

**MOLECULAR MODELING STUDIES ON ZEOLITES
IN ORDER TO DESIGN CATALYSTS FOR THE
SYNTHESIS OF FINE CHEMICALS**

**Thesis submitted to the
University of Poona
for the Degree of**

**Doctor of Philosophy
in
CHEMISTRY**

By
Ramesh Chandra Deḡa

**Catalysis Division
National Chemical Laboratory
Pune-411 008
India**

May 1998

Dedicated
to
My parents and sisters



COMPUTERIZED

CERTIFICATE

This is to certify that the work presented in this thesis entitled, "MOLECULAR MODELING STUDIES ON ZEOLITES IN ORDER TO DESIGN CATALYSTS FOR THE SYNTHESIS OF FINE CHEMICALS" by Ramesh Chandra Deka, for the degree of Doctor of Philosophy, was carried out by the candidate under my supervision in the Catalysis Division, National Chemical Laboratory, Pune, India. Any material that has been obtained from other sources has been duly acknowledged in the thesis.

Date: 14 May 1998

Place: Pune



DR. RAJAPPAN VETRIVEL

(Research Guide)

ACKNOWLEDGEMENTS

It is a pleasure to show my regards to my research guide, Dr. R. Vetrivel, Scientist, Catalysis Division, National Chemical Laboratory, Pune, for his invaluable guidance and constant encouragement during the thesis work. I am deeply indebted to him for the knowledge and experience I gained in molecular modelling through his earnest efforts.

I take this opportunity to thank Dr. S. Sivasanker, Prof. S. Pal and Dr. Dewi Lewis for their active interest and fruitful discussions on several aspects of the thesis work.

I thank my collaborators Dr. A. Chatterjee, Dr. A.P. Singh, Dr. T. Selvam, Dr. P. Bharathi, Mrs. S. Sharma and Mr. S. Waghmode for their co-operation.

I am thankful to my labmates and friends Ajitha, Sailaja, Mahesh, Ramda, Nayana, Aparna, Uttam, Debnath, Kailash, Chandrakumar, Damodaran, Shamasundar, Uddhav, Manoj, Yogita and Sangita for the cordial atmosphere which I enjoyed in the lab. I specially thank Mr. M. Krishnamurthy for his timely help.

I don't have enough words to express my thanks to my friends Prodeepda, Dipakda, Puyam, Vinod, Sharmaji, Venkat, Shekhar, Sunny, Kutty, Newman, Nandan, Jayachandran, Seshu, Suju, Shivashankar and Pallan who made my stay at NCL comfortable and memorable.

I heartily acknowledge Kamaleswar, Rama, Diganta, Baishali, Ghanashyam and Dipak for their well wishes. I am grateful to my family members for their moral support.

I sincerely thank all the research scholars, scientific and non-scientific staff of the Catalysis Division, for their friendly association and help.

I take this opportunity to thank Dr. A. V. Ramaswamy, Head, Catalysis Division, for his personal interest and encouragement.

I thank Dr. Paul Ratnasamy, Director, NCL, for the facilities of the Laboratory and for allowing me to submit this work in the form of thesis.

Finally, I would like to thank CSIR, New Delhi, for financial support in the form of research fellowship.

Ramesh Ch. Deka

Ramesh Ch. Deka

ABBREVIATIONS USED IN THIS THESIS

CAN	Cancrinite
CNDO	Complete Neglect of Differential Overlap
CPK	Corey-Pauling-Koltun
CVFF	Consistent Valence Force Field
DFT	Density Functional Theory
DIBP	Diisopropylbiphenyl
EA	Electron Affinity
EB	Ethylbenzene
EM	Energy Minimization
FAU	Faujasite
GAMESS	General Atomic and Molecular Electronic Structure System
HOMO	Highest Occupied Molecular Orbital
HSAB	Hard-Soft Acid-Base
IBB	Isobutylbenzene
IBEB	Isobutylethylbenzene
IP	Ionization Potential
LTL	Zeolite L
LUMO	Lowest Unoccupied Molecular Orbital
MAZ	Mazzite
MC	Monte Carlo
MD	Molecular Dynamics
MNDO	Modified Neglect of Diatomic Overlap
MOR	Mordenite
MSD	Mean Square Displacement
MTW	ZSM-12
OFF	Offretite
PC	Personal Computer
PHF	Periodic Hartree-Fock
PMH	Principle of Maximum Hardness
QC	Quantum Chemical
XPS	X-ray Photoelectron Spectroscopy

CONTENTS

CHAPTER 1

GENERAL INTRODUCTION AND SCOPE OF THE THESIS	1
1.ZEOLITES: A GENERAL OVERVIEW	1
2.SCOPE OF THE THESIS	3
3.BASICS OF SIMULATION METHODS	5
3.1. Force Field	5
3.1.1 Long range interaction	6
3.1.2 Short range interaction	6
3.1.3 Force field parameters	8
3.2. Energy Minimization	10
3.2.1 Steepest descent method	10
3.2.2 Conjugate gradient method	11
3.2.3 Newton-Rophson method	11
3.3. Monte Carlo Technique	12
3.4. Molecular Dynamics	13
3.5. Quantum Chemical calculations	15
3.6. Molecular Graphics Methods	16
4. SUMMARY	17
REFERENCES	17

CHAPTER 2

MOLECULAR GRAPHICS AND STRUCTUREAL FITTING OF AROMATICS IN LARGE PORE ZEOLITES	23
1. INTRODUCTION	24
2. METHODOLOGY	25
2.1 Display of Molecules and Zeolites	25
2.2 Real Time Motions	26
2.3 Geometric Measurements	27
2.4 Further of Graphics Facilities	27
3. RESULTS AND DISCUSSION	27
3.1 Fitting of Molecules Inside Zeolites by Molecular Graphics	27

3.2 Analysis of Simulation Results by Molecular Graphics	37
4. CONCLUSIONS	38
REFERENCES	38
CHAPTER 3	
LOCATION AND ENERGETICS OF ALKYLAROMATICS IN LARGE PORE ZEOLITES FROM HYBRID METHOD	40
1. INTRODUCTION	41
2. METHODOLOGY	42
3. RESULTS AND DISCUSSION	44
3.1. Minimum Energy Locations for the Isomers of DIBP	44
3.2. Minimum Energy Locations for the Isomers of IBEB	47
4. CONCLUSIONS	49
REFERENCES	49
CHAPTER 4	
ADSORPTION SITES AND DIFFUSION MECHANISM OF ALKYLAROMATIC IN LARGE PORE ZEOLITE CATALYSTS AS PREDICTED BY MOLECULAR MODELING TECHNIQUES	51
1. INTRODUCTION	52
2. METHODOLOGY	54
3. RESULTS AND DISCUSSION	55
3.1 Diffusion of DIBP Isomers in LTL, MOR and MTW	56
3.1.1 Zeolite L	56
3.1.2 Mordenite	58
3.1.3 ZSM-12	58
3.2 Diffusion of Alkylbenzenes in Large Pore Zeolites	61
3.2.1 Zeolites with pore diameter $\geq 7.0\text{\AA}$	61
3.2.2 Zeolites with pore diameter $\leq 7.0\text{\AA}$	67
3.2.3 Influence of pore architecture in diffusion	73
4. CONCLUSIONS	75
REFERENCES	75

CHAPTER 5

MOLECULAR DYNAMICS STUDIES ON DIFFUSION OF AROMATICS IN MORDENITE	79
1.INTRODUCTION	80
2.METHODOLOGY	81
3.RESULTS AND DISCUSSION	82
3.1 Adsorption Sites and Energetics	82
3.2 Coefficients of Self-Diffusion	85
4.CONCLUSIONS	87
REFERENCES	87

CHAPTER 6

INFLUENCE OF ZEOLITE COMPOSITION ON ACIDITY AND ETHYLATION ACTIVITY: A QUANTUM CHEMICAL STUDY	90
1.INTRODUCTION	91
2.METHODOLOGY	93
2.1.Theory	93
2.2.Computational Details	96
3.RESULTS AND DISCUSSION	97
3.1. Influence of Mordeinite Pore on Frontier Molecular Orbitals of Guest Molecular	97
3.2. Influence of Chemical Composition on Acidity	100
3.2.1. Calculation with 3-21G basis set	100
3.2.2. Calculations with DZV basis set	103
3.3.Influence of Chemical Composition on Ethylation Activity	104
4. CONCLUSIONS	106
REFERENCES	106

CHAPTER 7

SUMMARY AND CONCLUSIONS	110
REFERENCES	115
CURRICULUM VITAE	
LIST OF PUBLICATIONS	

CHAPTER 1

TH 1129

GENERAL INTRODUCTION AND SCOPE OF THE THESIS

1. ZEOLITES: A GENERAL OVERVIEW

Zeolites are framework structures with large cages and channels made up of an extensive linkage of SiO_4 tetrahedra joined together through the oxygen atoms. Commonly the element Al is substituted for some of the Si atoms. In these aluminosilicates an additional cation is incorporated interstitially within the lattice so that its electron is donated to the Al site to satisfy the bonding requirements of a tetrahedral framework. According to Smith,¹ “a zeolite is an aluminosilicate with a framework structure enclosing cavities occupied by large ions and water molecules, both of which have considerable freedom of movement, permitting ion-exchange and reversible dehydration.” However, synthetic zeolites include numerous examples that do not meet one or more of these criteria. The effective pore sizes in zeolites range from $\sim 3 \text{ \AA}$ to over 10 \AA , which is sufficient to permit the diffusion of catalytically interesting organic molecules. This fact combined with the possibility of generating active sites inside the channels and cavities of zeolites produces a very unique type of catalyst, which by itself can be considered as a catalytic microreactor.²

Zeolites were discovered in 1756 by the Swedish mineralogist Axel Fredrick Cronstedt.³ He examined two samples, one of Finish origin and the other one brought from Iceland. When heated in the flame of a blowpipe, the samples emitted gas and puffed up. The minerals were named zeolites which mean “boiling stones” in Greek (*Zeo* = boil and *lithos* = stone). The history of zeolite research began with the synthesis experiments of Sameshima in Japan⁴ and Barrer in UK.⁵ But the full recognition of the industrial potential of zeolite materials came only in the 1950's when researchers at Union Carbide succeeded in the synthesis of zeolites A and X and developed commercial technologies of gas purification, separation and catalysis using zeolites. Today, synthetic zeolites play a major role in petroleum and petrochemical catalysis, radioactive waste storage, water treatment,

gas separation and animal feed supplements, all because of their exceptional abilities for ion exchange and sorption.⁶ In addition, there is a growing interest in the synthesis of fine chemicals.⁷⁻¹¹

In general, hydrated zeolites can be represented by the formula: $M^{+n}_{x/n}[(AlO_2)_x(SiO_2)_y] wH_2O$ where M is a cation which can belong to the group IA or IIA or can be an organic cation, n is the cation valence, w is the number of water molecules and y/x is the Si to Al ratio in the structure. The square bracket contains the framework atoms while the remaining atoms reside in specific sites in the channels. Crystalline structures of the zeolite type but containing tetrahedrally coordinated Si, Al, P as well as transition metals and many other group elements with varying valency such as, B, Ga, Fe, Cr, Ti, V, Mn, Co, Zn, Cu etc., have also been synthesized with the generic name of zeotype, including AlPO₄, SAPO, MeAPO and MeAPSO type molecular sieves.^{12,13} All these tetrahedrally coordinated atoms are generally called the T-atoms. When a trivalent atom is present in the zeolite framework, a negative charge is created in the lattice, which is compensated by cations like sodium, potassium, etc. Brönsted acid sites are developed when the cation is exchanged by a proton. The proton is attached to the oxygen atom bridging the silicon and aluminum atoms, resulting in the acidic hydroxyl group which is the site responsible for the Brönsted acidity of zeolites.

The acid sites of zeolites, in combination with their well-defined pore architecture, make zeolites suitable as a shape selective solid acid catalyst. Whereas the ion-exchange capacity is controlled by composition rather than zeolite structure, the use as a catalyst is strongly dependent on the structure. Therefore, the synthesis of zeolites with new structures is one of the main topics in zeolite research. The compilation of structural information on zeolites is available in the *Atlas of Zeolite Structure Types*.¹⁴ Further information on zeolites can be found in a review article by Higgins,¹⁵ in a classic book by Breck¹⁶ and more recent results, in a book by Szostak.¹⁷ Because zeolite synthesis is time consuming and their use in catalysis is mainly based on trial and error methods, the need for theoretical predictions of zeolite properties, adsorption, diffusion and interaction of reactants and product molecules are evident. The understanding of these properties of zeolites can greatly facilitate the design of zeolite catalysts. A large intensification of the theoretical studies of zeolites can be seen in the last ten years.¹⁸⁻²¹ The recent book edited

by Catlow²² is an excellent source of information on theoretical modeling of zeolite structures and their reactivity. Most of the earlier theoretical studies were mainly focused on the relation between the zeolite framework structure and the molecules or ions present within the zeolite framework.

The principal techniques used in molecular modeling are molecular graphics, energy minimization, Monte Carlo, molecular dynamics and quantum chemical calculations. Monte Carlo and molecular dynamics methods are attractive alternative to experiments because these methods, in principle, provide information for conditions under which experiments are not feasible. Previous simulations based on molecular dynamics²³⁻²⁵ and Monte Carlo methods^{26,27} tended to concentrate on small guest molecules, since these two methods need to perform for relatively long time scales. For large molecules of catalytic relevance, it is necessary to perform computationally less demanding techniques, such as energy minimization before applying these computationally expensive techniques.

2. SCOPE OF THE THESIS

In this thesis, we describe modeling of large organic molecules which are catalytically important and we will show that computational techniques yield detailed and reliable information on both structural and dynamical properties of sorbed species. We describe the modeling of sorption sites, diffusion mechanisms, diffusivity of the aromatics and their electronic interaction with the zeolite host. The aim of the thesis is to find out suitable zeolite catalysts for the selective synthesis of 4,4'-diisopropylbiphenyl (DIBP) and para-isobutylethylbenzene (*p*-IBEB) because of their importance in industries. The modeling methods used and the computational approaches are generalized so as to study the adsorption of any large molecules inside the zeolites. Molecular modeling studies to investigate regiospecific alkylation of biphenyl and isobutylbenzene are carried out with their importance, in mind as intermediates for liquid crystal polymers and α -(4-isobutylphenyl) propionic acid, a popular analgesic drug called ibuprofen, respectively.

⇒ In this chapter, we present a brief introduction to zeolites and their catalytic activity.

The need for theoretical studies to understand diffusion mechanism of aromatic molecules and their interactions with zeolite hosts are stressed. Later sections of this

chapter present the theoretical principles used in molecular modeling and a brief introduction to the main features of each technique.

- ⇒ In Chapter 2, the importance of molecular graphics for visualization of zeolite structures and fitting of different organic molecules such as isomers of DIBP, ethylbenzene, isobutylbenzene and *o*-, *p*- and *m*-IBEB inside various zeolites are discussed. Using molecular graphics, it is possible to study how well the reactant and product molecules fit in the pores of different zeolites and it gives a preliminary screening method to identify the list of promising zeolites suitable for a specific reaction. This chapter also outlines the visualization and interpretation of structural data derived from elaborate calculations that lead to an understanding of the structure-property interplay.
- ⇒ In Chapter 3, we have investigated the sorption sites for the aromatics in different zeolites and calculated their adsorption energy values using a hybrid technique²⁸ which combines molecular dynamics and Monte Carlo methods with energy minimization. In this method, a library of different conformations of the sorbate molecule is generated by a molecular dynamics simulation and each of these conformations is then inserted, using a Monte Carlo method into random adsorption locations in the host framework. Suitable candidate 'adsorption-complexes', are accepted which pass the specified geometric as well as energetic constraints. Subsequently their energy values are minimized using standard techniques. The adsorption energy values calculated for the isomers of DIBP in zeolite-L, mordenite and ZSM-12 show that 4,4'-DIBP has favourable adsorption energy in ZSM-12.
- ⇒ In Chapter 4, we describe the diffusion behavior of aromatics in different large pore zeolites using force field energy minimization technique. We have calculated the diffusion energy barriers of several alkylaromatics in various zeolites to predict their shape selective behavior in alkylation of biphenyl and isobutylbenzene. Recently, this methodology has been developed as computationally efficient procedure to evaluate the diffusion energy barrier.^{29,30} It is found that the efficiency for selective production of 4,4'-DIBP in zeolite L (LTL), mordenite (MOR) and ZSM-12 (MTW) increase in the order: LTL < MOR < MTW. The efficiency for selective production of *p*-IBEB in

several zeolites are analyzed in terms of the interaction energy and energy barriers. It is found that MOR is the most suitable shape selective catalyst.

⇒ In Chapter 5, we report the results of molecular dynamics simulation of alkylbenzenes inside the pores of mordenite. We have compared the diffusion energy barriers calculated using force field energy minimization with the diffusivity of the molecules by molecular dynamics calculations. The diffusion behavior of the molecules at room temperatures is focused in this chapter.

⇒ In Chapter 6, the results of *ab initio* quantum chemical calculations on representative zeolite cluster models and the aromatic molecules are presented. The change in HOMO-LUMO energy of the molecules at different locations inside zeolite cavity is studied. Acidity of zeolite cluster is derived using the local Hard-Soft Acid-Base principle originally proposed by Pearson.³¹ We have investigated the acidity of zeolite clusters using new acidity parameters, the relative electrophilicity and nucleophilicity. Variations in the acidity of the zeolite due to isomorphous substitution of Si by Al, Ga or B have been predicted accurately using these calculations.

⇒ In Chapter 7, the salient conclusions derived in this thesis are summarised.

3. BASICS OF SIMULATION METHODS

Computer simulation at atomic level and electronic level are possible with classical mechanics and quantum mechanics, respectively. These methods are fairly standardized for chemical applications and their principles are described in the following sections.

3.1. Force Field

The forces acting between the atoms in a molecule or chemical systems could be mathematically defined through force field expressions. The results of all classical simulation methods (energy minimization, Monte Carlo, molecular dynamics) depend directly on the reliability of the force field parameters used.

The interatomic potential V for a system of n particles describes the variation of the total potential energy of the system as a function of the nuclear coordinates, r_1, \dots, r_n . i.e.

$$V = V(r_1, \dots, r_n) \quad (1)$$

In practice, V is generally broken down into 'pair,' 'three-body,' 'four-body' and higher order terms:

$$V = \sum_{i,j=1}^{\prime} V(r_i, r_j) + \sum_{i,j,k=1}^{\prime} V(r_i, r_j, r_k) + \sum_{i,j,k,l=1}^{\prime} V(r_i, r_j, r_k, r_l) + \dots \quad (2)$$

where the first term refers to a sum over all pairs of atoms, the second over all triplets and the third over all quartets, with the summation containing in principle up to 'N-body' terms. The primes indicate that in the summation a given term is only included once.

The majority of simulations approximate V simply by the pair potential term, which is usually decomposed into coulombic and non-coulombic terms (ϕ):

$$V(r_i, r_j) = \frac{q_i q_j}{r_{ij}} + \phi(r_{ij}) \quad (3)$$

The first term represents the long range electrostatic interactions between a pair of atoms with effective charges q_i and q_j while the second term is a two-body short range interaction.

3.1.1. Long range interactions

The long range interaction between ions is given by Coulomb's law as:

$$V(r) = \sum_{ij} \frac{q_i q_j}{r_{ij}} \quad (4)$$

where q_i and q_j are the effective charges on the atoms i and j separated by a distance r_{ij} . This expression converges very slowly as a result of the summation involving the r^{-1} term. The problem is overcome by using the Ewald summation technique³² which manipulates the sum by first adding and then subtracting a Gaussian charge distribution to each point in the array. The individual terms in the array are then rearranged into a rapidly and slowly converging series and taking advantage of the periodicity of the lattice, the slowly converging series is Fourier transformed into reciprocal space where convergence is rapid.³³ Either formal or partial charges may be suitable for zeolite ions. The use of formal charges with appropriate defined potentials was justified by Jackson and Catlow,³⁴ while van Beest *et al.*³⁵ gave a set of recommended partial charges derived using quantum chemical methods.

3.1.2 Short range interactions

The short range interaction combines a number of components including non-bonded interactions, electronic polarizability and, where relevant, covalent interactions, modeled by bond-bending and bond-stretching terms. For zeolite lattice this can be

represented by several ways. The expressions that model the system most accurately are considered below.

(a) Buckingham Potential: The basic form for Buckingham potential describing the interaction of a pair of ions is given as:

$$\phi_{ij} = A_{ij} \exp\left(\frac{-r_{ij}}{\rho_{ij}}\right) - \frac{C_{ij}}{r_{ij}^6} \quad (5)$$

Here i and j refer to the interacting ions, A_{ij} , ρ_{ij} and C_{ij} are variable parameters in the description of the short range potential. This expression comprises an attractive term and an exponential repulsive term. The two components correspond to a contribution of attractive dispersive forces (r^{-6}) and a term modeling the electron cloud overlaps which produces a repulsive force.

(b) Lennard-Jones potential: When considering intermolecular interactions between sorbed molecules and the zeolite lattice, the Lennard-Jones 12, 6 potential is considered to be an appropriate representation;

$$\phi_{ij} = \frac{A}{(r_{ij})^{12}} - \frac{B}{(r_{ij})^6} \quad (6)$$

where A and B are constants of repulsion and attraction due to dispersion forces, respectively.

(c) Bond-stretching: Bond-stretching terms are used in modeling bonded interactions in covalent systems, e.g. the hydroxyl group in zeolites. A Morse potential can be used for such interaction:

$$\phi_{ij} = D_b [1 - \exp\{-\alpha (r_{ij} - r_0)\}]^2 - D_b \quad (7)$$

where D_b is the bond dissociation energy for the bond between atoms i and j , r_0 is the equilibrium bond distance, r_{ij} is the bond length and α is a constant defining the shape of the potential energy well and can be obtained from spectroscopic data. A simple alternative is the widely used harmonic potential:

$$\phi_{ij} = \frac{1}{2} k_{ij} (r_{ij} - r_0)^2 \quad (8)$$

where k_{ij} is the harmonic force constant.

(d) *Bond-bending*: For modeling covalent and semi-covalent nature or angle dependency of the zeolite structure and in the adsorbates as well, a three-body potential needs to be considered in the potential function. The most common representation of the bond bending force is:

$$\phi_{ijk} = \frac{1}{2} k_{ijk} (\theta - \theta_0)^2 \quad (9)$$

where k_{ijk} is the bond-bending force constant between bonds ij and ik , θ_0 is the equilibrium bond angle and θ is the bond angle at atom i between atoms i , j and k .

(e) *Torsional terms*: Four-body torsional potential is used to study organic molecules particularly planar adsorbate molecules such as ethylene and benzene in zeolites.³⁶ Two planes are defined, between the ions, i , j and k and between j , k and l with the potential energy being dependent on n times the angle between these planes, thus giving rise to a minimum when the angle is 0 and multiples of $2\pi/n$ radians. The analytical form of the potential is given as:

$$\phi_{ijkl} = k_{ijkl} [1 \pm \cos(n\phi)] \quad (10)$$

where ϕ is the torsion angle, k_{ijkl} is the torsional constant and n is an integer which gives the periodicity of the torsion. There are also several other expressions defining the potential for out-of-plane bending, hydrogen bonding etc. Their contributions are fairly small and that too in special cases, where molecules can exist in unusual conformations.

3.1.3. Force field parameters

Having defined the forms of the interatomic interactions, the next step is to determine the variable parameters in these expressions. Two main approaches, namely empirical fitting and direct calculation are usually employed in the derivation of potential parameters.

(a) *Empirical fitting*: The 'empirical fitting' procedure starts with an initial guess of the parameters, they are then adjusted systematically, usually via a least squares fitting technique, until the differences between the calculated and experimental structure and properties are minimized. This method requires the availability of structural data and preferably other data such as elastic and dielectric constants.

(b) *Direct calculation*: Potentials may be calculated directly using quantum mechanical methods ranging from electron gas techniques³⁷ to *ab initio* quantum chemical calculations

using Hartree-Fock method.³⁸ Density Functional Theory (DFT) has also been used to calculate the potential parameters.³⁹ In these methods the interaction energy between a pair or periodic array of atoms can be calculated for a range of distances and the resulting

Table 1. Parameters used in force field energy minimization calculations.

Atoms ^a		Bond length parameters: $E = k_1 (r - r_0)^2$		
		r_0 (Å)	k_1 (kcal mol ⁻¹ Å ⁻²)	
c	h	1.1050	340.6175	
cp	h	1.0800	363.4164	
cp	cp	1.3400	480.0000	
cp	c	1.5100	283.0924	

Atoms			Bond angle parameters: $E = k_2 (\theta - \theta_0)^2$	
			θ_0	k_2 (kcal mol ⁻¹ degree ⁻²)
h	c	h	109.4000	39.5000
h	c	c	110.0000	44.4000
cp	cp	h	120.0000	37.0000
cp	cp	cp	120.0000	90.0000
h	c	cp	110.0000	44.4000
c	cp	cp	120.0000	44.2000
cp	c	cp	110.5000	46.6000

Atoms				Torsion parameter: $k_\phi (1 + \cos(n\phi - \phi_0))$		
				k_ϕ (kcal mol ⁻¹)	n	ϕ_0
*	cp	cp	*	12.0000	2	180.000

Atoms				Out-of-plane parameter: $E = k_\chi (1 + \cos(n\chi - \chi_0))$		
				k_χ (kcal mol ⁻¹)	n	χ_0
cp	cp	cp	*	0.3700	2	180.0000

Atoms		Nonbonded parameters: $E = A_{ij}/r^{12} - B_{ij}/r^6$; $A_{ij} = (A_i A_j)^{1/2}$; $B_{ij} = (B_i B_j)^{1/2}$	
		A (kcal mol ⁻¹ Å ¹²)	B (kcal mol ⁻¹ Å ⁶)
h		7108.4660	32.87076
c		1790340.7240	528.48190
o		272894.7846	498.87880
cp		2968753.3590	1325.70810
si		3149175.0000	710.00000

^a Atom types: h = hydrogen; c = aliphatic carbon; cp = aromatic carbon; o = zeolite oxygen; si = zeolite silicon.

* indicates any atom of the periodic table.

potential energy curve is fitted to a suitable functional form. Pairs or cluster of atoms may be embedded in some representation of the surrounding crystal. These methods can, in principle, calculate potentials for any interaction, but constrained only by the computational resources to develop an exhaustive list.

We have used an empirically fitted potential parameter set, consistent valence force field (CVFF)⁴⁰ for our calculations. These potentials are reported in the literature and are extensively used. A list of the CVFF potential parameter used is given in Table 1.

Using the above mentioned force field expressions, a range of computational techniques can be employed for calculating structural properties and the dynamic behaviour of molecules inside zeolites. In the following section the computational basis of such methods is described.

3.2. Energy Minimization

Energy minimization (EM) technique is the simplest approach to determine the minimum energy configuration of a molecule or crystal, where the interatomic interactions are known through force field expressions. It requires the specification of an initial configuration or 'starting point'; the energy is calculated using knowledge of force field expressions and parameters. The system is then driven down in energy to the nearest minimum. A wide variety of algorithms are available, which are classified according to the order of the derivative of the total energy function that is employed in the calculation. The simplest methods employ the energy function alone and search over configuration space until the minimum is located. Much greater efficiency is obtained using gradient techniques in which the first derivatives of energy with respect to all the structural variables X_i ($\delta E/\delta X_i$) are calculated. These then guide the direction of minimization. Rapid convergence can be achieved when knowledge of second derivatives is also used to guide the minimization direction. The following methods are widely used:

3.2.1. Steepest descent method

The direction of steepest descent of $f(X)$ at the point X is given by the vector $-\nabla f(X)$ which is denoted by $-g_k$. If the direction of step at each successive point X_k is the vector of steepest descent $-g_k$, the iterative procedure is called the method of steepest descent. It is defined by⁴¹

$$X_{k+1} = X_k - \lambda_k g_k, \quad k = 0, 1, 2, \dots, \lambda_k > 0 \quad (11)$$

where λ_k is a scalar quantity that determines the step length in direction $-g_k$.

3.2.2. Conjugate gradients method

In this method the displacement vector S_k uses information on the previous values of the gradients which speeds up convergence.⁴¹ Thus the expression for S_k is:

$$S_k = -g_k + \beta_k \cdot S_{k-1} \quad (12)$$

$$\text{where } \beta_k = \frac{g_{k-1}^T \cdot g_{k-1}}{g_{k-2}^T \cdot g_{k-2}}$$

Here the g_k are vectors whose components are the derivatives with respect to individual coordinates and the superscript, T, indicates the transpose of the vector.

3.2.3. Newton-Raphson method

In this method, the iterative minimization proceeds according to the expression:

$$X_{k+1} = X_k - H_k g_k, \quad k = 0, 1, 2, \dots \quad (13)$$

where the matrix $H_k = W_{ij}^{-1}$, in which the elements W_{ij} are the second derivatives, $(\delta^2 E / \delta X_i \delta X_j)$. Newton-Raphson method converges more rapidly and is far less computationally expensive than gradient techniques. The major computational problem remains in the need to store the inverse of the second derivative matrix.

Energy minimization methods can be applied effectively to large complex systems and are making an increasingly important contribution to solve crystal structure related problems. However, these methods are limited for several reasons; they inherently omit any representation of atomic motions and time dependent phenomena. There is another major difficulty in the minimization techniques - they can only be guaranteed to locate the nearest local minimum to the starting point of the calculation. The only real solution to the problem is to sample large numbers of starting points in order to ensure that all low energy minima have been identified. A number of sophisticated mathematical procedures have been developed with the aim to simplifying the overall potential energy surface and 'washing out' local minima⁴² but there can never be a guarantee that the 'global' minimum - the minimum configuration corresponding to the lowest energy has been identified.

Despite these limitations, energy minimization techniques are straight forward, robust and readily applicable. These methods are ideally suited to large and complex systems such as zeolites. Fruitful applications of this method have been reported in zeolite

science to model crystal structures^{43,44} and sorption sites.^{45,46} The influences of organic templates on the synthesis of microporous materials have been studied by combining with molecular dynamics and Monte Carlo methods.^{47,48} We have used energy minimization techniques to study the sorption, energetics and diffusion of aromatics in large pore zeolites (Chapters 3 & 4).

3.3. Monte Carlo Technique

The Monte Carlo (MC) simulation method is well suited to the study of molecules sorbed in zeolites. The simulation proceeds via the generation of successive configurations of the ensemble by a series of random moves which can be a molecular translation, molecular rotation, insertion or deletion of molecule etc. Once a sufficient number of configurations is generated, ensemble averages are calculated. In generating such ensembles, it is essential to formulate an 'acceptance' criterion, that is a procedure that determines whether a new configuration created by a move will be acceptable within the ensemble. MC simulations are most commonly run in the canonical (NVT) ensemble in which both volume and temperature are fixed. The most commonly used approach is the Metropolis method, which are given below:⁴⁹

1. When a new configuration, v' is generated from the old configuration, v the change in configuration changes the energy of the system by the amount

$$\Delta E_{vv'} = E_{v'} - E_v.$$

This energy difference governs the relative probability of configurations through the Boltzmann distribution and one can build this probability into the Monte Carlo trajectory by a criterion for accepting and rejecting moves to new configurations. If

$\Delta E_{vv'}$ is positive the Boltzmann factor $B = \exp(-\Delta E_{vv'}/kT)$ is calculated.

2. If the energy change $\Delta E_{vv'}$ is negative or zero, the configuration is accepted.
3. If $\Delta E_{vv'}$ is positive, a random number (P) between 0 and 1 is generated.
4. If $P \leq B$, the move is accepted. Otherwise the move to a new configuration in the next step is rejected.

MC simulations are performed on ensembles containing several thousand particles, to which periodic boundary conditions are applied in the case of the simulation of zeolites. The simulation again starts with an equilibration phase during which the system is

equilibrated followed by a 'simulated run' in which, typically, several million configurations are generated.^{50,51}

This method can be used to locate the sorption site, determine sorption equilibria and various thermodynamic functions at higher temperatures.⁵²⁻⁵⁴ Stroud *et al.*⁵² have studied the adsorption of methane in zeolite A and calculated the heat capacity, isosteric heat of adsorption and adsorption isotherm using MC methods. Yashonath *et al.*⁵³ in their simulation studies attempted to understand the behaviour of sorbed methane in terms of the temperature dependence of its binding and mobility in zeolite Y. Recently, Smit and coworkers⁵⁵⁻⁵⁸ have studied the location and conformation of *n*-alkanes in different zeolites using a novel Monte Carlo technique called configurational-bias Monte Carlo. Freeman *et al.*²⁸ have developed a technique which blends molecular dynamics, Monte Carlo and energy minimization methods to locate the global energy minimum site for sorbed molecules. We have used (in Chapter 3) this hybrid technique to determine the minimum energy configuration of the aromatics inside the pore of various zeolites.

3.4. Molecular Dynamics

Molecular dynamics (MD) simulation is perhaps the most powerful computational technique available for obtaining information on the time dependent properties of molecular or atomic motion in zeolite crystals. It is used to obtain thermodynamic quantities and detailed dynamical information on sorption and diffusion processes in zeolite systems. For instance, the extent to which intermolecular vibration and framework motion assist sorption and diffusion of molecules can be simulated. The major limitation is its inability to model diffusion of larger sorbed molecules and electronic polarizability due to the huge amount of computer time and memory requirements.

MD technique proceeds by deriving explicit numerical solution of Newton's equation of motion. It requires the initial coordinates and velocities of particles which are assigned based on X-ray crystal structure and temperature of simulation. With the knowledge of the interatomic potential among the particles, the forces acting on the particle can be calculated. Periodic boundary conditions are generally applied in order to replicate the basic simulation box infinitely in three directions. Initially, the random velocities are assigned and then the velocities are scaled over many time steps to converge to an

equilibrated state. In the limit of an infinitesimal value of time step, Δt , the coordinates X_i and velocities V_i of the i^{th} particle after Δt can be written as:

$$X_i(t + \Delta t) = X_i(t) + V_i(t) \Delta t, \quad (14)$$

$$V_i(t + \Delta t) = V_i(t) + \frac{f_i}{m_i}(t) \Delta t, \quad (15)$$

where f_i is the force acting on the i^{th} particle and m_i is its mass. One important factor in MD simulation is the choice of Δt . It must be smaller than the time scale of any important dynamical processes at the atomic or molecular level. Thus, it must be at least an order of magnitude smaller than the typical period of atomic vibrations (10^{-12} - 10^{-13} s). A very small time step consumes a lot of computational resources and large time steps can introduce errors as dynamics of atoms or conformation of molecules may not be noticed. Values in the range 10^{-14} - 10^{-15} s generally represent the best compromise as discussed in detail by Jacobs and Rycerz.⁵⁹ Of the three types of algorithms used in contemporary MD studies, namely the Verlet⁶⁰, Beeman⁶¹ and Gear,⁶² the Verlet method with leap-frog formulation has been found to be readily applicable for studying zeolitic materials.⁶³

One of the most useful properties of a zeolite is its ability to control the diffusion of the different sorbed molecules, which can be calculated from MD simulations. The property of usual interest in MD simulations is the diffusion coefficient which is calculated from the well known Einstein formula⁶⁴ as given below:

$$D = \lim_{t \rightarrow \infty} \frac{\langle |r(t) - r(0)|^2 \rangle}{6t} \quad (16)$$

where $r(t)$ and $r(0)$ are respectively the final and initial position of a particle, for a time interval t and D is the diffusion coefficient. The numerator, $\langle |r(t) - r(0)|^2 \rangle$ is generally called mean square displacement of the particle.

Previous work on the application of MD to zeolite systems concentrated on the diffusion of small molecules in zeolite pores. Typical studies include diffusion of methane in NaY by Yashonath *et al.*⁶⁵, xenon in silicalite by Pickett *et al.*²³ water in ferrierite by Leherte *et al.*⁶⁶ and diffusion of O_2 and N_2 in NaA by Miyamoto and coworkers.⁶⁷ The dynamics of even large molecules such as porphyrin inside faujasite zeolite has been studied.⁶⁸ Other typical examples on MD simulations of hydrocarbons in zeolites are those

of Hernandez and Catlow⁶⁹ and Demontis and Suffritti.⁷⁰ We have calculated (Chapter 5) the diffusivity of *o*-, *m*- and *p*-IBEB in mordenite using MD technique.

3.5. Quantum Chemical Calculations

Various types of simulation techniques discussed above are used for adsorption and diffusion studies on zeolites. For the application of zeolites as useful catalysts, the mechanism of reaction following the adsorption of molecules on the active sites have to be understood. This process is often complicated to deal with experimental techniques due to the high reaction rates involved. Quantum chemical calculations can be divided into two types, semi-empirical methods (such as CNDO, MNDO etc.) and non-empirical (*ab initio*, DFT etc.) methods. Semi-empirical methods neglect many of the differential overlap approximations while the non-empirical methods evaluate all overlap integrals. The goal of either method is to obtain the wave function of orbital $\phi(r)$ occupied by each electron, the eigenvalue (or orbital energy) ϵ_i corresponding to that orbital, the total energy E_{tot} and the atomic force F on each atom by solving the Schrödinger wave equation.

Quantum chemical calculation is a fairly standard technique used for studying chemisorption and reaction mechanism on zeolite surfaces. The use of quantum chemical methods in zeolite systems is two fold. It can be used to identify reaction pathways and sorbed intermediate species in the cages of zeolites. Reactivity is studied using finite molecular clusters to represent a particular site in zeolite structure.⁷¹⁻⁸¹ In addition, it is widely used in the derivation of force field parameters for use in static and molecular dynamic simulations.^{35,38,82-85} Potential parameters derived from *ab initio* methods are used for obtaining structural informations of zeolites. Generally calculations on zeolites involve the use of zeolite fragments treated as clusters so as to mimic the infinite crystal. The cluster size depends on the level of approximation or sophistication of the calculations. A plausible way to terminate the cluster is to embed them in a surrounding lattice of zeolite structure represented as point charges or alternatively terminate them with hydrogen atoms. More details on quantum chemical calculations on zeolite system can be found in a recent review by Sauer.⁸⁶ Recently, periodic Hartree-Fock (PHF) calculations of siliceous mordenite, have been performed by White and Hess.⁸⁷ They have also examined the electrostatic potential of silicalite⁸⁸ using PHF method. However, the computational efforts involved is large for these type of calculations.

An alternative way to overcome the limitation of small cluster models was used by Redondo and Hay who used semi-empirical quantum chemical calculations (MNDO) to study acid sites in zeolite ZSM-5.⁸⁹ In their study each of the 12-T distinct T-sites was modeled by a large cluster of the appropriate geometry containing about 100 atoms. Using a large cluster, Gale *et al.*⁹⁰ performed semi-empirical calculations on the interaction between methanol and Brønsted acid sites in ZSM-5 and found the methanol to be hydrogen bonded to the framework proton. In a recent study, Mota *et al.*⁹¹ performed a semi-empirical MNDO calculation of simple alkylcarbenium ions on a large and more realistic cluster, comprising a hexagonal prism and sodalite unit to investigate different adsorption sites on zeolite Y. Chatterjee and Vetrivel^{92,93} studied the role of templating organic molecules in the synthesis of ZSM-5 using MNDO method. An extensive study on comparison of various sizes used in *ab initio* calculations and force field methods were presented by van Santen and coworkers.⁹⁴ In Chapter 6 we are presenting semi-empirical MNDO method to study the change in HOMO-LUMO energy values of aromatics inside the channel of mordenite. *Ab initio* calculations on zeolite clusters are carried out in order to understand their acidity and reactivity.

3.6. Molecular Graphics Methods

Finally, this work on available computational techniques for studying zeolites will not be completed without mentioning the molecular graphics techniques. The role of molecular graphics in elucidating and analyzing simulation results is clearly demonstrated by Freeman and Catlow.⁹⁵ In EM calculations, the structure of the relaxed zeolite and the geometry of the adsorption site can be visualized and analyzed using molecular graphics. In MD simulations, the migration of molecules in real time can be animated. The shape selective properties of zeolites can be qualitatively predicted with the aid of molecular graphics fittings. For instance, the interactive matching of molecules with zeolite pore can predict which molecules can enter the pores to reach the active site on the basis of either their size or steric requirements before performing detailed calculations. We have studied the shape selective properties of various zeolites for the synthesis of 4,4'-DIBP and *p*-IBEB (Chapter 2).

4. SUMMARY

In this chapter, a brief introduction has been provided on the structure and catalytic properties of zeolites. It is followed by the section describing the aims and outcome of the thesis. Further, we have described the basics of widely used computational techniques and their role in the studies of zeolites and their catalytic activities. Energy minimization of a zeolite structure with adsorbate molecules will help in determining the minimum energy location of the molecule inside the zeolite pore. The application of Monte Carlo and molecular dynamic simulations will help in determining the adsorption sites and diffusivity of sorbed molecules at temperatures above the ambient conditions, respectively. Predicting the reaction mechanism and probing the catalytic properties of different zeolites are possible using the *ab initio* quantum chemical technique.

REFERENCES

1. J.V. Smith, *Chem. Rev.*, 88 (1988) 149.
2. A. Corma, *Chem. Rev.*, 95 (1995) 559.
3. A.F. Cronstedt, *Svenska Vetenskaps Akademiens Handlingar, Stockholm*, 17 (1756) 120.
4. J. Sameshima, *Bull. Chem. Soc. Japan*, 4 (1929) 96.
5. R.M. Barrer, *J. Soc. Chem. Ind.*, 64 (1945) 130.
6. A. Dyer, *Chem. Ind. (London)*, (1984) 241.
7. W.F. Hölderich, M. Hesse and F. Näumann, *Angew. Chem. Int. Ed. Engl.*, 27 (1988) 226.
8. W.F. Hölderich, *Catal. Sci. Tech.*, 1 (1991) 31.
9. Y. Sugi and M. Toba, *Catal. Today*, 19 (1994) 187.
10. C.B. Dartt and M.E. Davis, *Catal. Today*, 19 (1994) 151.
11. P.B. Venuto, *Microporous Mater.*, 2 (1994) 297.
12. S.T. Wilson, B.M. Lok, C.A. Mesina, T.R. Cannan and E.M. Flanigen, *J. Am. Chem. Soc.*, 104 (1982) 1146.
13. M.E. Davis, C. Montes, P.E. Hathway and J.M. Garces, *Stud. Surf. Sci. Catal.*, 49 (1989) 199.
14. W.M. Meier, D.H. Olson and Ch. Baerlocher, *Atlas of Zeolite structure Types*, 4th ed.

- Elsevier, New York, 1996.
15. J.B. Higgins, in *Silica: Physical Behavior, Geochemistry, and Materials Applications*, P.J. Heaney, C.T. Prewitt and G.V. Gibbs (eds.), Mineralogical Soc. of America, Washington, 1994.
 16. D.W. Breck, *Zeolite Molecular Sieves, Structure, Chemistry and Use*, John Wiley & Sons, New York, 1974.
 17. R. Szostak, *Molecular sieves: Principles of Synthesis and Identification*, Van Nostrand Reinhold, New York, 1989.
 18. R. Vetrivel, C.R.A. Catlow and E.A. Colbourn, *J. Chem. Soc., Faraday Trans. 2*, 85 (1989) 497.
 19. J. Sauer, *Chem. Rev.*, 89 (1989) 199.
 20. R.A. van Santen and G.J. Kramer, *Chem. Rev.*, 95 (1995) 637.
 21. A.A. Demkov and O.F. Sankey, in *Access in Nanoporous Materials*, T.J. Pinnavaia and M.F. Thorpe (eds.), Plenum Press, New York, 1995, p. 273.
 22. *Modelling of Structure and reactivity in Zeolites*, C.R.A. Catlow (ed.), Academic Press, London, 1992.
 23. S.D. Pickett, A.K. Nowak, J.M. Thomas, B.K. Peterson, J.F.P. Swift, A.K. Cheetham, C.J.J. den Ouden, B. Smit and M.F.M. Post, *J. Phys. Chem.*, 94 (1990) 1233.
 24. P. Demontis, E.S. Foix, G.B. Suffritti and S. Quartieri, *J. Phys. Chem.*, 94 (1990) 4329.
 25. R.L. June, A.T. Bell and D.N. Theodorou, *J. Phys. Chem.* 94 (1990) 8232.
 26. R.L. June, A.T. Bell and D.N. Theodorou, *J. Phys. Chem.*, 94 (1990) 1508.
 27. K. Watanabe, N. Austin and M.R. Stapleton, *Molecular Simulation*, 15 (1995) 197.
 28. C.M. Freeman, C.R.A. Catlow, J.M. Thomas and S. Brode, *Chem. Phys. Lett.*, 186 (1991) 137.
 29. J.A. Horsley, J.D. Fellmann, E.G. Derouane and C.M. Freeman, *J. Catal.*, 147 (1994) 231.
 30. R.C. Deka and R. Vetrivel, *Chem. Commun.*, (1996) 2397.
 31. R.G. Pearson, *J. Am. Chem. Soc.*, 85 (1963) 3533.
 32. P.P. Ewald, *Ann. Phys.*, 64 (1921) 253.

33. M.P. Tosi, *Solid State Phys.*, 16 (1964)1.
34. R.A. Jackson and C.R.A. Catlow, *Molecular Simulation*, 1 (1988) 207.
35. B.W.H. van Beest, G.J. Kramer and R.A. van Santen, *Phys. Rev. Lett.*, 64 (1990) 1955.
36. J.O. Titiloye, P.Tschaufeser and S.C. Parker, in *Spectroscopic and Computational Studies of supramolecular Systems*, J.E.D. Davies (ed.), Kluwer Academic Publishers, Dordrecht, 1992, p. 137.
37. W.C. Mackrodt and R.F. Stewart, *J. Phys. C*, 12 (1979) 5015.
38. J.D. Gale, C.R.A. Catlow and W.C. Mackrodt, *Modelling Simul. Mater. Sci. Eng.*, 1 (1992) 73
39. M. Sierka and J. Sauer, *Faraday Discuss.*, 106 (1997) 41.
40. P. Dauber-Osguthorpe, V.A. Roberts, D.J. Osguthorpe, J. Wolff, M. Genest and A.T. Hagler, *Proteins: Struct., Function Genetics*, 4 (1988) 21.
41. K.V. Mital, *Optimization Methods in Operations Reserach and Systems Analysis*, Wiley Eastern Limited, New Delhi, 1983.
42. J. Kostrowicki and H.A. Sheraga, *J. Phys. Chem.*, 96 (1992) 7442.
43. R.G. Bell, R.A. Jackson and C.R.A. Catlow, *J. Chem. Soc., Chem. Commun.*, (1990) 782.
44. C.R.A. Catlow, J.M. Thomas, C.M. Freeman, P.A. Wright and R.G. Bell, *Proc. R. Soc. London. A*, 442 (1993) 85.
45. A.R. George, C.M. Freeman and C.R.A. Catlow, *Zeolites*, 17 (1996) 466.
46. A.R. George, C.R.A. Catlow and J.M. Thomas, *Microporous Mater.*, 11 (1997) 97.
47. D.W. Lewis, C.M. Freeman and C.R.A. Catlow, *J. Phys. Chem.*, 99 (1995) 11194.
48. D.W. Lewis, C.R.A. Catlow and J.M. Thomas, *Chem. Mater.*, 8 (1996) 1112
49. (a) D. Chandler, *Introduction to Modern Statistical Mechanics*, Oxford University Press, New York, 1987. (b) C.R.A. Catlow, in *Computer Modelling in Inorganic Crystallography*, C.R.A. Catlow (ed.), Academic Press, London, 1997, p. 1.
50. M.P. Allen and D.J. Tildesley, *Computer Simulation of Liquids*, Oxford University

Press, 1987.

51. *Computer Modelling of Fluids, Polymers and Solids*, C.R.A. Catlow, S.C. Parker and M.P. Allen (eds.), Vol. 293, NATO Series, Kluwer Academic Publishers, Dordrecht, 1990.
52. H.J.F. Stroud, E. Richard, P. Limcharoen and N.G. Parsonage, *J. Chem. Soc., Faraday Trans. 1*, 72 (1976) 72.
53. S. Yashonath, J.M. Thomas, A.K. Nowak and A.K. Cheetham, *Nature*, 331 (1988) 601.
54. J. Karger, M. Petzold, H. Pfeifer, S. Ernst and J. Weitkamp, *J. Catal.*, 136 (1992) 283.
55. B. Smit and J.I. Siepmann, *Science*, 264 (1994) 1118.
56. B. Smit and J.I. Siepmann, *J. Phys. Chem.*, 98 (1994) 8442.
57. S.P. Bates, W.J.M. van Well, R.A. van Santen and B. Smit, *J. Am. Chem. Soc.*, 118 (1996) 6753.
58. S.P. Bates, W.J.M. van Well, R.A. van Santen and B. Smit, *J. Phys. Chem.*, 100 (1996) 17573.
59. P.W.M. Jacobs and Z.A. Rycerz, in *Computer Modelling in Inorganic Crystallography*, C.R.A. Catlow (ed.), Academic Press, London, 1997.
60. L. Verlet, *Phys. Rev.*, 159 (1967) 98.
61. D. Beeman, *J. Comput. Phys.*, 20 (1976) 130.
62. C.W. Gear, in *Numerical Initial Value Problems in Ordinary Differential Equations*, Prentice Hall Publishers, New York (1971).
63. P. Demontis and G.B. Suffritti, *J. Phys. Chem. B*, 101 (1997) 5789.
64. A. Einstein, *Ann. Phys. (Lipizig)*, 17 (1905) 549; English translation in A. Einstein, *Investigations on the Theory of the Brownian Movement*, Dover, New York, 1956.
65. S. Yashonath, P. Demontis and M.L. Klein, *Chem. Phys. Lett.*, 153 (1988) 551.
66. L. Leherte, G.C. Lie, K.N. Swamy, E. Clementi, E. G. Derouane and J.M. Andre, *Chem. Phys. Lett.*, 145 (1988) 237.

67. M. Kubo and A. Miyamoto, in *Computer Aided Innovation of New Materials II*, M. Doyama *et al.* (eds.), Elsevier, Amsterdam, 1993, p. 295.
68. T. Sato, K. Sugao, Y. Oumi, R. Vetrivel, M. Chatterjee, A. Chatterjee, M. Kubo, A. Stirling, A. Fahmi and A. Miyamoto, *Appl. Surf. Sci.*, 119 (1997) 346.
69. E. Hernandez and C.R.A. Catlow, *Proc. R. Soc. Lond. A*, 448 (1995) 143.
70. P. Demontis and G.B. Suffritti, *Chem. Rev.*, 97 (1997) 2845.
71. G.M. Zhidomirov and V.B. Kazansky, *Adv. Catal.*, 34 (1986) 131.
72. R. Vetrivel, C.R.A. Catlow and E.A. Colbourn, *Proc. R. Soc. London A*, 417 (1988) 81.
73. R. Vetrivel, C.R.A. Catlow and E.A. Colbourn, *J. Phys. Chem.*, 93 (1989) 4594.
74. G.J. Kramer and R.A. van Santen, *J. Am. Chem. Soc.*, 115 (1993) 2887.
75. E.H. Teunissen, R.A. van Santen, A.P.J. Jansen and F.B. van Duijneveldt, *J. Phys. Chem.*, 97 (1993) 203.
76. E. Broclawik, H. Himei, M. Yamadaya, M. Kubo, A. Miyamoto and R. Vetrivel, *J. Chem. Phys.*, 103 (1995) 2102.
77. H. Himei, M. Yamadaya, M. Kubo, R. Vetrivel, E. Broclawik and A. Miyamoto, *J. Phys. Chem.*, 99 (1995) 12461.
78. M. Yamadaya, H. Himei, T. Kanougi, Y. Oumi, M. Kubo, A. Stirling, R. Vetrivel, E. Broclawik and A. Miyamoto, *Stud. Surf. Sci. Catal.*, 105 (1997) 1485.
79. R. Shah, J.D. Gale and M.C. Payne, *J. Phys. Chem.*, 100 (1996) 11688.
80. P.E. Sinclair and C.R.A. Catlow, *J. Chem. Soc., Faraday Trans.*, 92 (1996) 2099.
81. P.E. Sinclair and C.R.A. Catlow, *J. Chem. Soc., Faraday Trans.*, 93 (1997) 333.
82. G.J. Kramer, N. Farragher, B.W.H. van Beest and R.A. van Santen, *Phys. Rev. B*, 43 (1991) 5068.
83. J.B. Nicholas, R.E. Winans, R.J. Harrison, L.E. Iton, L.A. Curtiss and A.J. Hopfinger, *J. Phys. Chem.*, 96 (1992) 7958.
84. J.-R. Hill and J. Sauer, *J. Phys. Chem.*, 98 (1994) 1238.
85. J.-R. Hill and J. Sauer, *J. Phys. Chem.*, 99 (1995) 9536.

86. J. Sauer, *Stud. Surf. Sci. Catal.*, 84 (1994) 2039.
87. J.C. White and A.C. Hess, *J. Phys. Chem.*, 97 (1993) 6398.
88. J.C. White and A.C. Hess, *J. Phys. Chem.*, 97 (1993) 8703.
89. A. Redondo and P.J. Hay, *J. Phys. Chem.*, 97 (1993) 11754.
90. J.D. Gale, C.R.A. Catlow and A.K. Cheetham, *J. Chem. Soc., Chem. Commun.*, (1991) 178.
91. C.J.A. Mota, P.M. Esteves and M.B. de Amorim, *J. Phys. Chem.*, 100 (1996) 12418.
92. A. Chatterjee and R. Vetrivel, *J. Chem. Soc., Faraday Trans.*, 91 (1995) 4313.
93. A. Chatterjee and R. Vetrivel, *J. Mol. Catal.*, 106 (1996) 75.
94. G.J. Kramer, A.J.M. de Man and R.A. van Santen, *J. Am. Chem. Soc.*, 113 (1991) 6435.
95. C. Freeman and R. Catlow, *Chem. Ind. (London)*, (1990) 796.

CHAPTER 2

MOLECULAR GRAPHICS AND STRUCTURAL FITTING OF AROMATICS IN LARGE PORE ZEOLITES

ABSTRACT

In this chapter, we describe the usefulness of molecular graphics studies as a powerful and reliable method for quick screening of zeolites for selective synthesis of 4,4'-diisopropylbiphenyl and *p*-isobutylethylbenzene. Molecular graphics fitting of the isomers of diisopropylbiphenyl and isobutylethylbenzene in various zeolites indicate that large pore zeolites are needed for the synthesis of these alkylaromatics. Within the large pore zeolites, the importance of size and shape of the pores are clearly indicated by the molecular graphics studies. We have extensively used molecular graphics studies to analyze the results of our classical mechanics simulations and quantum chemical calculations. Animation of the dynamics of molecules inside zeolite during the energy minimization and molecular dynamics calculations brings out several intrinsic characteristics of zeolites-molecule interactions.

1. INTRODUCTION

The application of molecular graphics technique to the study of problems in protein crystallography¹ and medicinal chemistry² has enjoyed spectacular growth. Molecular graphics method has been introduced in the field of catalysis with the desire to understand the science behind catalysis.³⁻⁵ Another reason for the increasing use of molecular graphics is the need and benefit of computational analysis of experimental data. The availability of crystal structure databases⁶ combined with molecular graphics facilities to display them have opened the way for the rapid screening of a range of materials for potential catalytic application. Occasionally, simple arguments based on molecular size and shape may allow the investigator an important insight into the steric interactions which underly in a catalytic process.

Zeolite research is one of the most rapidly developing fields in catalytic chemistry.⁷ These materials, based on silicon, aluminium and oxygen frameworks, have complicated structures characterized by interconnected cavities and channels, presenting the ideal environment for shape selective catalysis. The catalytic behaviour of most of the zeolites arises from the Brönsted acid sites as the active sites. These active sites are located inside the intriguing pore structures. In such cases molecular graphics is useful to provide better understanding of the active sites.

Molecular graphics method provides an indication of the types of molecule that can be accommodated within the zeolite pores. We have carried out a preliminary screening process using molecular graphics to identify the most suitable zeolite for selective synthesis of 4,4'-diisopropylbiphenyl (DIBP) and *p*-isobutylethylbenzene (IBEB), respectively. 4,4'-DIBP is quite valuable because of its application in liquid crystals and high performance polymers.^{8,9} Separation of the isomers of DIBP is difficult and costly process. So, there is a strong incentive for the development of a catalyst that would selectively produce the 4,4'-DIBP. The alkylation of biphenyl with propene over acidic faujasite (FAU), zeolite-L (LTL), mordenite (MOR) and ZSM-12 (MTW) have been attempted.¹⁰ Zeolites are obvious candidates as catalysts for the selective production of 4,4'-DIBP. Size and shape differences between the 4,4'-, 4,3'- and 3,3'-DIBP lead to large differences in diffusion rates within the pores of these zeolites, which are reflected in the product yields.

HX and HY zeolites have been used as disproportionating catalysts to convert *o*- and/or *m*-isobutylethylbenzene into *p*-isobutylethylbenzene (IBEB) which is an intermediate in the synthesis of α -(4-isobutylphenyl) propionic acid.¹¹ This substance is better known as ibuprofen. *p*-IBEB can also be synthesized by alkylation of isobutylbenzene with ethene over Lewis acid catalysts¹² in which the selectivity toward *p*-IBEB is typically 17.6 %. The possibility of using zeolite catalysts for the production of *p*-IBEB by disproportionation of isobutylbenzene and a polyalkylbenzene over HY zeolite¹³ has been shown to lead to better selectivity (46.3 %). Although HY zeolite is better than conventional catalyst, selection of this specific zeolite is a random choice rather than a logical selection and no experimental results are available for any other zeolites.

Zeolites with a wide range of pore sizes are available. So, a screening process is desired prior to actual catalytic testing in a reactor. Hence, we have analyzed the efficacy of different zeolites using molecular graphics methods. In this chapter, we will present the molecular graphics studies with the aim of screening and predicting shape selective behaviour of zeolites for the above reactions. Using molecular graphics, it is possible to rapidly visualize how well the various reactant or product molecules fit inside the pores of zeolites. More details applications of molecular graphics method in zeolite systems can be found in an article by Freeman *et al.*¹⁴

2. METHODOLOGY

There are several public domain and commercial software packages available for molecular graphics applications. These software packages could be implemented in either personal computer (PC) or in workstations. In this thesis, all the molecular graphics studies were carried out using SiliconGraphics Inc., USA-Indigo2 workstation with 64 bit R 4400 CPU @ 150 MHz, including 8 Graphics + 2 Raster engines for advanced graphics features. The software used is Insight II package supplied by Biosym Inc., USA. This facility provides several analysis features which are listed below.

2.1. Display of Molecules and Zeolites

When the positions of atoms in molecules or solid lattice are known, they could be visualized as molecular graphics pictures. For zeolite lattice, when the coordinates of atoms in asymmetric unit cell, unit cell parameters and symmetry space group are known,

it is possible to apply symmetry operators and display the atoms in one or more unit cells. Although theoretically, the number of atoms that could be displayed is limited only by the memory of the workstation, for all practical purposes ~5000 atoms could be displayed. Different kinds of atoms are displayed in different colours. The simplest way to display an atom is as a “dot”. The atoms which lie within bonding distances are connected by sticks, which represent the bonds. These sticks have the colour of both the atoms which are connected by the bonds (Figure 1a). To increase the clarity, the width of the bonds could

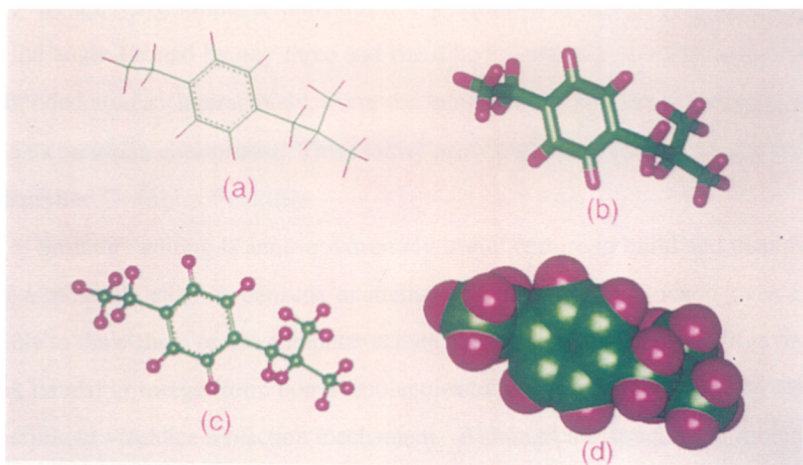


Figure 1. Different display styles of a typical example molecule, *p*-isobutylethylbenzene; (a) stick model, (b) rod model, (c) ball and stick model and (d) CPK model.

be increased to make them look like “rods” (Figure 1b). More realistic visualization could be made by “ball and stick” representations (Figure 1c), where the atoms are small spheres connected by stick-like bonds. A space filling model by rendering the actual ionic or van der Waals radii to the atoms according to Corey-Pauling-Koltun (CPK)¹⁵ model is also possible (Figure 1d). This CPK model provides the real perspective of the shape and size of the molecules and that of interstitial spaces inside zeolites. We used van der Waals radii: Si = 0.45Å, H = 1.10Å, C = 1.55Å and O = 1.35Å.

2.2. Real Time Motions

Another valuable facility available in the molecular graphics method is the translation and rotation of the displayed chemical system. Imaginary horizontal (X-axis)

and vertical (Y-axis) axes run across the computer screen, where the molecular graphics pictures are displayed. The axis perpendicular to the computer screen is Z-axis. It is possible to translate or rotate the molecules along these three cartesian axes by the use of keyboard or mouse in order to visualize them from different directions. This facility is also extremely useful to understand the structural fitting and orientation of molecules inside zeolites.

2.3. Geometric Measurements

By applying simple arithmetics, it is possible to calculate the distance between any two, the angle formed by any three and the dihedral angle formed by any four bonded or non-bonded atoms. Interactively, using the mouse or the keyboard, choosing an atom will locate its cartesian coordinates. This facility provides quantitative structural fitting.

2.4. Further Graphics Facilities

Structure editing is another extremely useful feature to build and display molecules. As if a molecule such as benzene or methane is drawn with a pencil over a paper, it is possible to draw them on the computer screen using the mouse. Further it is possible to cut (break bonds) or merge (form bonds) molecules to form new molecules. By this process, it is possible to visualize a reaction mechanism. Although the structure of molecules formed by this method may not be chemically reasonable, simple energy minimization could render the exact geometry for the molecule.

3. RESULTS AND DISCUSSION

3.1. Fitting of Molecules Inside Zeolites by Molecular Graphics

All the aromatic molecules are minimized after building on the computer screen in order to arrive at their minimum energy configurations. We performed molecular graphics screening with the minimized structures of the molecules. The size and shapes of the molecules are critical parameters that decide the selectivity of the reaction. The molecular size of a guest molecule is usually characterized by a critical diameter, d_c ¹⁶, a Lennard-Jones length constant, s_m ¹⁷, or a minimum kinetic diameter of the molecule, d_m ¹⁸. The minimum kinetic diameter can be calculated from the minimum equilibrium cross sectional diameter and is often used to characterize how difficult it is for a molecule to penetrate through a zeolite channel.¹⁸ The value of the Lennard-Jones length constant can be

determined either from the transport properties (viscosity, thermal conductivity) or from detailed measurements of the deviations from the ideal gas law (second virial coefficients)¹⁹ This method gives a spherical representation of the molecule. When a molecule is within a cage of a zeolite, this Lennard-Jones potential length constant may give some indication of the interaction between the molecule and surrounding oxygen ions. However, molecules should not be viewed as rigid spheres, nor should zeolite channels be viewed as rigid walls. For the case where the molecular diameter is close to but still smaller than the zeolite channel diameter, the molecule might experience a net attraction when passing through the channels. If the molecular diameter is slightly larger than the zeolite channel diameter, the molecule might experience a net repulsive force instead. If the molecular diameter is much larger than the channel diameter, the molecule can no longer enter the zeolite due to the strong repulsive force from the channels.

Neither zeolite channel diameter nor molecular diameter can be described by a precise number. In the electron cloud model of the atom, the probability density distribution theoretically reaches zero only at infinity. The electron density, however, falls off so rapidly at a short distance from the nucleus that some approximation of size can be made. In the case of zeolites, different radii of oxygen, such as 1.3 Å (Flanigen *et al.*¹⁷) 1.35 Å (Olson *et al.*²⁰) and 1.4 Å (Ruthven²¹) were used which could result in different values of the same pore. The calculation of the free diameter of a zeolite channel is also slightly dependent on the choice of diametrically opposing oxygens.¹⁷ The vibration of the crystal lattice and the possible distortions of both molecule and zeolite when the molecule penetrates through the lattice make it even more difficult to assess the precise diameter of either molecule or zeolite pore. It is an oversimplification to characterize a nonspherical molecule by either a minimum diameter or a Lennard-Jones potential length constant. Furthermore, the molecular sizes defined by above methods pose problems such as, either they are too difficult to estimate or the estimated values are not reliable. For example, the critical molecular diameters of 6.8 Å for *p*-xylene and 7.4 Å for *o*- & *m*- xylene¹⁸ do not explain how zeolite ZSM-5 with a diameter of 5.1 Å to 5.4 Å in an efficient molecular sieve for their separation. Similarly, 1,3,5-triethylbenzene, with critical diameter of 9.2 Å diffuses in zeolites with 12-m ring with diameter of 7.4 Å.¹⁸ Thus, critical diameter is not a true measure of the size of the molecule. Hence, we use more realistic values to describe

the size and shape of the molecules as described in the previous section. Conformational analysis is performed to make sure that the global minima is achieved by allowing cooperative motion of the alkyl groups and by determining the strain energy values for different conformers of the molecules.

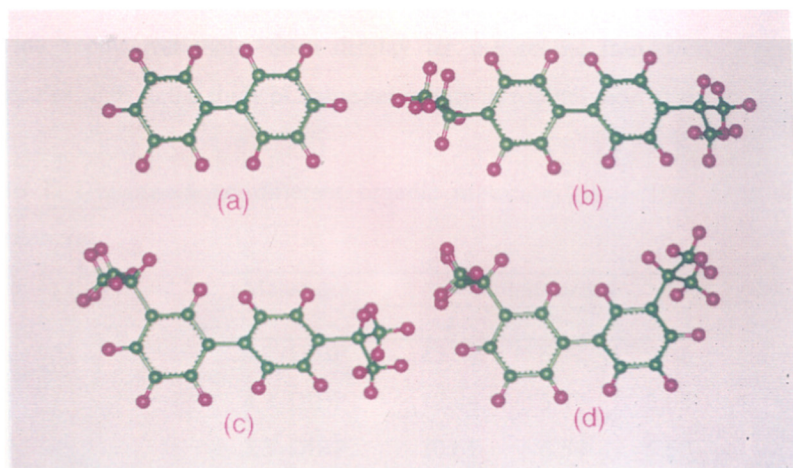


Figure 2. Molecular graphics pictures (ball and stick model) of biphenyl and isomers of diisopropylbiphenyl molecules; (a) BP, (b) 4,4'-DIBP, (c) 4,3'-DIBP and (d) 3,3'-DIBP.

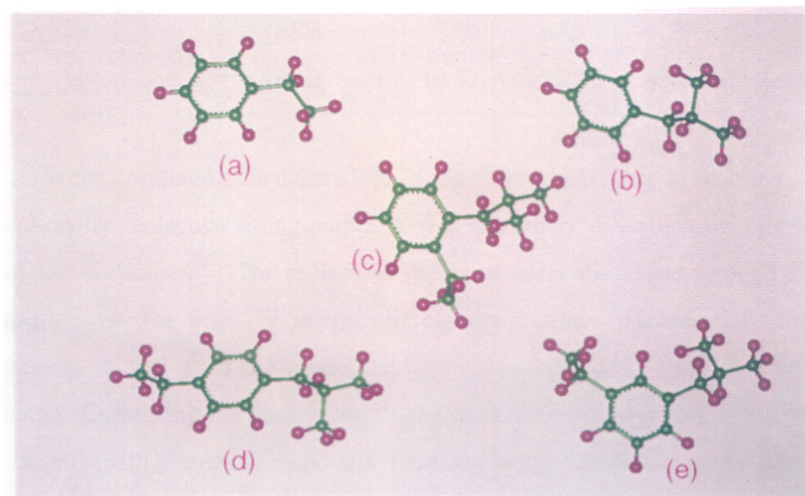


Figure 3. Molecular graphics pictures (ball and stick model) of ethylbenzene, isobutylbenzene and isomers of isobutylethylbenzene molecules; (a) EB, (b) IBB, (c) *o*-IBEB, (d) *p*-IBEB and (e) *m*-IBEB.

Figure 2 shows biphenyl and the isomers of DIBP at their minimum energy configuration. The minimum energy configuration of ethylbenzene (EB), isobutylbenzene (IBB) and the isomers of IBEB are shown in Figure 3. For the energetically favorable conformation, the three largest dimensions ($a \times b \times c$) of the molecules are given in Table 1. Graphical representations of the atoms as spheres with their actual van der Waals radii provide a powerful tool. Such display for the zeolite framework atoms and sorbate molecules leads to the study of shape selectivity in zeolite-guest systems.

Table 1. Dimensions of different organic molecules as derived from the force-field calculations.

Molecules	Dimensions/Å		
	a	b	c
4,4'-DIBP	13.85	6.77	4.36
4,3'-DIBP	12.44	5.87	5.05
3,3'-DIBP	10.61	6.54	5.50
EB	6.32	4.97	2.74
IBB	7.93	5.07	3.88
<i>m</i> -IBEB	8.45	5.95	5.55
<i>o</i> -IBEB	7.50	6.85	5.55
<i>p</i> -IBEB	10.47	5.22	4.46

When correlating the dimensions of the molecules (Table 1) with the pore diameter of zeolites for molecular fitting purposes, it is customary to neglect the largest dimension (a) of the molecules.²² The molecules prefer to enter the cages through their smallest dimensions on the basis of interaction energy criteria. Hence, only the other two dimensions (b and c) of the molecules have to be compared with the size of the pore openings. Comparing the dimensions (b and c) of the molecules in Table 1, it is observed that 'small' (with 8-member rings) and 'medium' (with 10-member rings) pore zeolites are too small to accommodate isomers of DIBP and IBEB, while 'large' pore zeolites are suitable for the diffusion of these molecules.

Figure 4 shows the pore architectures of FAU, LTL, MOR, MTW, mazzite (MAZ), offretite (OFF) and cancrinite (CAN) relevant to molecular shape selective catalysis. The zeolite FAU has framework structures consisting of linked β or sodalite cages. A sodalite

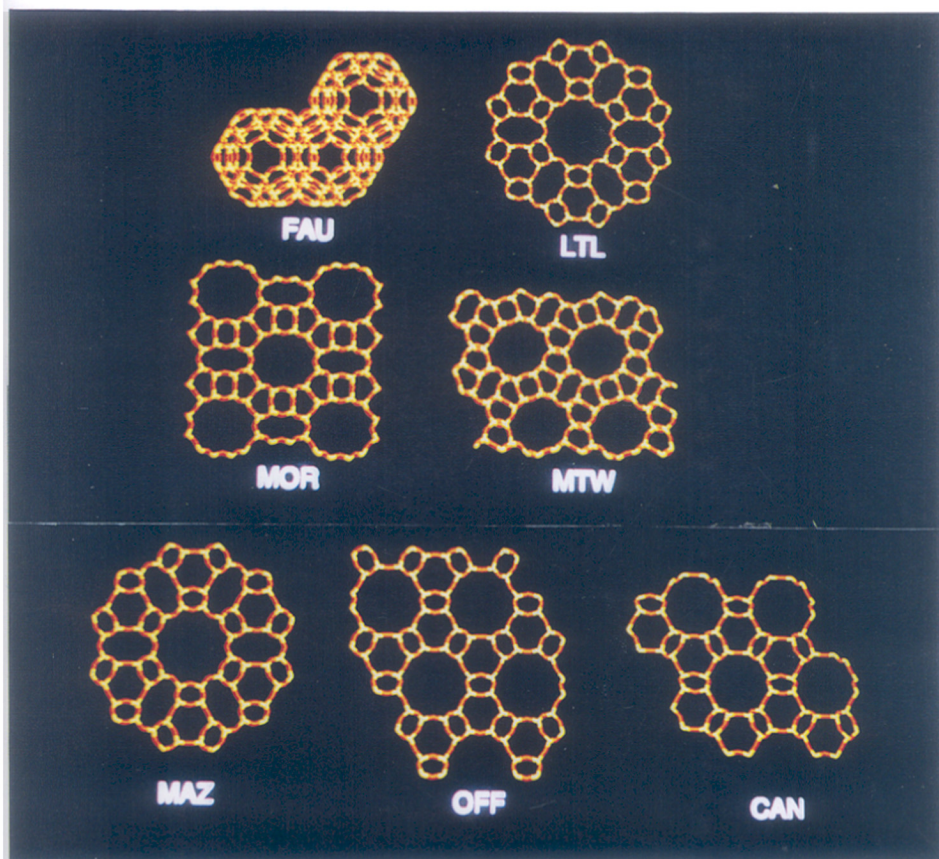


Figure 4. Molecular graphics pictures (stick model) of different large pore zeolites viewed through the channel direction (please see text for the code).

cage structure is made up of 24 tetrahedra arranged as six four-ring faces and eight six-ring faces in a cage-like fashion. Linking sodalite cages by double six-rings through four of the eight six-ring faces in tetrahedral arrays results in the framework structures of FAU. FAU, apart from having β cages also have hexagonal prisms formed by double six-rings and the supercages with a twelve member ring entrance window. Zeolite L (LTL) also has a twelve member channel which extends along the c-axis. Its framework is made up of

polyhedron cages called cancrinite cages. In the LTL topology, cancrinite cages are joined to three neighbouring ones via oxygen bridges to form 8-ring and circular 12-ring channels in the stacking direction. The diameter of the larger channel increases between the 12-ring windows, giving the channel an undulating character. Although 8-rings are present both parallel and perpendicular to the 12-ring channels, they are so much distorted that for all practical purposes only one-dimensional 12-ring channel system is available for molecular motion. In MOR topology, units of four 5-rings are joined to one another via common edges to form chains. Mirror images of these chains are connected to form corrugated sheets. Finally, sheets displaced by half a translation are connected to one another via oxygen bridges to form elliptical 12-ring channels and 8-ring along the corrugations. The 8-ring openings of adjacent 12-ring channels are displaced with respect to one another, so the 8-ring channel is tortuous. Consequently, the channel system is essentially one-dimensional. The MTW structure contains partial features of the ferrierite and the mordenite framework. It also contains both four-member rings and five-member rings within its structure. The largest opening in this structure is a 12-m ring, which is highly nonplanar. The pore walls of MAZ framework are constructed from 4-rings and 6-rings. In the MAZ topology, two types of smaller channels are present: the first consists of stacked gmelinite cages surrounded by six-member rings; the second is between two cross-linked rows of cages and is surrounded by eight-member rings. In the OFF structure, 4-rings, 6-rings and 8-rings are present in the pore walls. The 8-rings in b-direction have free

Table 2. Chemical composition and pore diameter of selected large pore zeolites.

Zeolite	Unit cell composition	Pore diameter (Å)
FAU	$\text{Na}_{58} [(\text{AlO}_2)_{58} (\text{SiO}_2)_{134}] \cdot 240 \text{ H}_2\text{O}$	7.4
LTL	$\text{K}_9 [(\text{AlO}_2)_9 (\text{SiO}_2)_{27}] \cdot 21 \text{ H}_2\text{O}$	7.1
MAZ	$\text{Na}_{10} [(\text{AlO}_2)_{10} (\text{SiO}_2)_{26}] \cdot 28 \text{ H}_2\text{O}$	7.4
MOR	$\text{Na}_8 [(\text{AlO}_2)_8 (\text{SiO}_2)_{40}] \cdot 24 \text{ H}_2\text{O}$	6.5×7.0
OFF	$(\text{Ca}, \text{Mg})_{1.5}\text{K} [(\text{AlO}_2)_4 (\text{SiO}_2)_{14}] \cdot 14 \text{ H}_2\text{O}$	6.7
MTW	$\text{Na}_n [(\text{AlO}_2)_n (\text{SiO}_2)_{28-n}] \cdot \sim 4 \text{ H}_2\text{O}$	5.7×6.2
CAN	$\text{Na}_6 [(\text{AlO}_2)_6 (\text{SiO}_2)_6] \cdot \text{CaCO}_3 \cdot 2 \text{ H}_2\text{O}$	5.9

diameters of $5.2 \text{ \AA} \times 3.8 \text{ \AA}$ and form narrow gates to the 12-member channel in the *c*-direction. The main feature of CAN is the single 12-ring channel parallel to the *c*-axis. The typical structural composition of the zeolites mentioned above and their pore diameters are given in Table 2.

Figure 5 shows CPK views of 4,4'-, 4,3'- and 3,3'-DIBP in LTL. It appears to have plenty of empty space for each of the molecules inside the pore of LTL. Hence LTL would not be expected to produce 4,4'-DIBP selectively. Figure 6 shows CPK views of the isomers of DIBP in MOR. In contrast to LTL, there is very less empty space for each of the molecules in mordenite pore. Moreover, the 3,3'-DIBP fits slightly well in the cross section of mordenite channel. This indicates that mordenite would be better shape selective catalyst than zeolite L. The CPK views of the three isomers of DIBP in MTW are shown in Figure 7. The 4,4'-DIBP has a compact cross section by virtue of the fact that the three bulky components (the two isopropyl groups and the biphenyl ring) are arranged linearly. In contrast, these components are not arranged linearly in the 4,3' and 3,3' isomers. With one isopropyl group placed on the side of biphenyl ring in 4,3' isomer and both isopropyl groups on the same side of biphenyl ring in 3,3' isomer, these two isomers are less well packed in the channel of MTW. For all the three isomers there are some overlap of the atoms of DIBP molecules with zeolite framework. However, in the case of 4,4' isomer there is a significant amount of space between the molecule and the atoms of the zeolite framework. The 4,4' isomer can therefore easily move through the channel. In the cases of 4,3' and 3,3' isomers, there are significant overlap between the molecules and pore wall because of the isopropyl groups placed on the lateral side of biphenyl ring. Hence, the diffusion of these isomers will be significantly impeded by steric interactions with the atoms forming the channel of MTW.

Molecular graphics method is extended to study the fitting of alkylbenzenes such as ethylbenzene, isobutylbenzene and isomers of isobutylethylbenzene. Figures 8-14 show the molecular graphics fitting of the three isomers of IBEB in various large pore zeolites. It is apparent from the figures that all the three isomers can easily diffuse through the pores of FAU, LTL and MAZ. In these cases the fit for *o*- & *m*-IBEB does not appear to be noticeably worse than that for the *p*-isomer. The pore sizes of OFF, MTW and CAN are slightly smaller. The fits for all the three isomers are not good since there are overlaps of

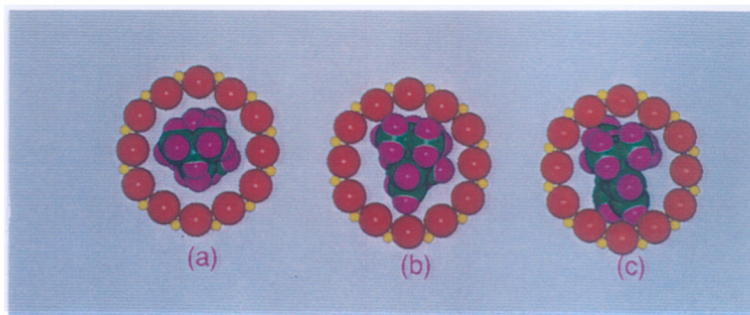


Figure 5. CPK models of (a) 4,4'-DIBP, (b) 4,3'-DIBP and (c) 3,3'-DIBP in zeolite L. Carbon atoms are green, hydrogen atoms are pink, silicons are yellow and oxygens are red.

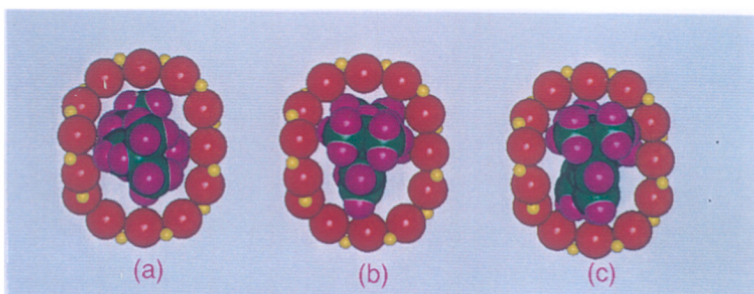


Figure 6. CPK models of (a) 4,4'-DIBP, (b) 4,3'-DIBP and (c) 3,3'-DIBP in mordenite. Carbon atoms are green, hydrogen atoms are pink, silicons are yellow and oxygens are red.

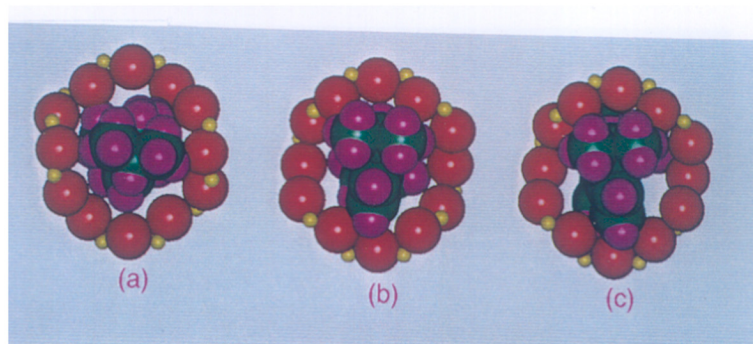


Figure 7. Space filling models of (a) 4,4'-DIBP, (b) 4,3'-DIBP and (c) 3,3'-DIBP in ZSM-12. Carbon atoms are green, hydrogens are pink, silicons are yellow and oxygens are red.

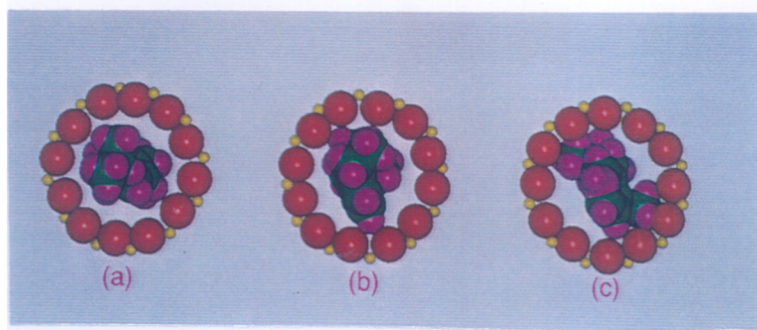


Figure 8. CPK models of (a) *p*-IBEB, (b) *m*-IBEB and (c) *o*-IBEB in faujasite. Carbon atoms are green, hydrogens are pink, silicons are yellow and oxygens are red.

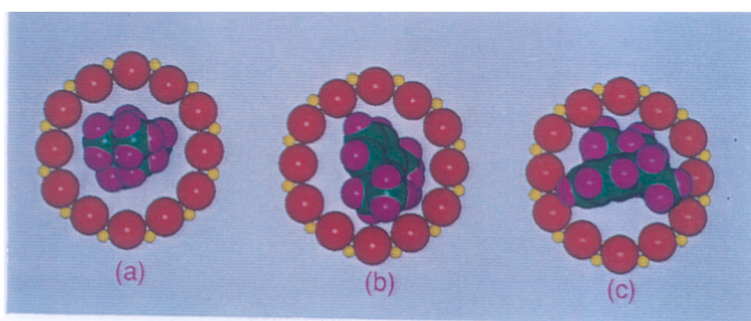


Figure 9. CPK models of (a) *p*-IBEB, (b) *m*-IBEB and (c) *o*-IBEB in zeolite L. Carbon atoms are green, hydrogens are pink, silicons are yellow and oxygens are red.

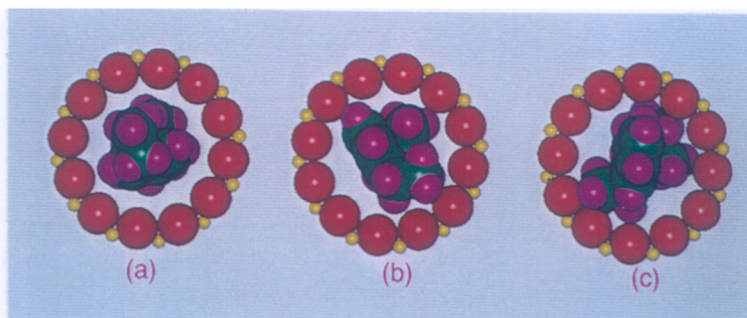


Figure 10. CPK models of (a) *p*-IBEB, (b) *m*-IBEB and (c) *o*-IBEB in mazzite. Carbon atoms are green, hydrogens are pink, silicons are yellow and oxygens are red.

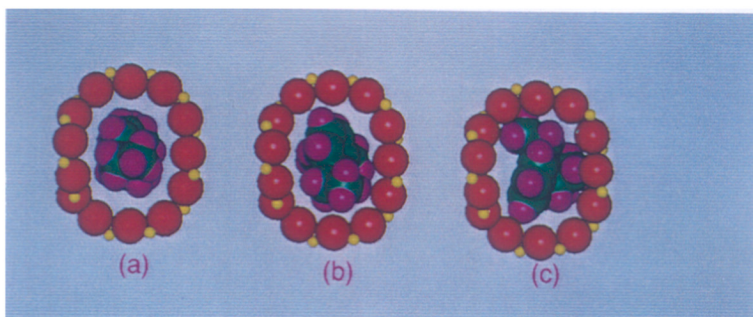


Figure 11. CPK models of (a) *p*-IBEB, (b) *m*-IBEB and (c) *o*-IBEB in mordenite. Carbon atoms are green, hydrogens are pink, silicons are yellow and oxygens are red.

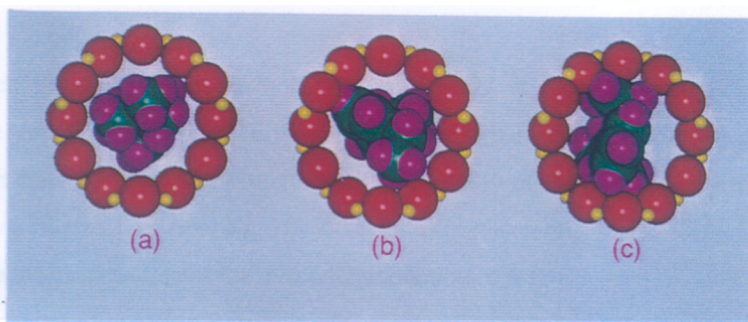


Figure 12. CPK models of (a) *p*-IBEB, (b) *m*-IBEB and (c) *o*-IBEB in offretite. Carbon atoms are green, hydrogens are pink, silicons are yellow and oxygens are red.

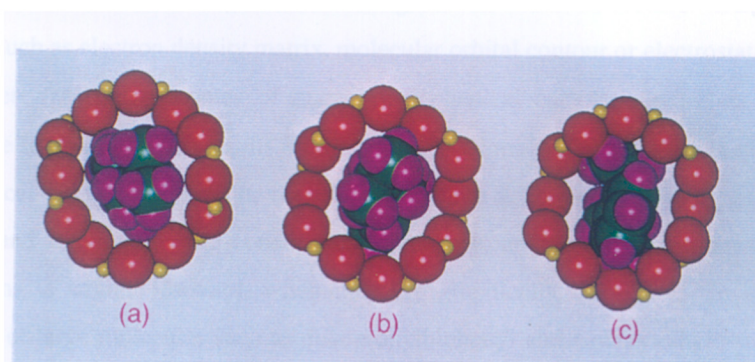


Figure 13. CPK models of (a) *p*-IBEB, (b) *m*-IBEB and (c) *o*-IBEB in ZSM-12. Carbon atoms are green, hydrogens are pink, silicons are yellow and oxygens are red.

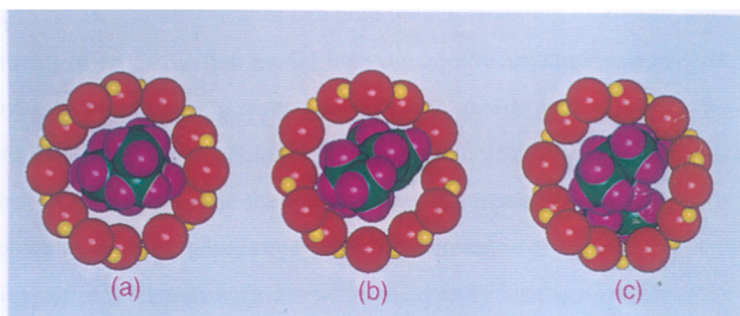


Figure 14. CPK models of (a) *p*-IBEB, (b) *m*-IBEB and (c) *o*-IBEB in cancrinite. Carbon atoms are green, hydrogens are pink, silicons are yellow and oxygens are red.

the van der Waals surfaces of the molecules and zeolites at several points. This suggests that there could be significant difference in energy barriers for diffusion of the three isomers in these zeolites. The visual inspection of the fit of the isomers of IBEB inside the pores of various zeolites from Figures 8-14, indicate that zeolites with elliptical pores (ca. MOR) are the best candidates for selective production of *p*-IBEB.

3.2. Analysis of Simulation Results by Molecular Graphics

Today, with the advent of modern computers and sophisticated software packages, it is possible to carry out accurate calculations. The results of classical mechanics calculations have numerous orientations/configurations of the molecules. Large array of numbers such as electron density matrix, molecular orbital contour or electrostatic potential contour, etc. are the outcomes of quantum mechanical calculations. It is practically impossible to analyze these results without the use of molecular graphics method. First, the graphical display of the results saves plenty of time to be invested in going through the numbers and arriving at valid conclusions. Secondly, understanding the outcome of the calculations is straight forward, when they are graphically displayed. In case of the dynamics of large molecules such as diisopropylbiphenyl and isobutylethylbenzene inside the complex microporous structures of zeolite, it is impossible to understand the nature of interactions without the help of molecular graphics. Thus molecular graphics is widely used throughout this thesis.

4. CONCLUSIONS

Molecular graphics studies can help in understanding of zeolite structure and in the development of an interaction model between zeolite structure and sorbate molecules. It can provide a preliminary screening of possible zeolite catalysts for a specific reaction before further detailed calculations. The use of molecular graphics technique combined with other calculations lead to the study of science of catalysis and to design new industrial catalysts with improved selectivity. With the increase in computer power and the growing availability of user friendly software will undoubtedly lead to a fruitful interaction between molecular graphics and catalysis research.

In this work, we have used molecular graphics to understand the intriguing pore architecture in several large pore zeolites. Molecular graphics has been applied to study the structural fitting of the aromatic molecules inside these zeolites to understand their shape selective properties as described in this chapter. Further molecular graphics is used to analyze the different configuration and orientations of molecules inside the zeolites during the course of diffusion. The diffusion is simulated using energy minimization as well as molecular dynamics calculations as described in Chapters 4 and 5, respectively.

REFERENCES

1. T.A. Jones, *J. Appl. Cryst.*, 11 (1978) 268.
2. J.G. Vinter, *Chem. Br.*, 21 (1985) 1.
3. S. Ramdas, J.M. Thomas, P.W. Betteridge, A.K. Cheetham and E.K. Davies, *Angew. Chem. Int. Ed. Engl.*, 23 (1984) 671.
4. S. Ramdas and J.M. Thomas, *Chem. Br.*, 21 (1985) 16.
5. C. Freeman and R. Catlow, *Chem. Ind (London)*, (1990) 796.
6. *Inorganic Crystal Structure Database*, produced by Prof. Bergerhoff and coworkers of Anorganische-Chemisches, Institut der Univeritat Bonn.
7. P.B. Venuto, *Microporous Mater.*, 2 (1994) 297.
8. H.W. Hill and J.T. Edmonds Jr., *US Patent*, 3 396 110 (1968).
9. S. Jinbo, M. Ito, K. Otomo and H. Hiraide, *Japanese Patent*, 61 231 030 (1986).
10. P.B. Venuto, *Stud. Surf. Sci. Catal.*, 105B (1997) 811.
11. C.B. Dartt and M.E. Davis, *Catal. Today*, 19 (1994) 151.

12. I. Shimizu, Y. Matsumura, Y. Tokumoto and K. Uchida, *European Patent*, 373 362, (1990).
13. Y. Tokumoto, I. Shimizu and S. Inoue, *European Patent*, 414 207, (1991).
14. C.M. Freeman, S.M. Levine, J.M. Newsam, J. Sauer, S.M. Tomlinson, J. Brickmann and R.G. Bell, in *Modelling of Structure and Reactivity in Zeolites*, C.R.A. Catlow (ed.), Academic Press, London, 1992.
15. C. Levinthal, *Sci. Am.*, 214 (1966) 42.
16. D.M. Ruthven, *Am. Chem. Soc. Symp. Ser.*, 40 (1977) 320.
17. E.M. Flanigen, J.M. Bennett, R.W. Grose, J.P. Cohen, R.L. Patton, R.M. Kirchner and J.V. Smith, *Nature*, 271 (1978) 512.
18. D.W. Breck, *Zeolite Molecular Sieves*, Wiley, New York, 1974.
19. R. Reid, J.M. Prausnitz and T.K. Sherwood, in *The Properties of Gases and Liquids*, McGraw-Hill, New York, 1977, p. 555.
20. D.H. Olson, G.T. Kokotailo, S.L. Lawton and W.M. Meier, *J. Phys. Chem.*, 85 (1981) 2238.
21. D.M. Ruthven, *Principles of Adsorption and Adsorption Process*, Wiley, New York, 1984.
22. A. Chatterjee and R. Vetrivel, *J. Chem. Soc., Faraday Trans.*, 91 (1995) 4313.

CHAPTER 3

LOCATION AND ENERGETICS OF ALKYLAROMATICS IN LARGE PORE ZEOLITES FROM HYBRID METHOD

ABSTRACT

We have investigated the minimum energy locations for isomers of DIBP and IBEB in large pore zeolites, using a hybrid method that combines molecular dynamics and Monte Carlo techniques with energy minimization. The minimum energy locations and the corresponding interaction energy values, reflect essentially the steric interaction between the guest molecule and the host zeolite framework. The location of the typical minimum energy configurations of these molecules inside the zeolites are analyzed by molecular graphics. Accordingly, these results provide clues for defining the diffusion path in energy minimization calculations. We propose, on the basis of this investigation, that ZSM-12 is a suitable host for the selective production of 4,4'-DIBP and mordenite is a suitable host for the selective production of *p*-IBEB.

1. INTRODUCTION

Regiospecific isopropylation of biphenyl to 4,4'-diisopropylbiphenyl (DIBP) among the other products is drawing attention as one of the key steps in developing advanced materials such as liquid crystals and liquid crystal polymers.¹⁻⁵ Acid zeolites have been shown to be efficient shape selective catalysts for this reaction and numerous experimental studies⁶⁻¹² are carried out with an aim of pointing out the best catalyst and the reasons for their efficiency. Among the various zeolites, it was found that mordenite (MOR) and ZSM-12 (MTW) show better efficiency in terms of alkylation activity and selectivity towards 4,4'-DIBP.^{11,12} Another interesting reaction is the alkylation of isobutylbenzene (IBB) to *p*-, *m*- and *o*-isobutylethylbenzene (IBEB). *p*-IBEB can be dehydrogenated in another process to form *p*-isobutylstyrene which is the key intermediate in the synthesis of the popular analgesic drug ibuprofen.¹³ Again acid zeolites are known to produce better selectivity in the formation of *p*-IBEB, for example, HY zeolite shows a better selectivity (46.3%) than the conventional catalysts (17.6%).¹³ Thus, there is an interest to study the location, binding energy and diffusion of the various isomers in the channels of zeolites, in order to find clues regarding how the selectivity towards 4,4'-DIBP and *p*-IBEB could be improved.

In this chapter, we present the results of a 'hybrid method' to locate the adsorption sites for three isomers of DIBP in three zeolites having different types of pore architecture. We chose three zeolites for the isomers of DIBP in which the alkylation reaction has been studied experimentally: zeolite L (LTL), MOR and MTW. The influence of the shape and size of the channels as well as the type of channel connections on the adsorption of the guest molecules are determined. We also present our results on the adsorption of isomers of IBEB in two large pore zeolites. We have chosen faujasite (FAU) and MOR considering their novel pore architectures. All these zeolite structures present different isotopic frameworks¹⁴ and many different Si/Al ratios are possible. As we are interested mainly in the influence of the size, shape and connectivity of the channels of zeolites on adsorption of aromatics, regardless of their chemical composition, we chose the fully siliceous form of each zeolite as the model system.

We have adopted the 'hybrid method' which combines molecular dynamics, Monte Carlo and energy minimization reported by Freeman *et al.*¹⁵ The energy minimization is

indeed, a computationally efficient procedure for locating the favourable adsorption sites for molecules inside the zeolites. However, the fundamental difficulty with energy minimization procedure is that it is necessary to specify a starting configuration to which minimization is applied. The “starting point” is generally chosen using intuition although various starting configurations could be considered. The procedure becomes increasingly tedious inspite of which it is not certain that all the favourable adsorption sites inside zeolites have been located. In order to overcome these difficulties Freeman *et al.*¹⁵ developed the ‘hybrid method’ where both the conformations of the sorbed molecule and the zeolite volume are sampled in an efficient manner, with favoured configurations then being subjected to energy minimization.

After a short description of the procedure used for the molecular modeling method in Section 2, we present in Section 3 the minimum energy positions, corresponding energy values as well as a relevant discussion on how these quantities are useful to relate shape and size of the guest molecules with the adsorption sites in the host zeolite lattice.

2. METHODOLOGY

As mentioned earlier, the ‘hybrid method’ involves a combined molecular dynamics, Monte Carlo and energy minimization technique to probe the interactions between guest molecule and zeolite framework. The method was originally developed and applied to locate low energy sorption sites of butene isomers in a purely siliceous silicalite-1 type structure.¹⁵ This technique has been successfully applied to study sorbate-zeolite interactions in several cases.¹⁶⁻²⁰ Lewis *et al.*^{21,22} have studied the locations of organic templates inside various zeolites and predicted their templating ability for the synthesis of microporous materials using this technique.

The method starts with a high temperature molecular dynamics (MD) run to generate a library of conformations of the sorbate molecule. We have generated 100 initial configurations from a high temperature (1000 K) MD run. These conformations are then inserted, using a Monte Carlo method into random locations in the zeolite framework. Suitable candidate structures are accepted according to supplied geometric and energetic constraints. Subsequently, the 100 accepted structures are minimized using force field techniques, holding the zeolite framework rigid. For these 100 representative adsorption

sites, the interaction energy between the zeolite host and the molecule are calculated. We calculate interaction energy (E_{inter}) which includes effect of conformational change when the sorbate molecule is placed within the framework:

$$E_{inter} = E_{host-guest} - E_{guest}$$

where $E_{host-guest}$ is the total energy of the framework-sorbate combination and E_{guest} is the minimum energy of an isolated gas-phase molecule. The interaction energy is the energy of the host-guest system minus the energy of each component evaluated separately. Since the host zeolite is held rigid the energy of the host is not considered here. The above procedures allow us to determine the minimum energy adsorption sites for a particular 'zeolite-molecule' combination. The energies obtained are a measure of the "match" between the sorbate geometry and the topology of the host framework. The mean interaction energy value is also calculated for the 100 minimized configurations.

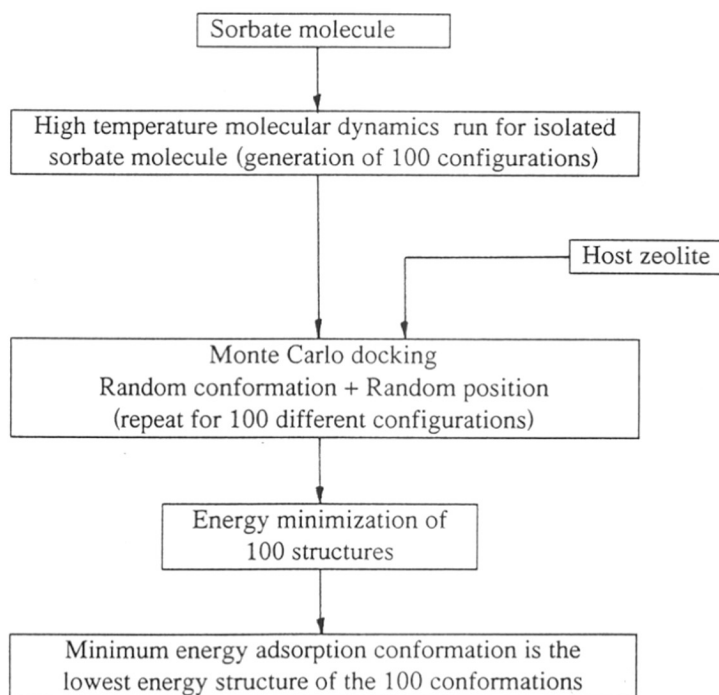


Figure 1. A flow diagram representing the hybrid method.

The methodology is conveniently represented by means of a flow diagram as shown in Figure 1. This methodology is available as an automated procedure in the “solid docker” module of the “Catalysis and Sorption” software package.²³ Consistent valence force field (CVFF)²⁴ has been widely used and found to give results in good agreement with experimental heats of adsorption.^{21,22,25} Hence, all the calculations are carried out using the CVFF and the computations are made in a SiliconGraphics Indigo2 workstation using the program DISCOVER²⁶

3. RESULTS AND DISCUSSION

3.1. Minimum Energy Location for the Isomers of DIBP

The minimum energy values among the calculated interaction energies for the isomers of DIBP in LTL, MOR and MTW are given in Table 1. The mean energy values over the 100 minimized configuration are also shown in Table 1. It is seen from the table that 3,3'-DIBP is less strongly adsorbed in LTL. In all cases 3,3'-DIBP has unfavourable mean energy which can be explained by its low affinity to the pore wall. The positive value of mean energy of 3,3'-DIBP in MTW indicates that it has repulsive interaction with the wall of MTW. This indicates that it will be difficult for this isomer to enter and diffuse through the 12-m channel of MTW. In all the three zeolites 4,4'-DIBP has favourable interaction energy; this can be explained by its least conformational flexibility, which increases its affinity to the pore wall. Mean energy values given in Table 1 do not follow the trend of minimum energy values. The diffusion behaviour will depend on the energetics of all possible configurations inside the zeolite channel. Hence to understand the

Table 1. Minimum interaction energies and mean energies (kJ/mol) of isomers of DIBP in the silica form of zeolites LTL, MOR and MTW

Zeolite code	Minimum energy			Mean energy		
	4,4'-DIBP	4,3'-DIBP	3,3'-DIBP	4,4'-DIBP	4,3'-DIBP	3,3'-DIBP
LTL	-132.60	-121.51	-51.08	-95.25	-95.98	-8.43
MOR	-208.52	-191.90	-192.26	-195.61	-146.40	-139.06
MTW	-248.31	-200.75	-208.18	-214.37	-148.28	34.20

diffusion behaviour of the molecules, we calculated the ratio of mean energy to minimum energy and they are presented in Table 2. This ratio will vary in the range of 1 to 0 depending on the difference between the minimum and mean values. This ratio is a measure of diffusivity and the larger values will correspond to better diffusivity. In general, it is observed that the diffusivity of 4,4'-DIBP is high. In case of LTL alone, the diffusivity of 4,3'-DIBP is slightly higher than 4,4'-DIBP. In MOR, the diffusivity of all isomers are found to lie in a very short range (ca. between 0.92 and 0.72). But there is large difference in the diffusivity as predicted by these ratios for the three isomers in MTW. From these results it can be concluded that there will be significant difference in the diffusion energy barriers for the isomer of DIBP in MTW.

Table 2. Ratio of mean energy/minimum energy values for the isomers of DIBP in LTL, MOR and MTW.

Zeolite code	Mean energy /minimum energy		
	4,4'-DIBP	4,3'-DIBP	3,3'-DIBP
LTL	0.72	0.79	0.17
MOR	0.92	0.76	0.72
MTW	0.86	0.73	0.14

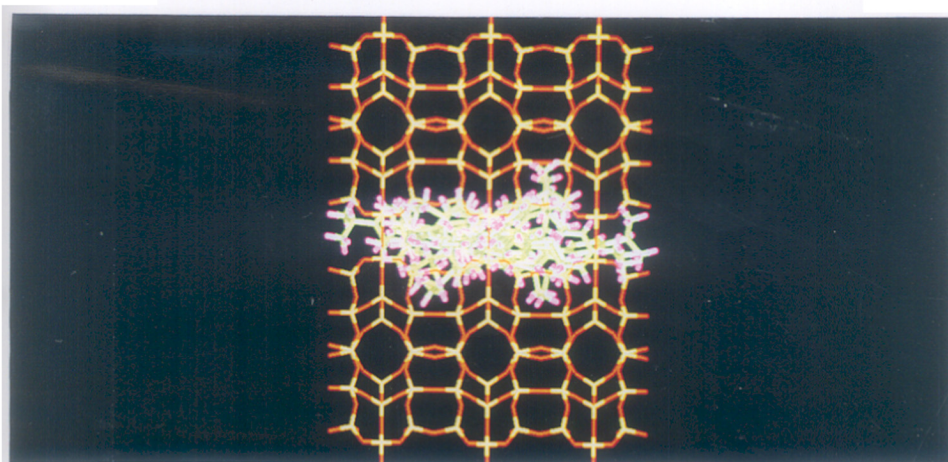


Figure 2. The distribution of 10 configurations of 4,4'-DIBP in LTL generated by the Monte Carlo docking technique and energy minimization. The view is across the cross-section of the 12-m channel.

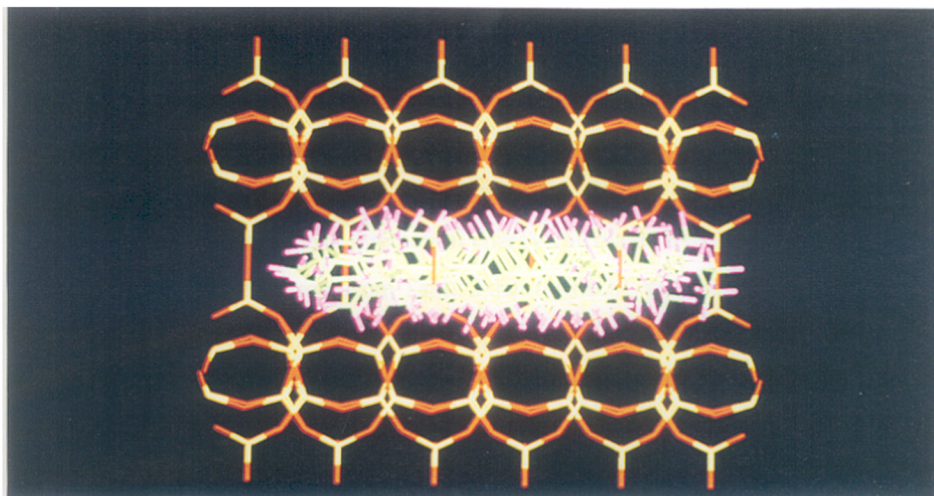


Figure 3. The distribution of 10 configurations of 4,4'-DIBP in MOR generated by the Monte Carlo docking technique and energy minimization. The view is across the cross-section of the 12-m channel.

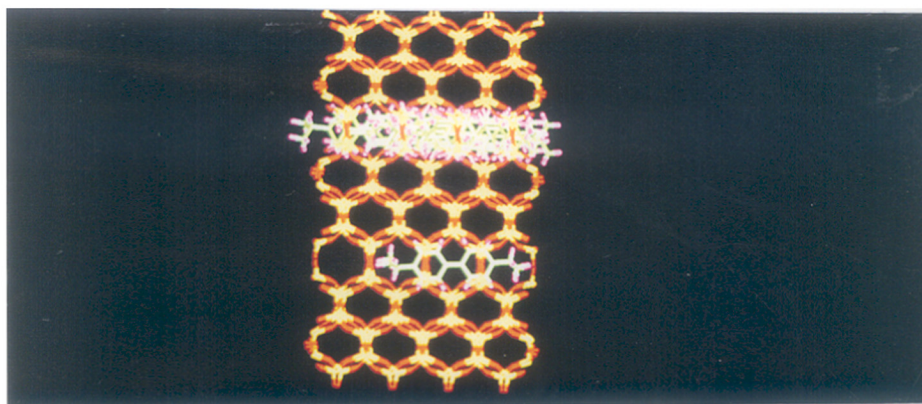


Figure 4. The distribution of 10 configurations of 4,4'-DIBP in MTW generated by the Monte Carlo docking technique and energy minimization. The view is across the cross-section of the 12-m channel.

The minimum energy positions correspond to molecules sorbed only in the 12-m channel. This is exemplified by Figures 2-4, which show 10 minimum energy configurations for 4,4'-DIBP in LTL, MOR and MTW, respectively.

3.2. Minimum Energy Locations for the Isomers of IBEB

The interaction energies for the isomers of IBEB in FAU and MOR for the deepest minima as well as the mean interaction energy calculated over the 100 configurations are given in Table 3. It is seen from Table 3 that for MOR the minimum interaction energy

Table 3. Minimum interaction energies and mean energies (kJ/mol) of IBEB isomers in the silica form of zeolites MOR and FAU

Zeolite code	Minimum energy			Mean energy		
	<i>p</i> -IBEB	<i>m</i> -IBEB	<i>o</i> -IBEB	<i>p</i> -IBEB	<i>m</i> -IBEB	<i>o</i> -IBEB
MOR	-95.10	-86.04	-95.10	-62.96	-47.29	-48.49
FAU	-45.74	-44.89	-62.63	-20.66	-12.62	-39.68

values for both *p*-IBEB and *o*-IBEB are almost same whereas *m*-IBEB has slightly unfavourable interaction energy. But the mean interaction energy values are in the order: *p*-IBEB < *o*-IBEB < *m*-IBEB. In the case of FAU, both minimum and mean energy values are in the order: *o*-IBEB < *p*-IBEB \cong *m*-IBEB. The calculated ratio of mean to minimum energy values are given in Table 4. It is observed that the diffusivity in FAU do not correspond to the size and shape of the molecules. This may be due to large supercages in FAU which do not have size preference for the isomers of IBEB. But the ratios (Table 4) of mean energy to minimum energy values are in the order: *p*-IBEB > *m*-IBEB > *o*-IBEB for mordenite. However, sampling of 100 configurations can not be used to make final conclusion on the diffusivity. They are useful to understand the location of adsorption sites.

Table 4. Ratio of mean energy/minimum energy values for the isomers of DIBP in FAU and MOR.

Zeolite code	Mean energy /minimum energy		
	<i>p</i> -IBEB	<i>m</i> -IBEB	<i>o</i> -IBEB
MOR	0.66	0.55	0.51
FAU	0.45	0.28	0.63

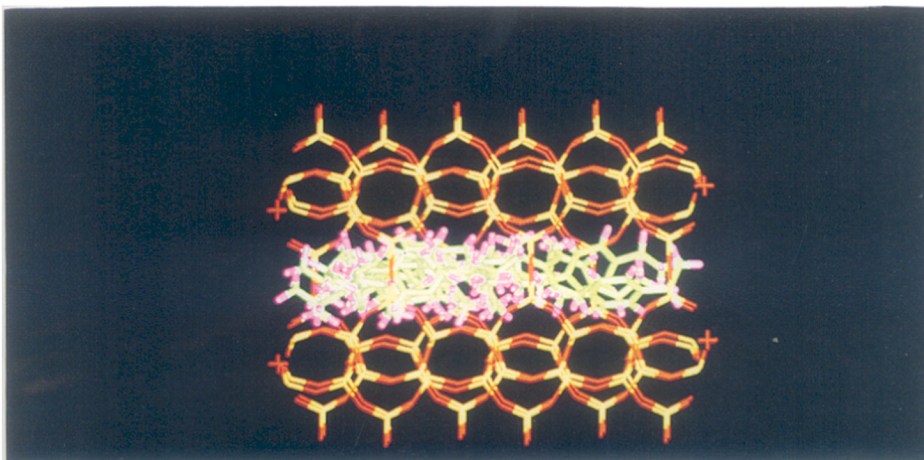


Figure 5. The distribution of 10 configurations of *p*-IBEB in MOR generated by the Monte Carlo docking technique and energy minimization. The view is across the cross-section of the 12-m channel.

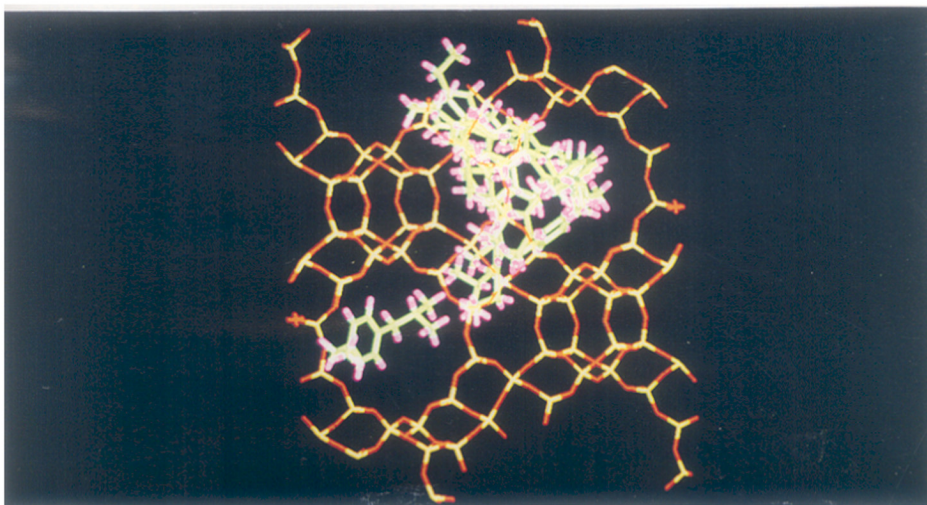


Figure 6. The distribution of 10 configurations of *p*-IBEB in FAU generated by the Monte Carlo docking technique and energy minimization.

The distribution of 10 minimum energy configurations of *p*-IBEB in mordenite and faujasite are shown in Figures 5 and 6, respectively. These results clearly indicate the preferred locations for the molecules and they provide guidelines to fix the diffusion path.

4. CONCLUSIONS

We have calculated the minimum interaction energies of DIBP isomers in LTL, MOR and MTW. The minimum energy configurations for the three isomers of DIBP are taken as the starting point for further detailed diffusion calculations. This technique is used to find the minimum energy configurations of EB, IBB and IBEB isomers also in FAU and MOR. The favourable adsorption sites inside zeolites are understood from the minimum energy configuration and the results provide clues to choose the diffusion path to calculate diffusion energy barriers. The mean energy of 100 configurations and ratio of mean/minimum energy values are useful to qualitatively predict the diffusivity of the molecules in these zeolites. The minimum energy configurations for EB, IBB and isomers of IBEB are generated in other large pore zeolites, namely zeolite L, mazzite, offretite, ZSM-12 and cancrinite and these minimum energy configurations are used as the starting point for diffusion calculations which will be discussed in Chapter 4.

REFERENCES

1. D. Fraenkel, M. Cherniavsky, B. Ittah and M. Levy, *J. Catal.*, 110 (1986) 273.
2. T. Matsuzaki, Y. Sugi, T. Hanaoka, K. Takeuchi, H. Arakawa and G. Takeuchi, *Chem. Express*, 4 (1989) 413.
3. H.W. Hill and J.T. Edmonds Jr., *US Patent*, 3,396, 110 (1968).
4. S. Jinbo, M. Ito, K. Otomo and H. Hiraide, *Japanese Patent*, 61, 231, 030 (1986).
5. G.S. Lee, J.J. Maj, S.C. Rocke and J.M. Garces, *Catal. Lett.*, 2 (1989) 243.
6. Y. Sugi, T. Matsuzaki, T. Hanaoka, K. Takeuchi, T. Tokoro and G. Takeuchi, *Stud. Surf. Sci. Catal.*, 60 (1991) 303.
7. X. Tu, M. Matsumoto, T. Matsuzaki, H. Hanaoka, Y. Kubota, J.-H. Kim and Y. Sugi, *Catal. Lett.*, 21 (1993) 71.
8. J. Fellmann, *Catalytica Highlights*, 17 (1991) 1.
9. T. Matsuda, T. Urata, K. Saito and E. Kikuchi, in *Preprint of 37th Symposium on*

- Petrochemistry*, Japan Petroleum Institute, 1991, p. 80.
10. C.B. Dartt and M.E. Davis, *Catal. Today*, 19 (1994) 151.
 11. Y. Sugi and M. Toba, *Catal. Today*, 19 (1994) 187.
 12. A.S. Loktev and P.S. Chekriy, *Stud. Surf. Sci. Catal.*, 84 (1994) 1845.
 13. I. Shimizu, Y. Matsumura, Y. Tokumoto and K. Uchida, *European Patent*, 0, 373, 362 (1990).
 14. W.M. Meier, D.H. Olson and Ch. Baerlocher, *Atlas of Zeolite Structure Types*, Elsevier, New York, 1996.
 15. C.M. Freeman, C.R.A. Catlow, J.M. Thomas and S. Brode, *Chem. Phys. Lett.*, 186 (1991) 137.
 16. F. Jousse, L. Leherter and D.P. Vercauteren, *J. Mol. Catal. A*, 119 (1997) 165.
 17. A.I. Shubin, K. Zamaraev, J.M. Thomas, C.R.A. Catlow, *Proc. R. Soc. Lond. A*, 446 (1994) 411.
 18. A.R. George, C.R.A. Catlow and J.M. Thomas, *Microporous Mater.*, 11 (1997) 97.
 19. C.R.A. Catlow, J.D. Gale, D.H. Gay and D.W. Lewis, in *Access in Nanoporous Materials*, T.J. Pinnavaia and M.F. Thorpe (eds.) Plenum Press, New York, 1995, p. 241.
 20. J. Kindler, E. Geidel, K. Krause, G.E. Mills and H. Foster, *Stud. Surf. Sci. Catal.*, 94 (1995) 764.
 21. D.W. Lewis, C.M. Freeman and C.R.A. Catlow, *J. Phys. Chem.*, 99 (1995) 11194.
 22. D.W. Lewis, C.R.A. Catlow and J.M. Thomas, *Chem. Mater.*, 8 (1996) 1112.
 23. Catalysis, Biosym Technologies Inc: San Diego, 1993.
 24. P. Dauber-Osguthorpe, V.A. Roberts, D.J. Osguthorpe, J. Wolff, M. Genest and A.T. Hagler, *Proteins: Struct., Function Genetics*, 4 (1988) 21.
 25. N. Henson, A.K. Cheetham, A. Redondo, S.M. Levine and J.M. Newsam, *Stud. Surf. Sci. Catal.*, 84 (1994) 2059.
 26. Discover, Biosym Technologies Inc: San Diego, 1993.

CHAPTER 4

ADSORPTION SITES AND DIFFUSION MECHANISM OF ALKYLAROMATICS IN LARGE PORE ZEOLITE CATALYSTS AS PREDICTED BY MOLECULAR MODELING TECHNIQUES

ABSTRACT

In this chapter, we demonstrate the application of force field energy minimization technique to study the adsorption and diffusion behaviour of large molecules inside the micropores of zeolites. The periodic variations of interaction energy between the molecules and zeolite framework in the calculated diffusion energy profiles are used to predict the energy barrier for diffusion. Diffusion energy barriers calculated for the isomers of diisopropylbiphenyl (DIBP) in zeolite L (LTL), mordenite (MOR) and ZSM-12 (MTW) show that the selectivity for the 4,4'-DIBP will be in the order of LTL < MOR < MTW. The detailed analysis of the configurations of the molecules in the most favourable and unfavourable adsorption location, indicate that the 4,4'-DIBP has favourable interaction energies in all the zeolites with different pore architecture. Studies on diffusion of isomers of DIBP in LTL, MOR and MTW indicate that MTW is a good catalyst for selective synthesis of 4,4'-DIBP.

Force field energy minimization calculations are carried out to study the diffusion of alkylbenzenes namely, ethylbenzene (EB), isobutylbenzene (IBB) and isobutylethylbenzene (IBEB) isomers in several large pore zeolites. Among the zeolites with pore diameter $\geq 7.0 \text{ \AA}$, the cage to cage diffusion of the alkylbenzenes in faujasite (FAU) show no significant diffusion energy barrier for any of the molecule. Zeolite L shows a very small selectivity towards *p*-IBEB which is due to a rapid change in minimum energy configuration as the molecules diffuse along the pore. In the case of mazzite (MAZ), a high diffusion energy barrier is observed for *o*-IBEB compared to *m*- and *p*-isomers. Calculations of the diffusion energy profiles for the molecules in mordenite show that there is negligible energy barrier for the diffusion of *p*-IBEB, whereas an energy barrier of 17.95 kJ/mol exists for diffusion of *m*-IBEB and a significantly large energy barrier of 95.69

kJ/mol exists for *o*-IBEB. Thus, the efficiency of shape selective production of *p*-IBEB in these zeolites will be in the order: FAU ~ LTL < MAZ < MOR. Among the zeolites with pore diameter ≤ 7.0 Å, the efficiency of shape selective production of *p*-IBEB is in the order: OFF < MTW < CAN. However, the interaction energy values of IBEB isomers are unfavourable inside these zeolites. Diffusion energy barriers calculated for EB, IBB, *o*-, *m*- and *p*-IBEB in various zeolites indicate that mordenite is a good catalyst for selective synthesis of *p*-IBEB.

1. INTRODUCTION

The structure of zeolite catalysts is characterized by the presence of regularly repeating intracrystalline cavities and pores, whose dimensions lie in the range 3-10 Å which is commensurable with molecular dimensions.¹ A fascinating structure-related aspect of the zeolite catalysis is molecular shape selectivity.²⁻⁴ The subtle interplay of “configurational” diffusion and intrinsic kinetics of reactions in the intracrystalline pore system enable zeolite catalysts to differentiate between molecules or transition states involved in a reaction on the basis of their size and shape and thus direct the reaction along specific paths. The diffusion of molecules in zeolite pores plays the major role in the shape selective process. Understanding the mechanism of diffusion can greatly facilitate the design of zeolite catalysts. The diffusion behaviours of molecules in natural and synthetic zeolites are studied by several analytical⁵⁻¹⁵ and computational¹³⁻¹⁸ techniques. In the applications of zeolite catalysts, a clear picture of the nature and location of adsorbed molecules is of fundamental importance to understand the mechanism of the catalytic processes. The energetics of adsorption as a function of pore diameter has also been investigated experimentally.¹⁹ However, a systematic study of sorption in zeolites has not been performed and the experimental observations reported in the literature are sometimes contradictory.

Computer simulations, using molecular dynamics or Monte Carlo techniques, are attractive alternatives to experiments because these methods can, in principle, provide information for the conditions under which experiments are not feasible. Previous simulations, based on molecular dynamics calculations²⁰⁻²² or Monte Carlo calculations²³⁻²⁸ had tended to concentrate on small guest molecules and until now these techniques are not

used to study large molecules of catalytic relevance due to highly demanding computations.

Force field energy minimization technique is an efficient method for studying the location and conformation of large guest molecules within the micropores of zeolites. In order to screen large number of systems, this method is computationally less demanding and can therefore be used to study large molecules before applying computationally expensive techniques. We demonstrate here that this approach can be manifested to study diffusion behaviour of alkyaromatics in zeolites. We use this technique to study the adsorption and location of 4,4'-DIBP, 4,3'-DIBP and 3,3'-DIBP (structures are shown in Chapter 2) in fully siliceous form of large pore zeolites. The main objective of this work is to find out a suitable zeolite catalyst for selective synthesis of 4,4'-DIBP among other isomers possible. Only 4,4'-DIBP is a valuable compound because of its application in liquid crystal polymers.²⁹ Biphenyl has been alkylated with propene over H-FAU, H-LTL, H-MOR and H-MTW.^{30,31} H-FAU and H-LTL zeolites gave conversions and selectivities similar to an amorphous silica-alumina, whereas mordenite was found to be better selective catalyst for the production of 4,4'-DIBP. Loktev and Chekriy³² showed that ZSM-12 produced even higher selectivity for 4,4'-DIBP than mordenite.

p-IBEB is the key intermediate in the production of α -(4-isobutylphenyl) propionic acid, which is popularly known as ibuprofen.³³ The conventional synthesis route for the production of *p*-IBEB involves the alkylation of isobutylbenzene with ethylene over Lewis-acid catalysts³⁴ in which the selectivity towards *p*-IBEB is typically 17.6%. Recently, the possibility of using zeolite catalysts for the production of *p*-IBEB by disproportionation of isobutylbenzene and a polyalkylbenzene over HY zeolite³⁵ has been shown to lead to better selectivity (46.3%). Although HY zeolite is better than conventional catalyst, selection of this specific zeolite is a random choice rather than a logical selection and no experimental results are available for any other zeolites. Hence, we wanted to analyze the diffusion behaviours of these molecules in different zeolites and compare their shape selectivity. We have chosen large pore zeolites with one dimensional pores, where only single file diffusion is possible, zeolites with two dimensional pores, where different molecular reorientations are possible at channel intersections and zeolites with three dimensional pores where cage to cage translations through channels are possible,

with total dynamic freedom inside the cages. The influence of change in pore architecture on adsorption and diffusion behaviour of the molecules is studied in detail. Here, we describe the application of force field energy minimization calculations to search the most viable zeolite catalyst for the selective synthesis of *p*-IBEB.

2. METHODOLOGY

The minimum energy configurations of all the molecules obtained from the ‘hybrid method’ described in Chapter 3, are taken as the starting point for diffusion calculations. The molecular graphics analysis and the force field energy minimization calculations for diffusion of the alkylaromatics are carried out with the Insight II and Discover software packages³⁶ supplied by Biosym Technologies Inc., USA using CVFF³⁷ (consistent valence force field). All the calculations are carried out in a SiliconGraphics-Indigo2 workstation. The diffusion energy profiles are calculated for the isomers of DIBP in LTL, MOR and MTW. Diffusion behaviours of EB, IBB, *o*-, *m*- and *p*-IBEB are calculated in several large pore zeolites, namely FAU, LTL, MAZ, MOR, OFF, MTW and CAN. The crystal characteristics and the dimensions of the simulation boxes for these zeolites are given in Table 1. The zeolite structures are taken from the crystal structure reported for faujasite,³⁸ zeolite L,³⁹ mazzite,⁴⁰ mordenite,⁴¹ offretite,⁴² ZSM-12⁴³ and cancrinite.⁴⁴

Table 1. Crystal characteristics and the dimensions of the simulation boxes for different zeolites

Zeolite	Symmetry	Unit cell composition	Unit cell dimensions			Pore diameter (Å)	Number of unit cells
			a (Å)	b (Å)	c (Å)		
FAU	cubic	[SiO ₂] ₁₉₂	25.028	25.028	25.028	7.4	2×2×2
LTL	hexagonal	[SiO ₂] ₃₆	18.465	18.465	7.476	7.1	2×2×8
MAZ	hexagonal	[SiO ₂] ₃₆	18.392	18.392	7.646	7.4	2×2×8
MOR	orthorhombic	[SiO ₂] ₄₈	18.094	20.516	7.524	6.5×7.0	1.7×1.5×8
OFF	hexagonal	[SiO ₂] ₁₈	13.300	13.300	7.600	6.7	3×3×8
MTW	monoclinic	[SiO ₂] ₂₈	24.880	5.020	12.150	5.7×6.2	1.5×7×2
CAN	hexagonal	[SiO ₂] ₁₂	13.170	13.170	15.850	5.9	3×3×8

The interaction energy of each of the molecule with the zeolite framework is calculated using the expression that contains the terms corresponding to deformation of bond lengths, bond angles, torsion angles etc.⁴⁵ During the calculation of the interaction energy, the atoms in the zeolite lattice are assumed to be fixed at their crystallographically determined geometries. The sorbate molecule is forced to diffuse stepwise, in steps of 0.2 Å inside the 12-m channel between two points, which define the diffusion path. These two points are located at the mid-points of the pore apertures of the 12-m channel in LTL, MAZ, MOR, OFF, MTW and CAN. In the case of FAU, three points are defined at the centers of three consecutive supercages and force field calculations are performed. After each step, a strong harmonic potential constrains the molecule to lie at a fixed distance from these points, while its orientation and conformation corresponding to minimum energy are chosen. Thus the interaction energy is minimized at each step with respect to the internal degrees of freedom as well as the non-bonding interactions with the zeolite framework. The non-bonding interactions of the molecules with the zeolite framework are calculated by determining the long-range forces by classical electrostatic interactions and short-range interactions in terms of Lennard-Jones potentials.³⁷

3. RESULTS AND DISCUSSION

Shape selectivity in catalytic reactions is governed by several factors such as kinetics of the reaction and relative rates of diffusion of reactants, products or reaction intermediates.⁴⁶ The diffusivity and hence the shape selectivity is found to be dependent on the pore opening, the nature and number of acid sites, morphology as well as the rate of coke formation.⁴⁷⁻⁴⁹

When one considers the interactions between zeolites and sorbed molecules, the location and conformation of guest molecules within the micropores can have a profound effect on the subsequent chemistry of these systems. Molecular level information on the location and conformation of sorbed molecules is not always readily accessible by experimental means and recent advances in theoretical methods have made interaction energy calculations combined with molecular graphics an ideal candidate to address these problems. Similar approach has been recently applied and proven successful to study the diffusion behaviours of simple aromatics in ZSM-5,⁵⁰ selectivity in the formation of

different isomers of alkylnaphthalene,⁵¹ selectivity in the conversion of n-butene to isobutene in relation to several other products⁵² inside zeolites and role of eight member rings of mordenite in methanol amination.⁵³ The diffusion energy profiles for different molecules give a good indication of the relative rates of diffusion through the pore of the zeolite. The diffusion energy profile is the graph showing the variation of interaction energy between the molecules and the zeolite framework as the molecule diffuses through the channel of the zeolite. These profiles are useful to identify the most favourable and unfavourable adsorption sites for the molecules inside the zeolite channels and the intraparticle diffusion is not covered in this procedure. The results of this study are useful to compare the self-diffusion studies of molecules, particularly in relation to local diffusion behaviour of molecules in zeolites for the membrane applications.⁵⁴ The difference between the most favourable site (minimum energy) and the most unfavourable site (maximum energy) in the diffusion energy profile provides qualitative estimate of the diffusion energy barrier.^{55,56} For example, when energy barriers for all the isomers of DIBP and IBEB are comparable in a given zeolite, their diffusion rates should also be approximately the same.

We report here, the diffusion characteristics of the alkylaromatics in 12-m channels of a variety of different siliceous zeolites. First we will present the results for the diffusion of the isomer of DIBP in LTL, MOR and MTW where the selectivity found from experimental results is: $MTW > MOR > LTL$ in the second part we will present the diffusion behaviour of isomers of IBEB in FAU, LTL, MAZ, MOR OFF, MTW and CAN. Our emphasis is on the influence of the pore architecture of different zeolites in the diffusion energy profiles of the aromatics.

3.1. Diffusion of DIBP Isomers in LTL, MOR and MTW

3.1.1. Zeolite L

Zeolite L belongs to the hexagonal crystal class. The pore in zeolite L is circular with a pore diameter of 7.1 Å. It has a structure consisting of channels along the c-direction. The channels are built up of 'barrel-shaped' cages that are interconnected via 12-member pores. The 12-m rings are separated by 7.5 Å along the c-direction. The diameter of the barrel is largest (~12.6 Å) at the midway between the two consecutive 12-m rings. In the regions of the pore, midway between the two 12-m rings, there is sufficient

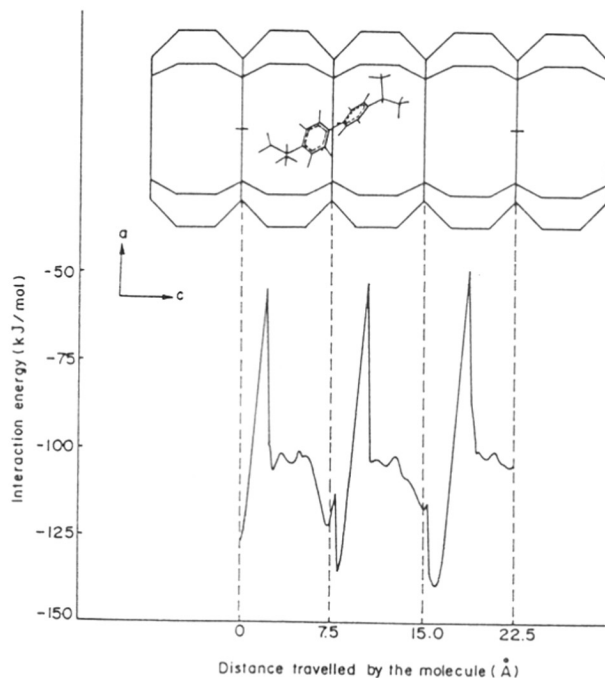


Figure 1. Variation of interaction energy of 4,4'-DIBP with zeolite L lattice during its diffusion along the c-axis. The molecular graphics picture of the cross section of the barrel shaped cages and a typical minimum energy configuration of 4,4'-DIBP as viewed from b-axis is also shown.

room for the sorbate to adopt several tilted configurations with the isopropyl groups projecting in different orientations with respect to the 12-m channel. The diffusion path for the molecules is defined by a pair of points marked as '+'s on the channel axis at opposite ends of the section of the channel under investigation, as shown in Figure 1. Figure 1 includes the diffusion energy profile for 4,4'-DIBP in LTL. The minimum energy configuration of 4,4'-DIBP in LTL is also shown in Figure 1. The diffusion calculations are carried out for 4,3'-DIBP and 3,3'-DIBP also. The diffusion energy barriers for all the three isomers of DIBP are given in Table 2. It is seen from Table 2 that the energy barriers for diffusion of all the three isomers are almost in the same order. We may conclude from this calculation that zeolite L may not be an efficient shape selective zeolite catalyst for selective synthesis of 4,4'-DIBP.

Table 2. Diffusion energy barriers in kJ/mol for different isomer of DIBP in large pore zeolites.

Alkylaromatics	Zeolites		
	LTL	MOR	MTW
4,4'-DIBP	86.66	13.26	34.66
4,3'-DIBP	71.18	24.23	133.62
3,3'-DIBP	79.43	53.31	193.91

3.1.2. Mordenite

Zeolite mordenite belongs to orthorhombic symmetry and has a pore structure that is effectively unidimensional. An elliptical 12-m channel ($6.5 \text{ \AA} \times 7.0 \text{ \AA}$) runs parallel to [001] and has small side pockets ($2.6 \text{ \AA} \times 5.7 \text{ \AA}$) parallel to the [010] direction which connects to the next 12-m channel. The calculated diffusion energy barriers of the molecules in mordenite are given in Table 2. It can be seen that the diffusion energy barriers for the isomers of DIBP are significantly different even though there is only small variation in the dimensions of the molecules. These results indicate the significance of the pore dimensions and shape also, since the mordenite has smaller pore with elliptical shape compared to large circular pores in LTL. The diffusion energy profile for 4,4'-DIBP in MOR is shown in Figure 2. The molecule passes through energy maxima and minima while diffusing through a unit cell; the variation of interaction energy values symmetrically repeats in the second and third unit cells also, as shown in Figure 2. The energy barrier for the diffusion of 4,4'-DIBP is $13.26 \text{ kJ mol}^{-1}$. However, there exists a high energy barrier of $24.23 \text{ kJ mol}^{-1}$ for 4,3'-DIBP, which is almost double of 4,4'-DIBP and even higher energy barrier of $53.31 \text{ kJ mol}^{-1}$ for *o*-IBEB. Due to high energy barriers for 4,3'-DIBP and 3,3'-DIBP isomers MOR is expected to give better selectivity for 4,4'-DIBP compared to LTL.

3.1.3. ZSM-12

ZSM-12 is another large pore zeolite. It has even more smaller pore diameter ($6.2 \times 5.7 \text{ \AA}$) with elliptical shape. The molecules are allowed to diffuse through 5 unit cells in the b-direction. The cross sectional view of the 12-m channel of MTW is shown in Figure 3. The variation of interaction energy between 4,4'-DIBP and the framework for three unit

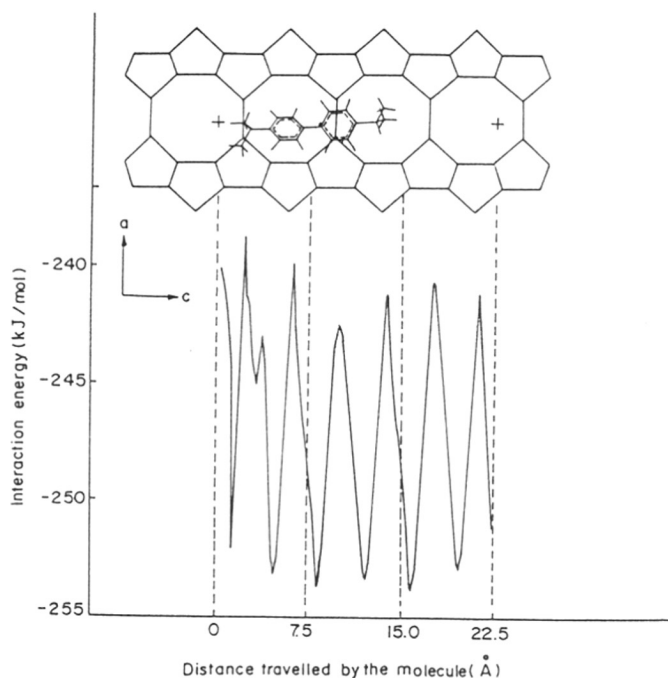


Figure 2. Variation of interaction energy of 4,4'-DIBP with mordenite lattice during its diffusion along the c-axis through the 12-m channel. The molecular graphics picture shows a typical minimum energy configuration of 4,4'-DIBP during the diffusion as viewed through b-axis.

cells as well as its minimum energy configuration in MTW is also shown in Figure 3. The diffusion energy profile shows a single maximum and a single minimum in each unit cell. The minimum and maximum energy occur when the atoms of the molecule are closer and farther, respectively, to the surface of the zeolite.

The comparisons of diffusion energy profiles for the three isomers of DIBP are shown in Figure 4. The diffusion energy barriers calculated from the energy profiles shown in Figure 4 are summarized in Table 2. The differences in the diffusion energy barriers of isomers of DIBP are very high. The large energy barriers for 4,3'-DIBP and 3,3'-DIBP could be correlated to their molecular sizes and flexibilities. All the molecules show energy profiles which uniformly repeat in the 3 unit cells considered. These results indicate that MTW is the best catalyst for the selective synthesis of 4,4'-DIBP, which is in excellent agreement with experiment.³²

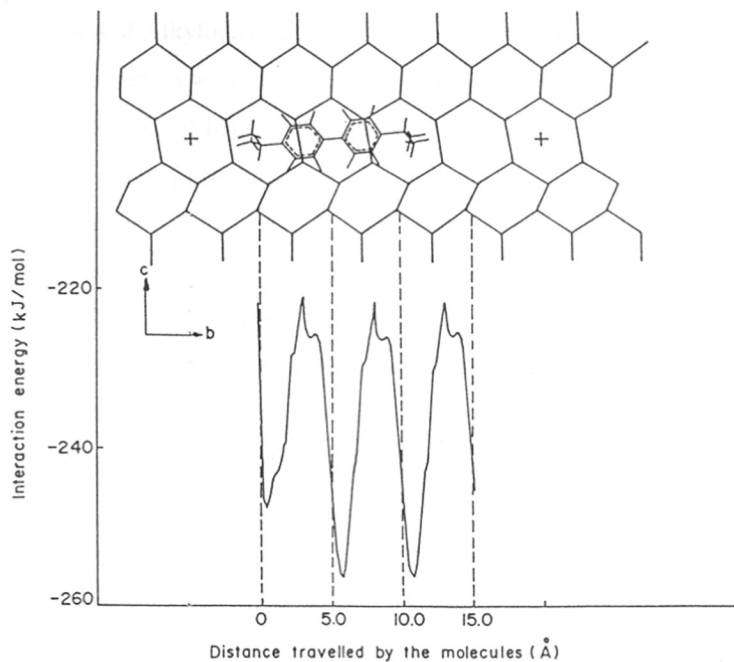


Figure 3. Variation of interaction energy of 4,4'-DIBP with ZSM-12 lattice during its diffusion along the b-axis through the 12-m channel. The molecular graphics picture shows a typical minimum energy configuration of 4,4'-DIBP during the diffusion as viewed through a-axis.

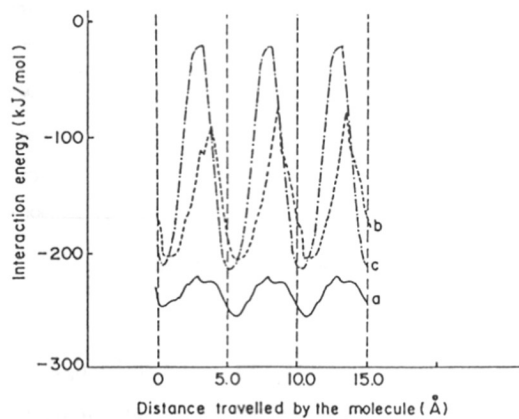


Figure 4. The diffusion energy profile for the isomers of DIBP when they diffuse through the 12-m channel in b-axis of ZSM-12. The regions of diffusion considered is same as Figure 3; 4,4'-DIBP (a), 4,3'-DIBP (b) and 3,3'-DIBP (c).

3.2. Diffusion of Alkylbenzenes in Large Pore Zeolites

In this section we will present the results for the diffusion of alkylbenzenes, namely EB, IBB and isomer of IBEB in various large pore zeolites.

3.2.1. Zeolites with pore diameter $\geq 7.0 \text{ \AA}$

3.2.1.1. Faujasite

Faujasite is a 3-dimensional zeolite with cubic symmetry, having 12-m ring openings of 7.4 \AA in diameter that provide access to a supercage of diameter 12.4 \AA . In our calculations, the diffusion paths for the alkylbenzenes in faujasite are defined by three points (A, B and C) at the centers of three consecutive supercages. The molecular graphics picture in Figure 5 shows the three supercages and diffusion path of the molecules from A

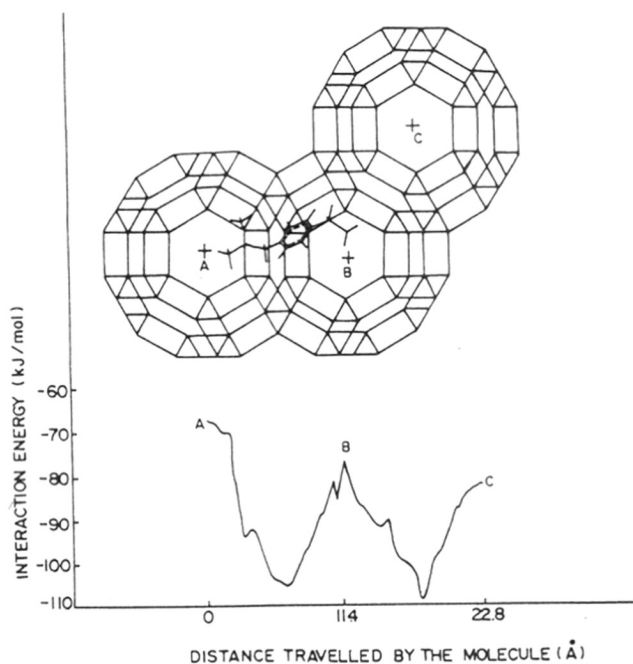


Figure 5. Variation of interaction energy of *p*-IBEB with faujasite lattice during 'cage to cage' diffusion through 12-m windows. The molecular graphics picture depicts the three supercages in different planes of the faujasite lattice. A typical minimum energy configuration of *p*-IBEB during the diffusion calculation is shown. A, B and C in the molecular graphics picture show the centres of the three supercages. In the graph, A, B and C show the interaction energy values near the centres of three supercages.

to C, via B. Figure 5 includes the diffusion energy profile for *p*-IBEB in faujasite. The minimum energy configuration of *p*-IBEB in faujasite is also shown in Figure 5. It is clear from Figure 5 that when the molecule moves from one supercage to another, the molecule energetically prefers to be near the wall rather than at the center of the supercage. Its interaction energy decreases and becomes minimum when the benzene ring of *p*-IBEB is near the center of the 12-member ring. As the molecule diffuses towards the center of the second supercage from 12-m ring its interaction energy increases and again becomes maximum near the center of the second supercage. Due to this high energy conformer, a diffusion energy barrier exists for cage-to-cage diffusion of the molecule in faujasite. Similar diffusion profiles are calculated for EB, IBB, *m*-IBEB and *o*-IBEB and the overall pattern of the diffusion energy profiles for all the molecules are found to be the same. The diffusion energy barriers of all the alkylbenzenes are given in Table 3. It is seen from Table 3 that the energy barriers for diffusions of all the molecules in faujasite are almost in the same order. We may conclude from this analysis that the pore system of faujasite places little constraint on the diffusion of different molecules. Hence, faujasite may not be a good shape selective zeolite catalyst for selective synthesis of *p*-IBEB.

Table 3. Diffusion energy barriers in kJ/mol for different molecules in large-pore zeolites

Alkylbenzenes	Zeolites			
	Faujasite	Zeolite L	Mazzite	Mordenite
EB	26.92	38.69	14.09	6.74
IBB	31.65	35.87	11.21	10.13
<i>m</i> -IBEB	28.38	43.69	9.78	17.95
<i>o</i> -IBEB	32.74	40.87	50.78	95.69
<i>p</i> -IBEB	31.65	28.43	10.69	6.44

3.2.1.2. Zeolite L

The pore architecture of LTL is already discussed in section 3.1.1. The walls of LTL are composed of 4-m rings and 8-m rings. The 8-m rings are highly elliptical and constitute the orifices of slit-like void volumes connecting neighbouring 12-m ring

channels. The 8-m rings are impermeable toward organic molecules. As mentioned earlier, the 12-m ring channels have barrel-shaped cross-section. In the regions of the pore, midway between the two 12-m rings, there is sufficient room for the sorbate to adopt several tilted configurations with the ethyl and isobutyl groups projecting in different orientations with respect to the 12-m channel, as shown in Figure 6. The diffusion path for the molecules is defined by a pair of points marked as '+'s on the channel axis at opposite ends of the section of the channel under investigation, as shown in Figure 7 and the

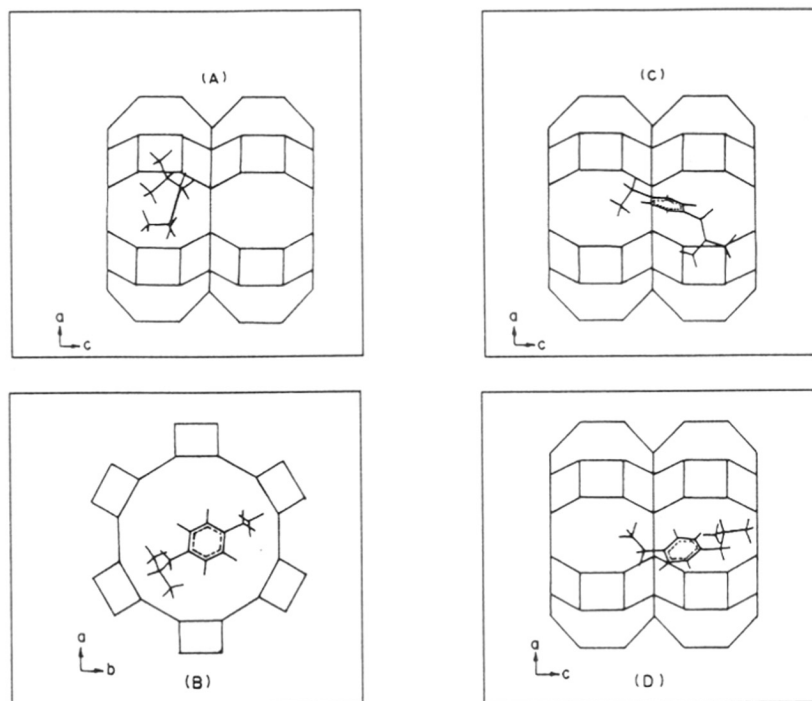


Figure 6. The molecular graphics picture showing the *p*-IBEB at various locations along the 12-m channel of zeolite L. The minimum energy configuration of *p*-IBEB is shown (A), when it is at the center of the barrel-shaped cage. The same minimum energy configuration as viewed from a perpendicular direction, (c-axis) that is along the axis of the 12-m channel is shown in (B). The configuration of *p*-IBEB (C) when it is crossing the 12-m ring connecting the barrels and the configuration (D) while diffusing towards the center of the barrel are also shown. The configurations C and D have relatively higher energy values than the configuration shown in (A).

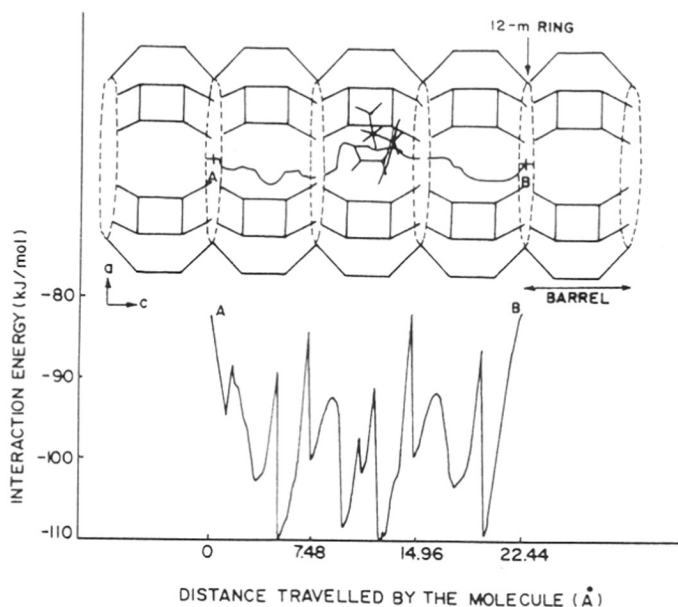


Figure 7. Variation of interaction energy of *p*-IBEB with zeolite L lattice during its diffusion along the *c*-axis through the barrel shaped cages. The molecular graphics picture shows the diffusion path of the molecule along with a typical minimum energy configuration of *p*-IBEB during the diffusion as viewed from the *b*-axis.

diffusion calculations are carried out in the same way as in faujasite. The energy profile for *p*-IBEB in zeolite L calculated by force field energy minimization techniques is shown in Figure 7 and the diffusion energy barriers for all the molecules are given in Table 3. From Table 3, it is seen that as in the case of faujasite there is no significant difference in the energy barrier for diffusion of the molecules in zeolite L. These calculations bring out the significance of the pore architecture. Zeolite L, with 2-dimensional pores is also not an efficient shape selective catalyst for the production of *p*-IBEB as in the case with 3-dimensional faujasite.

3.2.1.3. *Mazzite*

Zeolite mazzite is another hexagonal but one dimensional zeolite with pore diameter of 7.4 Å. Two types of smaller channels are present: the first consists of stacked gmelinite cages surrounded by six-member rings, the second is between two cross-linked

rows of cages and is surrounded by eight-member rings. The calculated diffusion energy barriers for the molecules in mazzite are given in Table 3. It can be seen from Table 3 that the diffusion energy barriers for EB, IBB *m*-IBEB and *p*-IBEB are in the same order, whereas there is a significantly high energy barrier for *o*-IBEB. The diffusion energy profile for *p*-IBEB in mazzite is plotted graphically in Figure 8. In the same figure the

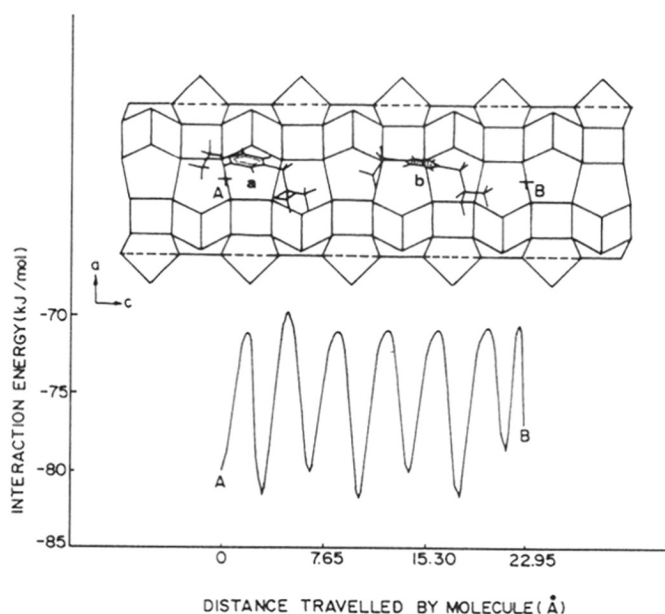


Figure 8. Variation of interaction energy of *p*-IBEB with mazzite framework as the molecule diffuses through 12-m channel. The molecular graphics picture shows a typical minimum (a) and a maximum (b) energy configurations of the molecule.

minimum and maximum energy configurations are also shown. The molecule passes through energy maxima and minima when it diffuses through the channel. There are alternative 8-m pockets in the channel of mazzite. The molecule adopts a minimum energy configuration when its phenyl ring is at the center of 8-m ring and the alkyl groups point towards other two 8-m rings. In other words, the maximum energy corresponds to the configuration in which phenyl ring as well as both the alkyl groups are in between the 8-m rings. Since there exists an energy barrier for diffusion of *o*-IBEB in mazzite, the diffusivity of other two isomers will be relatively faster than *o*-IBEB and mazzite will be a

selective catalyst compared to faujasite and zeolite L to produce *p* and *m*-isomers avoiding the formation of *o*-isomer.

3.2.1.4. Mordenite

The pore architecture of MOR is discussed in section 3.1.2. The calculated diffusion energy barriers of the molecules in mordenite are given in Table 3. It can be seen that the diffusion energy barriers for the isomers of IBEB are significantly different even though there are only small variations in the dimensions of the molecules. These results indicate the significance of the pore dimensions also, since the mordenite has small pore dimensions compared to other zeolites considered in this study. The diffusion energy barriers for *p*-IBEB and diffusion track for three carbon atoms (one aromatic carbon, two alkyl carbons) are shown in Figure 9. The molecule passes through energy maxima and

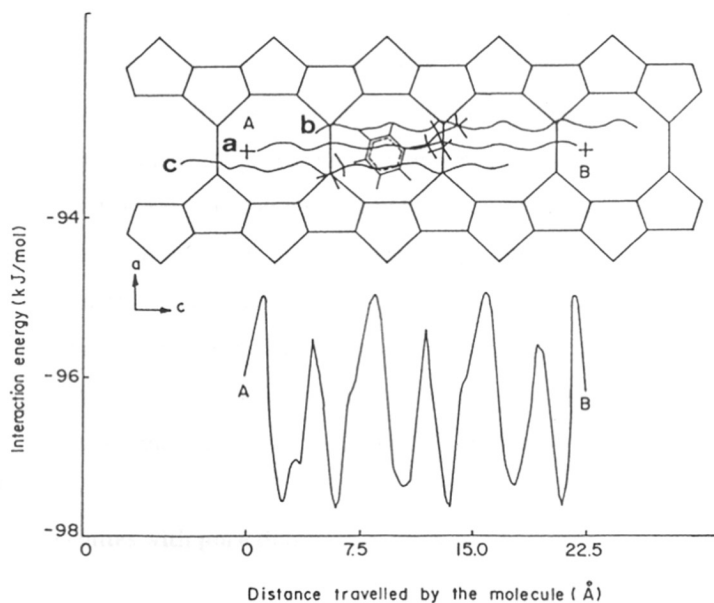


Figure 9. Variation of interaction energy of *p*-IBEB with mordenite framework as the molecule diffuses through the 12-m channel. The diffusion tracks for the motion of three carbon atoms are shown. The diffusion tracks of aromatic carbon atom to which the isobutyl group is bonded (a), the primary carbon in the isobutyl group (b) and the primary carbon in the ethyl group (c) are indicated to bring out their freedom of motion during the diffusion

minima while diffusing through a unit cell; the variation of interaction energy values symmetrically repeats in the second and third unit cells also, as shown in Figure 9. It is evident that the diffusion of EB and IBB have energy barriers of 6.74 kJ mol^{-1} and $10.13 \text{ kJ mol}^{-1}$ respectively. The energy barrier for the diffusion of *p*-IBEB is also of the same order (6.44 kJ mol^{-1}). However, there exists an energy barrier of $17.95 \text{ kJ mol}^{-1}$ for *m*-IBEB and a significantly large energy barrier of $95.69 \text{ kJ mol}^{-1}$ for *o*-IBEB. Hence mordenite is expected to be an efficient shape selective catalyst.

From the diffusion track of the different carbon atoms it is seen that as the alkyl groups move towards the zeolite framework its interaction energy decreases and becomes minimum. At maximum interaction energy, the molecule is parallel to the channel and the alkyl groups lie at the farthest distance from the zeolite framework. The same trend is found for diffusion of other molecules in mordenite.

These results also provide the information on the nature of sites inside mordenite where the molecules have favourable and unfavourable interactions. Figure 9 shows the position of *p*-IBEB in mordenite at its minimum energy configuration. It is seen from the figure that the molecule passes through two maxima and two minima, when it crosses each 8-m ring. The 8-m ring can be divided into 4 quarters. It is observed that when the phenyl ring of the molecule is at the beginning (0), center (0.5) or end (1) of the 8-m ring, the interaction of the molecule with the framework is most favourable while the unfavourable interaction corresponds to a configuration in which the phenyl ring is 0.25 or 0.75 through the 8-m ring. It is also observed that the favourable orientations of the molecule inside the 12-m ring are those in which the plane of the phenyl ring is parallel to the 8-m channel opening.

3.2.2. Zeolites with pore diameter < 7.0 Å

The diffusion energies for EB, IBB, *o*-IBEB, *p*-IBEB and *m*-IBEB are calculated in other large pore zeolites, such as offretite, ZSM-12 and cancrinite.

3.2.2.1. Offretite

The cross sectional view of the 12-m channel of OFF is shown in Figure 10. It has 8-m channels running perpendicular to the 12-m channel. The variation of the interaction energy between *p*-IBEB and the framework as well as the location and orientation of *p*-IBEB, when the interaction energy is minimum, is also shown in Figure 10. Similar

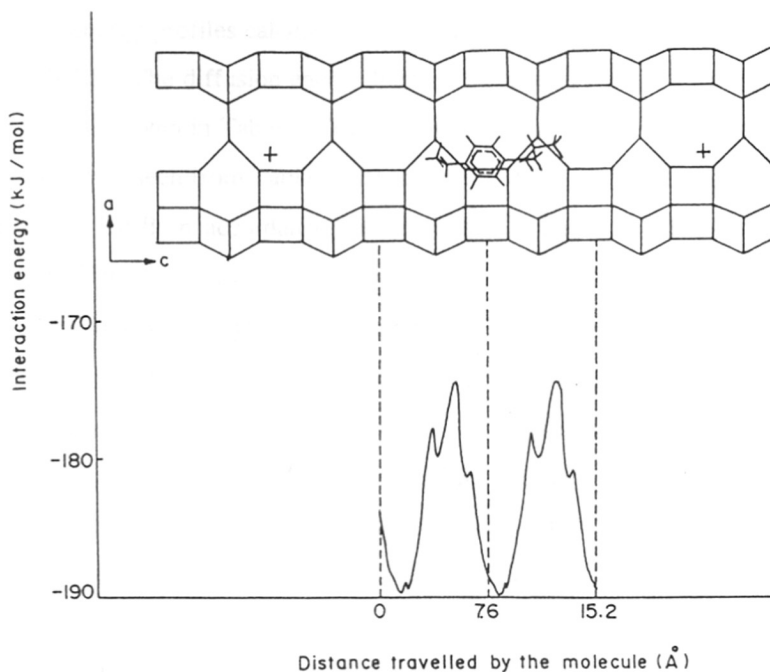


Figure 10. Variation of interaction energy of *p*-IBEB when it diffuses through 2 unit cells in the *c*-direction of OFF. The molecular graphics picture depicts the cross-section of 12-m channel. A typical minimum energy location of the *p*-IBEB in the diffusion path is also shown. The dotted lines are drawn to indicate the unit cells.

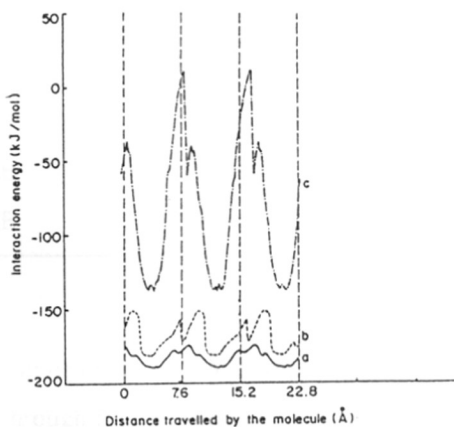


Figure 11. Variation of interaction energy of the isomers of IBEB, when they diffuse through the 12-m channel in the *c*-direction of OFF. The regions of diffusion considered is same as Figure 10; *p*-IBEB (a), *m*-IBEB (b) and *o*-IBEB (c).

diffusion energy profiles calculated for *o*-IBEB and *m*-IBEB are shown in Figure 11 along with *p*-IBEB. The diffusion energy barriers calculated from the energy profiles shown in Figure 11 are given in Table 4. Table 4 includes the diffusion energy barriers for EB and IBB also. It is seen from Table 4 that the energy barriers for EB and IBB are less than the isomers of IBEB in accordance with their size. The *o*-IBEB has the largest diffusion energy barrier. The reasons are its least flexibility and when the *o*-IBEB diffuses along the *c*-axis, the atoms of alkyl group in *o*-position have unfavourable interaction with zeolite surface due to the smaller dimension of the 12-*m* channel. It has positive interaction energy values in some locations while diffusing through the 12-*m* channel (from Figure 11). This indicates that *o*-IBEB cannot diffuse through the channel of OFF. Although the *m*-IBEB and *p*-IBEB isomers have favourable interaction energies it is necessary to have *o*-IBEB for disproportionation reaction. The high energy barriers for ortho isomer indicate that disproportionation reaction will not be possible in OFF. However, OFF seems to be a suitable catalyst for alkylation of IBB with ethylene for selective synthesis of *p*-IBEB. The energy barrier for *m*-IBEB is almost double of *p*-IBEB.

Table 4. Diffusion energy barriers in kJ/mol for different molecules in large-pore zeolites

Alkylbenzenes	Zeolites		
	OFF	MTW	CAN
EB	11.11	4.25	8.59
IBB	8.61	16.10	5.50
<i>m</i> -IBEB	30.00	38.21	81.51
<i>o</i> -IBEB	149.68	243.60	68.45
<i>p</i> -IBEB	15.43	19.13	14.65

3.2.2.2. ZSM-12

The pore architecture of MTW is discussed in section 3.1.3. The molecules are allowed to diffuse through 5 unit cells in the *b*-direction. The cross sectional view of the 12-*m* channel of MTW is shown in Figure 12. The variation of interaction energy between *p*-IBEB and the framework for three unit cells as well as its minimum energy configuration in MTW is also shown in Figure 12. The diffusion energy profile shows a single

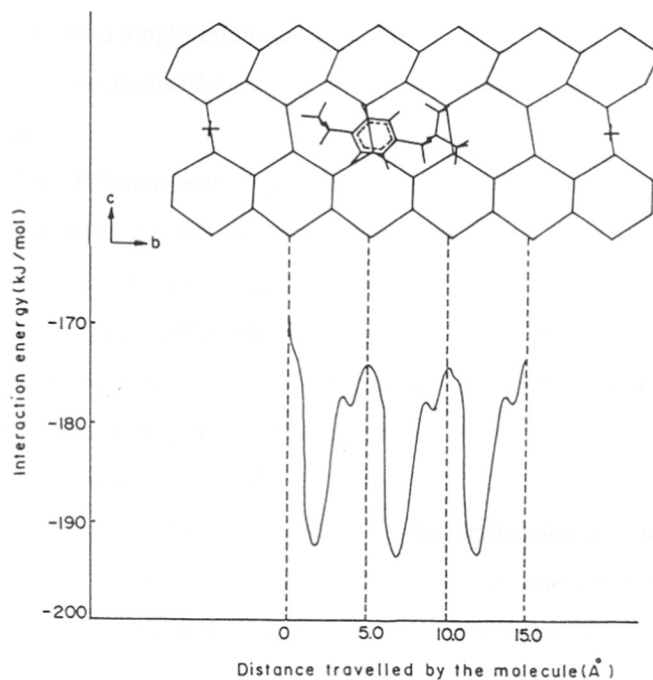


Figure 12. Variation of interaction energy of *p*-IBEB when it diffuses through 3 unit cells in the *b*-direction of MTW. The molecular graphics picture depicts the cross-section of 12-m channel. A typical minimum energy location of the *p*-IBEB in the diffusion path is also shown. The dotted lines are drawn to indicate the unit cells.

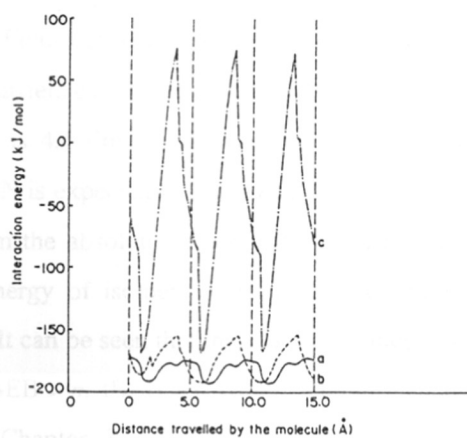


Figure 13. Variation of interaction energy of the isomers of IBEB, when they diffuse through the 12-m channel in the *b*-direction of MTW. The regions of diffusion considered is same as Figure 12; *p*-IBEB (a), *m*-IBEB (b) and *o*-IBEB (c).

maximum and a single minimum in each unit cell. The minimum and maximum energy occur when the atoms of the molecule are closer and farther, respectively, to the surface of the zeolite.

The diffusion energy profiles for all the three isomers are shown in Figure 13. Table 4 presents the diffusion energy barriers for all the five molecules. Although the difference in the diffusion energy barriers of *p*-IBEB and *m*-IBEB is not significant, the *o*-IBEB has a large diffusion energy barrier with positive interaction energy at some positions of the diffusion path. These values also indicate that zeolite MTW will not be suitable for the disproportionation reaction.

3.2.2.3. *Cancrinite*

Next, the diffusion behaviour of the molecules in cancrinite is studied. The symmetry and arrangement of the 12, 6 and 4-m channels in CAN are exactly same as in OFF. However, the pore diameter of CAN is considerably smaller (5.9 Å) than that of OFF (6.7 Å). The cross sectional view of the 12-m channel of CAN is shown in Figure 14. The molecules are diffused through 5 unit cells along the c-direction. The variation of the interaction energy between *p*-IBEB and CAN as the molecule diffuses in c-axis through three unit cells is shown in Figure 14. The minimum energy configuration of *p*-IBEB is also shown in Figure 14. The diffusion energy profile shows two peaks with maximum energy within a unit cell. This can be related to the presence of two intersecting 6-m ring within a unit cell. Figure 15 shows the diffusion energy profiles for the three isomers. The diffusion energy barriers calculated are again summarized in Table 4. The diffusion energy barrier of *o*-IBEB is 4.6 times and of *m*-IBEB is 5.6 times larger than that of *p*-IBEB. Hence, ideally CAN is expected to lead to better selectivity in the alkylation reaction. It is also observed from the absolute values that all the molecules are tightly fitting in CAN. The interaction energy of isomers of IBEB at their minimum energy configurations is given in Table 5. It can be seen that the absolute values of interaction also follow the same trend, namely *p*-IBEB > *m*-IBEB > *o*-IBEB. The influences of such energy characteristics are discussed in Chapter 3. In OFF and MTW, all the molecules have favourable interaction energy. It is pertinent to note that *o*-IBEB has a large positive interaction energy with CAN framework indicating a repulsive interaction. So, the entry of *o*-IBEB into channel of CAN itself has large activation energy barrier. Hence, in additions to the

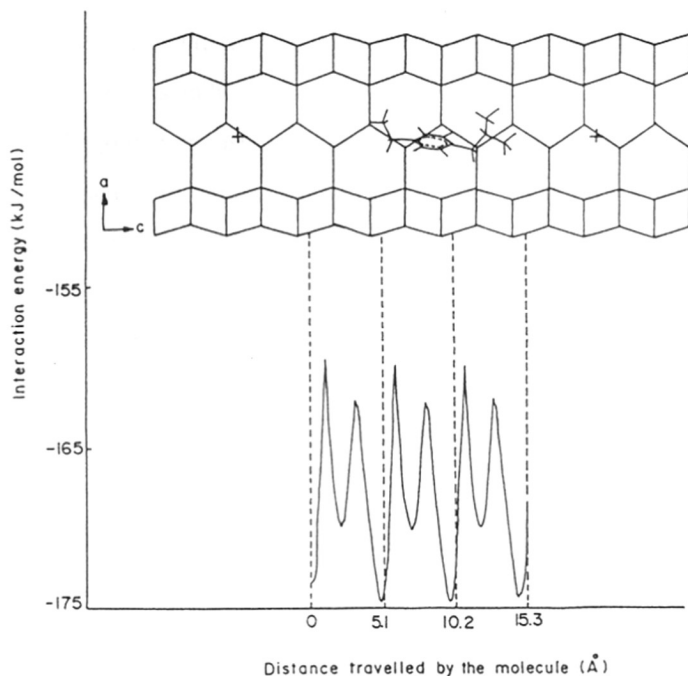


Figure 14. Variation of interaction energy of *p*-IBEB when it diffuses through 3 unit cells in the *c*-direction of CAN. The molecular graphics picture depicts the cross-section of 12-*m* channel. A typical minimum energy location of the *p*-IBEB in the diffusion path is also shown. The dotted lines are drawn to indicate the unit cells.

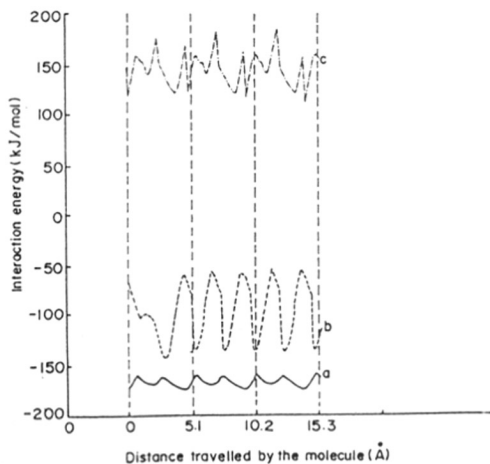


Figure 15. Variation of interaction energy of the isomers of IBEB, when they diffuse through the 12-*m* channel in the *c*-direction of CAN. The regions of diffusion considered is same as Figure 14; *p*-IBEB (a), *m*-IBEB (b) and *o*-IBEB (c).

diffusion energy barrier, the absolute value of interaction energy is also an important factor. These results indicate that if *o*-IBEB diffuses inside the channels of CAN, it is likely to undergo decomposition or cracking, which lead to deactivation of the zeolite due to coking.⁵⁷ Hence, by finding the ways to control the cracking, the potential of the shape selective properties of zeolites can be exploited.

Table 5. The interaction energy values (kJ/mol) of isomers of IBEB inside various zeolites at their minimum energy configuration

Molecule	Zeolites		
	OFF	MTW	CAN
<i>m</i> -IBEB	-181.64	-192.36	-151.96
<i>o</i> -IBEB	-138.39	-168.77	+184.03
<i>p</i> -IBEB	-189.90	-193.37	-174.51

3.2.3. Influence of Pore Architecture in Diffusion

From these studies we have seen that diffusion of molecules in zeolites depends on three important parameters, namely: (i) on the size of the molecules, (ii) on the pore diameter of the zeolites and (iii) pore architecture. The size and shape of the molecules are more flexible. In fact, the flexibility of the isomers of IBEB studied by conformational analysis indicate that their flexibility is in the order $p > m > o$. When the zeolite pore diameters match the dimensions of the molecules, the considerable increase in the diffusion energy barriers of *o*-IBEB and *m*-IBEB, compared to *p*-IBEB can be related to their flexibility. From the results presented here, the influence of pore architecture and pore dimensions could be discussed in detail. The figures presented here for the isomers of DIBP, *p*-IBEB, *o*- and *m*-IBEB follow almost the same trend but with varying diffusion energy barriers. As mentioned above, all the diffusion energy barrier values extracted from these studies are summarized in Tables 2-4. In general, it can be observed that 'channel-like' architecture as in MTW, MOR, CAN etc. are good for the selectivity than 'cage-like' architectures as in the case of FAU and LTL. Cages which are large enough to

accommodate all the molecules are leading to uniform diffusion behaviour for all the molecules with different sizes.

When the molecules diffuse through the channels of zeolites, they pass through surface and windows. From the analysis of the orientation and location of molecules in the minimum and maximum energy conformations, we observe that the alkyl groups in the molecules have favourable interaction with the surface in the zeolite framework, while the phenyl ring has an unfavourable interaction. As observed in the case of faujasite and zeolite L, the molecules prefer to change their orientation in which the alkyl groups can have more interaction with the surface. In mazzite also the adsorption sites, where alkyl groups are facing the 8-m windows in the zeolite framework are unfavourable. In mordenite, for all the isomers of IBEB, the alkyl groups have an end-to-end vector along the channel axis with phenyl plane facing the 8-m side pockets, during the diffusion. In cases, where the diameters of 12-m channels are getting smaller, the alkyl groups do not show such favourable interaction. The “window effect” discovered by Gorring⁵⁸ describes the non-linear relation between the diffusion coefficient and size of the molecule. Our results provide qualitative explanation based on the interaction of molecule with the surface and windows inside channels. However, it is necessary to calculate the electronic interactions of the alkyl and phenyl groups with the side pockets and pore walls of the zeolite to understand the ‘window effect’ quantitatively, which is attempted in Chapter 6.

In addition to the size as well as shape of the reactant molecules and the dimensions as well as architecture of the pores, there are factors such as Si/Al ratios, the number and nature of exchanged cations, temperature which influence the vibration of the framework and the nature of transition state also influence the shape selectivity in a minor way. ZSM-5 is known to be the best catalyst for the selective production of *p*-xylene than any other zeolite, independent of the Si/Al ratios and the exchanged cations,⁵⁹ which emphasize the importance of pore architecture. The transition state for 4,4'-DIBP and *p*-IBEB would be more “linear”. It is reasonable to assume that the transition states for the formation of 4,3'-DIBP, 3,3'-DIBP, *m*-IBEB and *o*-IBEB can have somewhat “bent” configuration, like these isomers themselves, resulting in higher activation energy values for diffusion of these molecules.

4. CONCLUSIONS

From the results presented here and on the lights of above discussions, the salient general features of the diffusion of the isomers of DIBP and IBEB can be summarized as given below.

(i) The diffusion characteristics of these molecules in the zeolite lattice depend on the molecular dimensions, pore diameter and the pore architecture of the zeolite.

(ii) The molecule-lattice interactions control the diffusion mechanism of molecules through the channel of a zeolite. The molecules prefer the configurations, where there is maximum interaction between the surface of the zeolite and the alkyl groups of the molecules.

(iii) Force field energy minimization calculation of the diffusion energy profile is simple technique relative to experimental studies of diffusion and reliable technique for logical catalyst screening.

(iv) For the diffusion of DIBP, these calculations show that significant energy barriers exist for 4,3'-DIBP and 3,3'-DIBP in MTW, 3,3'-DIBP in MOR and for none of them in LTL. Hence, the order of selectivity in the shape selective production of 4,4'-DIBP will be $MTW > MOR > LTL$ which is in the order predicted in the experimental study.³²

(v) For the diffusion of IBEB isomers, the order of selective production of *p*-IBEB among the zeolites with pore diameter $\geq 7.0 \text{ \AA}$, seems to be $MOR > MAZ > LTL \sim FAU$. CAN which has one dimensional pore and smallest diameter shows better selectivity for *p*-IBEB in the alkylation reaction. OFF has side pockets to the 12-m channel and shows less selectivity for alkylation. MTW has an intermediate selectivity and thus the order of selectivity in shape selective alkylation of IBB with ethylene to *p*-IBEB will be $CAN > MTW > OFF$. The interaction energy values of *p*-IBEB with the framework of OFF, MTW and CAN indicate its slow diffusion in these zeolites.

REFERENCES

1. L. Riekert, in *Advances in Catalysis*, D. D. Eley, H. Pines and P. B. Weisz (eds.), Vol. 21, Academic Press, New York, 1970, p. 281.
2. P.B. Weisz, in *New Horizons in Catalysis*, T. Seiyama and K. Tanabe (eds.), Vol.7A,

- Elsevier, Amsterdam, 1981, p. 3.
3. P.B. Weisz, *Chemtech*, 3 (1973) 498.
 4. E.G. Derouane, in *Catalysis by zeolites*, B. Imelik, C. Naccache, Y.B. Taarit, J.C. Vedrine, G. Coudurier and H. Praliaud (eds.), Vol. 5, Elsevier, Amsterdam, 1980, p. 5.
 5. C.N. Satterfield and J.R. Katzer, *Adv. Chem. Ser.*, 102 (1971)193.
 6. M. Bülow, P. Struve, G. Finger, C. Redszus, K. Ewrhardt, W. Schirmer and J. Kärger, *J. Chem. Soc., Faraday Trans. I*, 76 (1980) 597.
 7. W.O. Haag, R.M. Lago and P. B. Weisz, *Faraday Dis. Chem. Soc.*, 72 (1981) 317.
 8. R.R. Eckman and A.J. Vega, *J. Phys. Chem.*, 90 (1986) 4679.
 9. H. Pfeifer, *Phys. Rep.*, 26C (1976) 293.
 10. H. Jobic, A. Renouprez, M. Bee and C. Poinsignon, *J. Phys. Chem.*, 90 (1986) 1059.
 11. Y. Yasuda and A. Yamamoto, *J. Catal.*, 93 (1985) 176.
 12. J. Caro, M. Bülow, H. Jobic, J. Kärger and B. Zibrowius, in *Advances in Catalysis*, D.D. Eley, H. Pines, and P.B. Weisz, (eds.), Vol. 39, Academic Press, New York, 1993, p. 351.
 13. D.M. Ruthven, *Principles of Adsorption and Adsorption Processes*, John Wiley & Sons, New York, 1984.
 14. J. Karger and D.M. Ruthven, *Diffusion in Zeolites and other Microporous solids*, John Wiley & Sons, New York, 1992.
 15. B.F. Chmelka, D. Raftery, A.V. McCormick, L.C. de Menorval, R.D. Levine and A. Pines, *Phys. Rev. Lett.*, 66 (1991) 580.
 16. J. Kärger, M. Petzold, H. Pfeifer, S. Ernst and J. Weitkamp, *J. Catal.*, 136 (1992) 283.
 17. J. Xiao and J. Wei, *Chem. Eng. Sci.*, 47 (1992) 1143.
 18. *Modelling of Structure and Reactivity in Zeolites*, C.R.A. Catlow, (ed.), Academic Press, London, 1992.
 19. H. Stach, J. Jänchen, H. Thamm, E. Stiebitz and R.A. Vetter, *Ads. Sci. Technol.*, 3 (1986) 261.
 20. S. Yashonath and P. Santikary, *J. Phys. Chem.*, 97 (1993) 13778.
 21. R.L. June, A.T. Bell and D.N. Theodorou, *J. Phys. Chem.*, 96 (1992) 1051.

22. D. Dumont and D. Bougeard, *Zeolites*, 15 (1995) 650.
23. S.J. Goodbody, K. Watanabe, D. MacGowan, J.P.R.B. Walton and N. Quirke, *J. Chem. Soc., Faraday Trans.*, 87 (1991) 1951.
24. G.B. Woods and J.S. Rowlinson, *J. Chem. Soc., Faraday Trans.*, 85 (1989) 765.
25. F. Karavias and M.A. Myers, *Mol. Simul.*, 8 (1991) 23.
26. D.M. Rasmus and C.K. Hall, *AIChE J.*, 37 (1991) 769.
27. R.F. Cracknell and K.E. Gubbins, *Langmuir*, 9 (1993) 824.
28. K. Watanabe, N. Austin and M.R. Stapleton, *Mol. Simul.*, 15 (1995) 197.
29. D. Fraenkel, M. Cherniavsky, B. Ittah and M. Levy, *J. Catal.*, 110 (1986) 273.
30. G.S. Lee, J.J. Maj, S.C. Rocke and J.M. Garces, *Catal. Lett.*, 2 (1989) 243.
31. T. Matsuzaki, Y. Sugi, T. Hanaoka, K. Takeuchi, T. Tokoro and G. Takeuchi, *Chem. Express*, 4 (1989) 413.
32. A.S. Loktev and P.S. Chekriy, *Stud. Surf. Sci. Catal.*, 84 (1994) 1845.
33. J.-P. Rieu, A. Boucherle, H. Cousse and G. Mouzin, *Tetrahedron*, 42 (1986) 4095.
34. I. Shimizu, Y. Matsumura, Y. Tokumoto and K. Uchida, *Eur. Pat. Appl.*, 373 362, 1990.
35. Y. Tokumoto, I. Shimizu and S. Inoue, *Eur. Pat. Appl.*, 414 207, 1991.
36. DISCOVER, *Biosym Technologies Inc.*, 9685 Scranton Road, San Diego, CA, USA.
37. P. Dauber-Osguthorpe, V.A. Roberts, D.J. Osguthorpe, J. Wolff, M. Genest and A.T. Hagler, *Proteins: Structure, Function and Genetics*, 4 (1988) 31.
38. D.H. Olson, *J. Phys. Chem.*, 74 (1970) 2758.
39. J.M. Newsam, *J. Phys. Chem.*, 93 (1989) 7689.
40. E. Galli, *Cryst. Struct. Commun.*, 3 (1974) 339.
41. A. Alberti, P. Davoli and G. Vezzalini, *Z. Kristallogr.*, 175 (1986) 249.
42. J.A. Gard and J.M. Tait, *Acta Cryst. B*, 28 (1972) 825.
43. C.A. Fyfe, H. Gies, G.T. Kokotailo, B. Marler and D.E. Cox, *J. Phys. Chem.*, 94 (1990) 3718.
44. N. Bresciani Pahor, M. Calligaris, G. Nardin and L. Randaccio, *Acta Cryst. B* 38 (1982) 893.
45. A.T. Hagler, S. Lifson and P. Dauber, *J. Am. Chem. Soc.*, 101 (1979) 5122.
46. S. Morin, N.S. Gnep and M. Guisnet, *J. Catal.*, 159 (1996) 296.

47. Y.S. Bhat, J. Das, K.V. Rao and A.B. Halgeri, *J. Catal.*, 159 (1996) 368.
48. J.-H. Kim, A. Ishida, M. Okajima and M. Niwa, *J. Catal.*, 161 (1996) 387.
49. W.-H. Chen, A. Pradhan, S.-J. Jong, T.-Y. Lee, I. Wang, T.-C. Tsai and S.-B. Liu, *J. Catal.*, 163 (1996) 436.
50. Y. Nakazaki, N. Goto and T. Inui, *J. Catal.*, 136 (1992) 141.
51. J.A. Horsley, J.D. Fellmann, E.G. Derouane and C.M. Freeman, *J. Catal.*, 147 (1994) 231.
52. R. Millini and S. Rossini, *Stud. surf. Sci. Catal.*, 105 (1996) 1389.
53. T. Kiyoura, J. Ishikawa and H. Phala, *J. Catal.*, 170 (1997) 204.
54. R.R. Bhave, *Inorganic Membranes: Synthesis, Characteristics and Applications*, Van Nostrand Reinhold, New York, 1991.
55. R.C. Deka and R. Vetrivel, *Chem. Commun.*, (1996) 2397.
56. R.C. Deka and R. Vetrivel, *J. Catal.*, 174 (1998) 88.
57. J.N. Armor, *Appl. Catal.*, 78 (1991) 141.
58. R.L. Goring, *J. Catal.*, 31 (1973) 13.
59. A.J. Chandwadkar, R.A. Abdulla, S.G. Hegde and J.B. Nagy, *Zeolites*, 13 (1993) 470.

CHAPTER 5

MOLECULAR DYNAMICS STUDIES ON DIFFUSION OF AROMATICS IN MORDENITE

ABSTRACT

Molecular dynamics simulations are performed in order to study the dynamics of the isomers of isobutylethylbenzene (IBEB) in mordenite at 298 K. Diffusion of the isomers of IBEB show a linear variation for the mean square displacement (MSD) versus time plot. The MSD of *o*-IBEB is 6 \AA^2 after 20×10^{-12} s, whereas the MSD of *m*-IBEB is 175 \AA^2 after 20×10^{-12} s. However, *p*-IBEB has a MSD of more than 1000 \AA^2 after 20×10^{-12} s, subsequently the diffusion coefficients obtained at low sorbate concentration are in the order: *p*-IBEB > *m*-IBEB > *o*-IBEB. Due to the linear structure of *p*-IBEB, it diffuses faster along the 12-m channel of mordenite.

1. INTRODUCTION

The diffusion of aromatics in zeolites is of great interest in the context of separation and catalytic processes such as alkylation, transalkylation and isomerisation. For instance, the separation of *p*-xylene from C₈ aromatics (a mixture of the xylene isomers and ethylbenzene) is performed on the industrial scale using selective adsorption on zeolite molecular sieves.¹ The selectivity in a catalytic reaction can be determined from the diffusivity of the molecules involved in the reaction.² Several experimental studies to measure the diffusivity of aromatics inside zeolites, such as crystallographic,³⁻⁷ infrared,^{8,9} thermodynamic¹⁰ and NMR^{11,12} have been reviewed.¹³⁻¹⁵ The aim of these studies is to understand the sorption and diffusion behaviours of sorbates inside zeolites. However, a complete understanding of adsorption and diffusion in zeolites is hindered by the large discrepancies between the results obtained using different techniques.¹⁶

The need to gain a detailed insight into the behaviour of zeolite-sorbate systems on the molecular scale has inspired the development of computational methods to study such systems. Atomistic simulations based on interatomic potentials have proved to be of considerable value in studying the diffusion of organic molecules inside zeolites.¹⁷ An overview of the efforts in this area and the different techniques used has been compiled by Catlow.¹⁸ Among them, the molecular dynamics (MD) technique gives access to time-dependent and temperature-dependent properties and is often used to study various aspects of dynamics of sorbates. Since the first attempts to use MD for the simulation of diffusion processes in zeolites, sorbate molecules which could be represented by spherical particles have been preferentially chosen.¹⁹⁻³⁰ This was mainly due to the lesser computational effort required to model the interactions in such systems. This class of molecules includes noble gases (mainly Ar, Kr and Xe) and small spherically symmetric molecules like methane and CF₄. Trouw and Iton,¹⁹ Cohen de Lara *et al.*²⁰ and Yashonath *et al.*²¹ have studied the motion of methane in silicalite, NaA and faujasite, respectively. Although most of the MD simulations have been carried out in zeolites A, Y and silicalite, there are very few works in mordenite. Nowak *et al.*³¹ simulated the diffusion of methane in mordenite. El Amrani³² studied the diffusion of rare gases (Ne, Ar and Xe) in a model dealuminated mordenite. In most of the studies the sorbate molecules are modeled as soft spheres, interacting between them and with the framework atoms *via* Lennard-Jones or similar

potential functions. Moreover, interactions with Si or Al atoms of the framework are usually neglected, as they are considered shielded by the O atoms which cover the inner surfaces of the channels and cavities.

More complicated systems have been addressed by Leherter *et al.*,³³ who investigated the dynamics of water in ferrierite and by Demontis *et al.*,³⁴ who studied the diffusion of benzene in NaY. With the help of modern powerful computers it becomes possible for simulating large molecules inside zeolites. Goodbody *et al.*,³⁵ June *et al.*³⁶ and Hernandez and Catlow³⁷ simulated the behaviour of alkanes, such butane and hexane in silicalite for different loading of molecules. Schrimpf *et al.*³⁸ studied the structure, energetics and diffusion properties of *p*-xylene in NaY. Sastre *et al.*³⁹ used MD techniques to simulate the diffusion of a binary mixture of ortho and para-xylene in purely siliceous zeolite CIT-1. However, only little work has been undertaken until now to investigate the static and dynamic properties of aromatic compounds in mordenite by means of force field and MD simulations.⁴⁰⁻⁴³ Our energy minimization calculations showed that mordenite is the most efficient shape selective catalyst among the seven large pore zeolites analyzed. Hence, we chose to study the dynamics of these molecules inside mordenite by MD calculations to get further insight on the diffusion characteristics. In this work, we focus on the dynamics of ortho, meta and para-isobutylethylbenzene (IBEB) in mordenite. In order to locate the adsorption sites and to obtain the minimum energy pathway for diffusion of the aromatics, we performed constrained force field energy minimization calculations earlier (Chapter 4). Here, we describe our results on MD simulations performed at 298 K with an aim of investigating the diffusion process occurring in the time scale of the simulations. The dynamic properties studied include the probable adsorption sites, residence times in characteristic regions of the zeolite framework and self-diffusivity of the aromatics.

2. METHODOLOGY

Molecular dynamics simulation is carried out by solving Newton's equation of motion, using the Verlet algorithm.⁴⁴ The initial velocities have been assigned to all atoms of the system according to a Maxwell-Boltzmann distribution. The calculations are carried out at 298 K in the NVT (canonical) ensemble with full periodic boundary conditions. A

simulation box containing 8 unit cells of mordenite⁴⁵ (1152 atoms) and one sorbed molecule is considered. The zeolite frame was held fixed in our calculation. The interaction between the molecule and the mordenite framework is studied using the consistent valence force field (CVFF) parameters. Short-range host-guest interactions are calculated using Lennard-Jones potential.⁴⁶ These parameters are already listed in Table 1 of Chapter 1.

Simulations are performed using a time step of 1×10^{-15} s. Each of the IBEB isomers is initially located at their minimum energy configurations derived by force field energy minimization technique. The system is allowed to equilibrate for a 5×10^{-12} s period and then data are collected for a subsequent 20×10^{-12} s period. The results of the calculations are saved every 10×10^{-15} s and from these data, analyses of the diffusion process are undertaken. Mean square displacements (MSD) are calculated according to the well known Einstein Formula:

$$D = \frac{\langle |r(0) - r(t)|^2 \rangle}{6t} \quad (1)$$

where $\langle |r(0) - r(t)|^2 \rangle$ is the mean square displacement of the particles averaged on trajectories of duration, t . Pair distribution functions, $g(r)$, have also been calculated using standard procedure.⁴⁷ All simulations are performed using the program DISCOVER⁴⁸ supplied by Biosym Technologies Inc., USA.

3. RESULTS AND DISCUSSION

3.1. Adsorption Sites and Energetics

Force field energy minimization calculations were performed for the systematic search for minimum energy configurations. Figure 1 shows the minimum energy configurations of the isomers of IBEB in mordenite. In Figure 1a, the diffusion path of the *p*-IBEB is also shown. At minimum energy configuration, the molecule moves towards the walls of the zeolite from its centre. Smaller displacement of the molecule from the centre of zeolite channel is observed for *m*-IBEB and *o*-IBEB also. The molecular graphics analysis of the results of configurations generated during the MD simulation is carried out. These results provided information on the adsorption sites inside MOR and the modes

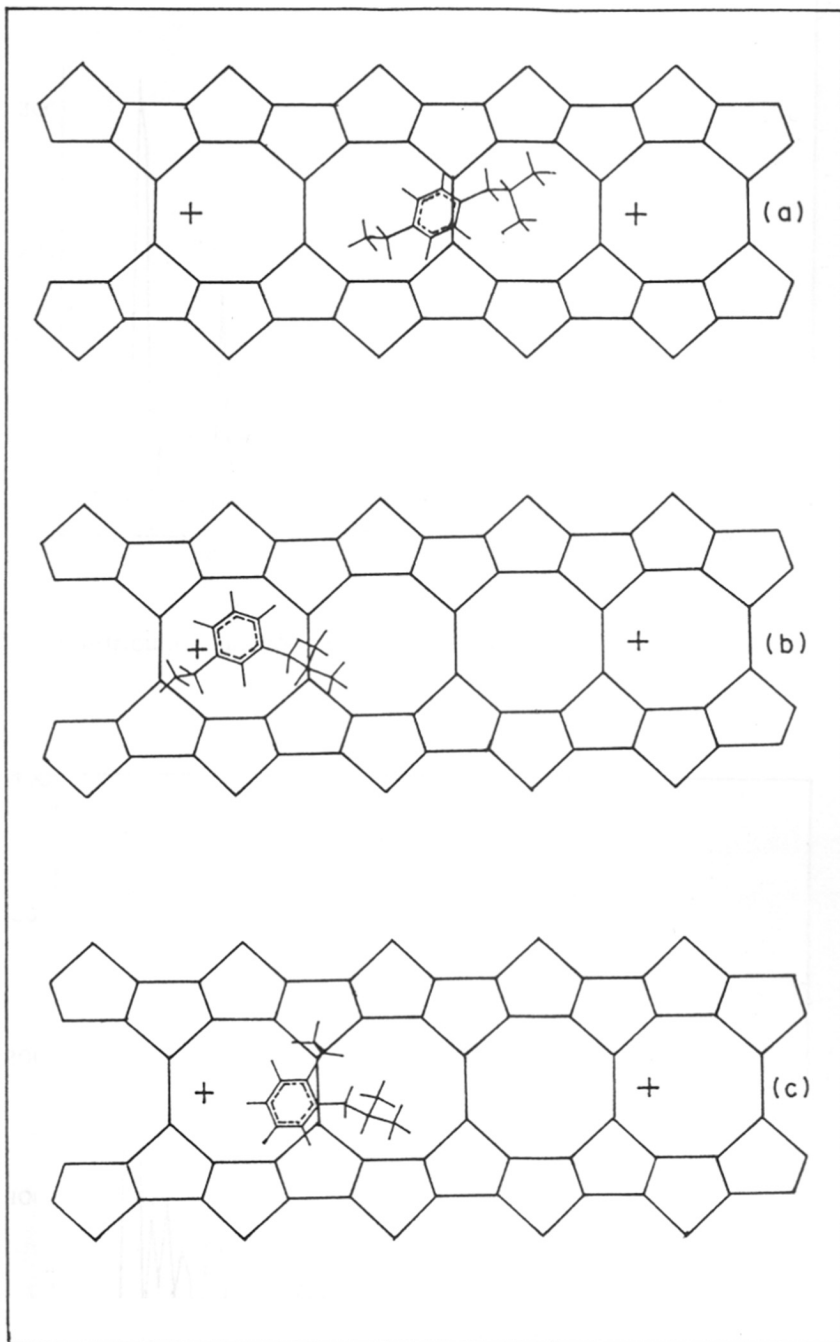


Figure 1. Minimum energy configurations of (a) *p*-IBEB, (b) *m*-IBEB and (c) *o*-IBEB obtained from the diffusion energy profiles calculated by force field energy minimization method.

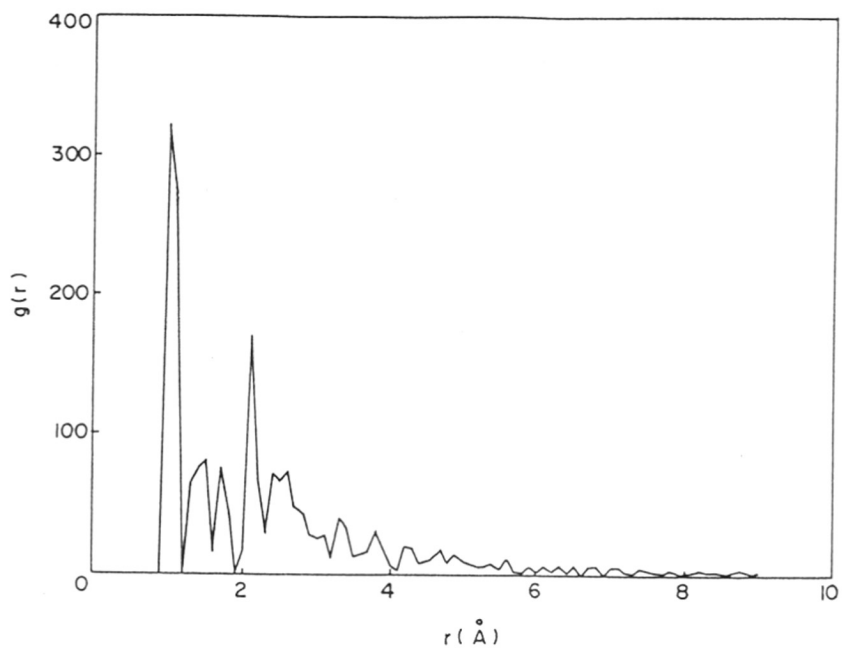


Figure 2. Pair distribution function for the centre of mass of *p*-IBEB in mordenite at 298 K.

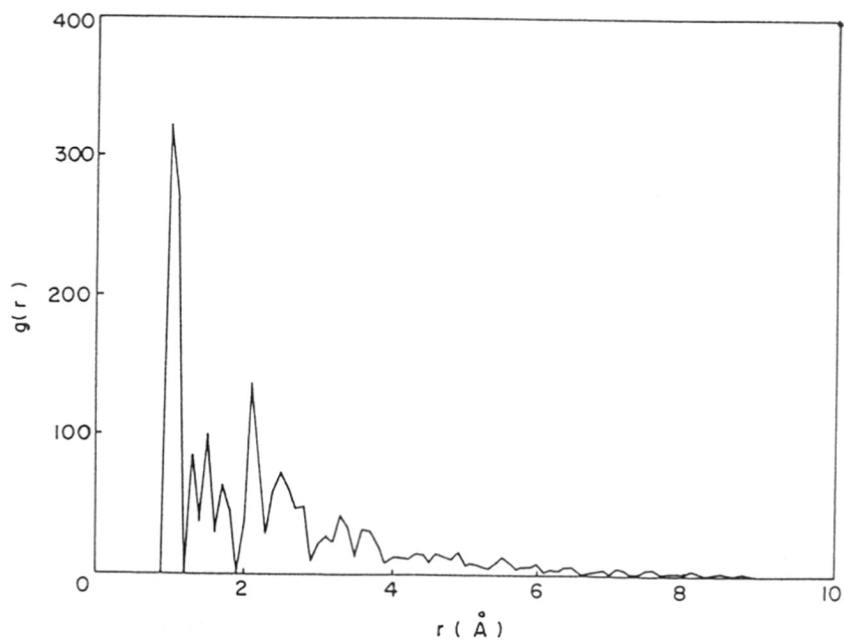


Figure 3. Pair distribution function for the centre of mass of *m*-IBEB in mordenite at 298 K.

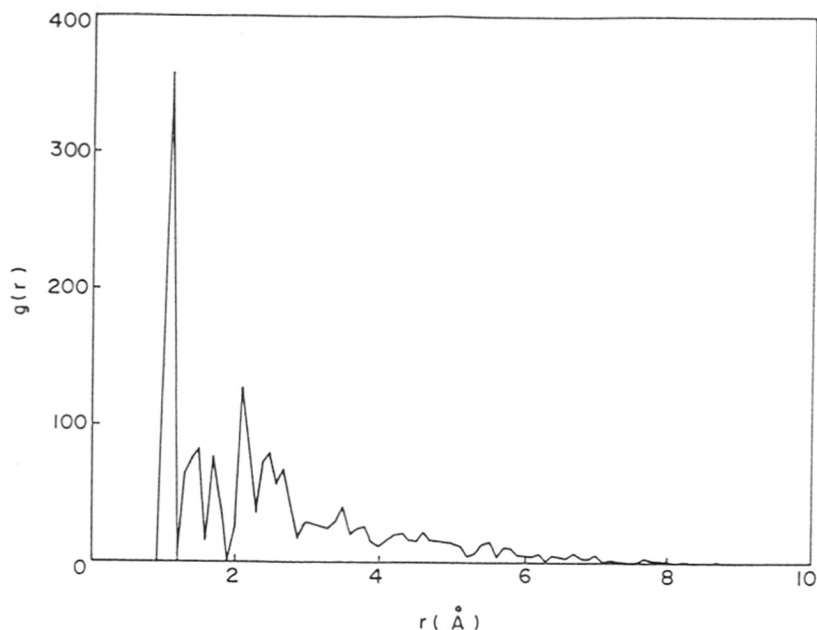


Figure 4. Pair distribution function for the centre of mass of *o*-IBEB in mordenite at 298 K.

of adsorption of isomers of IBEB. *p*-IBEB possesses more dynamic freedom inside the 12-m channel of MOR compared to *m*- and *o*-IBEB. The molecules are found to be displaced from the centre of the 12-m channel in most of the configurations during the simulation. An explanation for this phenomenon can be provided by the analysis of our MD results for the pair distribution functions, $g(r)$. Figures 2, 3 and 4 show the pair distribution functions for *p*-IBEB, *m*-IBEB and *o*-IBEB, respectively. These plots correspond for a loading of 1 molecule per 8 unit cells of MOR at 298 K. The structural distributions of the molecules during the simulation are evident from these figures.

3.2. Coefficients of Self-Diffusion

The diffusion coefficient of guest molecules is the most interesting dynamic property in the study of zeolite-sorbate systems. The coefficients of self-diffusion are computed from the MSD of the centre of mass of the guest molecule as a function of time. Figure 5 shows the MSD of the centres of masses of the isomers of IBEB with respect to time. The diffusion coefficient D can be calculated from the slope of the MSD plot according to the Einstein relation. The calculated diffusion coefficients of all the three

isomers are given in Table 1. The diffusivity of the three isomers are in the order of p -IBEB > m -IBEB > o -IBEB. These results are in correspondence with the size of the molecules and their flexibility. Similar trend was qualitatively predicted by the energy minimization calculations.

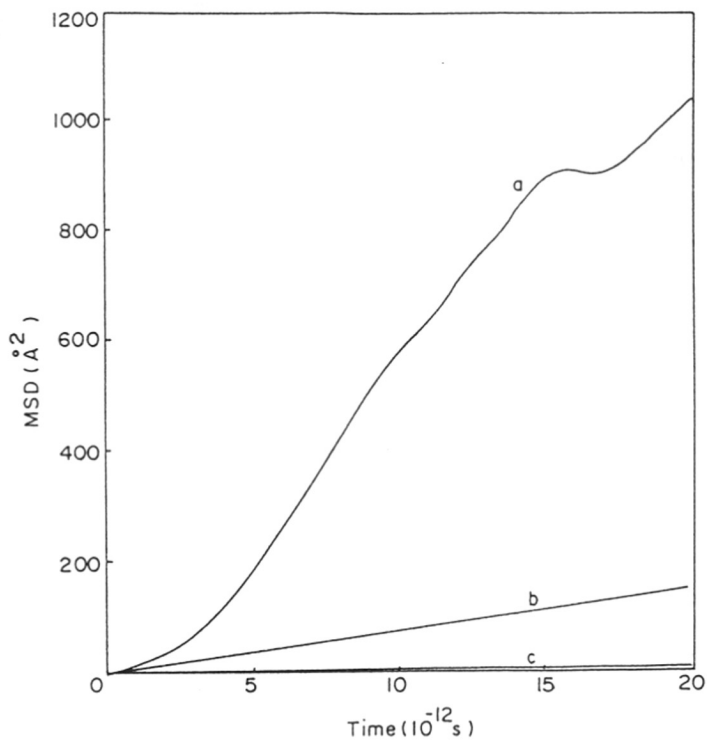


Figure 5. The variation of mean square displacement of the centre of the mass of the molecule with time of MD simulation; (a) p -IBEB, (b) m -IBEB and (c) o -IBEB.

Table 1. Self-diffusivities of the isomers of IBEB in mordenite from the plots in Figure 5.

Molecule	Self-diffusivity ($10^{-8} \text{ m}^2/\text{s}$)
p -IBEB	60.20
m -IBEB	7.39
o -IBEB	0.15

4. CONCLUSIONS

The dynamics of *o*-, *m*- and *p*-IBEB in purely siliceous mordenite are studied by MD technique. Earlier force field energy minimization calculations provided the starting minimum energy location for MD studies and our results validate such approach.

MD simulations are performed in order to study the behaviour of the isomers of IBEB at room temperature. The distributions of the molecules in the 12-m channel of mordenite give important information for the interpretation of the results derived from energy minimization calculation and further understanding of their adsorption characteristics. The diffusivities of the isomers of IBEB are found to decrease in the order: *p*-IBEB > *m*-IBEB > *o*-IBEB.

REFERENCES

1. R.W. Neuzil, *US Patent*, 3 558 730, 1971.
2. N.Y. Chen and W.E. Garwood, *J. Catal.*, 52 (1978) 453.
3. A.N. Fitch, H. Jobic and A.J. Renouprez, *J. Phys. Chem.*, 90 (1986) 1311.
4. M. Czjzek, T. Vogt and H. Fuess, *Zeolites*, 11 (1991) 832.
5. M. Czjzek, H. Fuess and T. Vogt, *J. Phys. Chem.*, 95 (1991) 5255.
6. C. Mellot, D. Espinat, B. Rebours, C. Baerlomer and P. Fischer, *Catal. Lett.*, 27 (1994) 159.
7. H. Klein and H. Fuess, in *Zeolites and Related Microporous Materials: State of the Art*, J. Weitkamp, H.G. Karge, H. Pfeifer and W. Holderich (eds.), Elsevier, Amsterdam, 1994.
8. A. Zecchina and C. Otero Arean, *Chem. Soc. Rev.*, (1996) 187.
9. F. Wakabayashi and K. Domen, *Catalysis Surveys from Japan*, 1 (1997) 181.
10. D.M. Ruthven and M. Gaddard, *Zeolites*, 6 (1986) 275.
11. J. Kärger and H. Pfeifer, *Zeolites*, 7 (1987) 90.
12. J. Kärger and D.M. Ruthven, *Diffusion in Zeolites and Other Microporous Solids*, John Wiley & Sons, New York, 1992.
13. J. Xiao and J. Wei, *Chem. Eng. Sci.*, 47 (1992) 1123.
14. J. Xiao and J. Wei, *Chem. Eng. Sci.*, 47 (1992) 1143.
15. N.Y. Chen, T.F. Degnan, Jr. and C.M. Smith, *Molecular Transport and Reaction in*

- Zeolites: Design and Application of Shape Selective Catalysts*, VCH Publishers, New York, 1994.
16. J. Kärger and D.M. Ruthven, *Zeolites*, 9 (1989) 267.
 17. J.M. Newsam, *Stud. Surf. Sci. Catal.*, 102 (1996) 231.
 18. *Modelling of Structure and Reactivity in Zeolites*, C.R.A. Catlow (ed.) Academic Press, London, 1992.
 19. F.R. Trouw and L.E. Iton, in *Zeolites for the Nineties, Recent Research Report*, H.C. Jansen, L. Moscou and M.F.M. Post (eds.), presented at the 8th International Zeolite Conference, Amsterdam, The Netherlands, 1989, p. 309.
 20. E. Cohen de Lara, R. Kahn, A.M. Goulay, *J. Chem. Phys.*, 90 (1989) 7482.
 21. S. Yashonath, P. Demontis and M.L. Klein, *Chem. Phys. Lett.*, 153 (1988) 551.
 22. R.L. June, A.T. Bell and D.N. Theodorou, *J. Phys. Chem.*, 94 (1990) 8232.
 23. A. Miyamoto, M. Kubo K. Matsuba and T. Inui, in *Computer Aided Innovation of New Materials II*, M. Doyama *et al.* (eds.), Elsevier, Amsterdam, 1993, p. 1025.
 24. C.R.A. Catlow, C.M. Freeman, B. Vessal, S.M. Tomiinson and M. Leslie, *J. Chem. Soc., Faraday Trans.*, 87 (1991) 1947.
 25. S. Yashonath and P. Santikary, *J. Phys. Chem.* 97 (1993) 13778.
 26. S. Bandyopadhyay and S. Yashonath, *Chem. Phys. Lett.*, 223 (1994) 363.
 27. P. Demontis, E.S. Fois, G.B. Suffritti and S. Quartieri, *J. Phys. Chem.*, 94 (1990) 4329.
 28. R.L. June, A.T. Bell and D.N. Theodorou, *J. Phys. Chem.*, 95 (1991) 8866.
 29. S.D. Pickett, A.K. Nowak, J.M. Thomas, B.K. Peterson, J.F.P. Swift, A.K. Cheetham, C.J.J. den Ouden, B. Smit and M.F.M. Post, *J. Phys. Chem.*, 94 (1990) 1233.
 30. D.N. Theodorou, R.Q. Snurr and A.T. Bell, in *Comprehensive Supramolecular Chemistry*, G. Alberti and T. Bein (eds.), Pergamon, Oxford, Vol. 7, 1996, p. 507.
 31. A.K. Nowak, C.J.J. den Ouden, S.D. Pickett, B. Smit, A.K. Cheetham, M.F.M. Post and J.M. Thomas, *J. Phys. Chem.*, 95 (1991) 848.
 32. S. El Amrani, *Etude de la diffusion des gaz rares dans les zeolithes par la dynamique moleculaire*, Thesis, University of Lyon, Lyon, France, 1990.
 33. L. Leherste, D.P. Vercauteren, E.G. Derouane, G.C. Lie, E. Clementi and J.-M. Andre, in *Zeolites: Facts, Figures, Future*, P.A. Jacobs and R.A. van Santen, (eds.), Elsevier,

- Amsterdam, 1989, p. 773.
34. P. Demontis, S. Yashonath and M.L. Klein, *J. Phys. Chem.*, 93 (1989) 5016.
 35. S.J. Goodbody, K. Watanabe, D. MacGowan, J.P.R.B. Walton and N. Quirke, *J. Chem. soc., Faraday Trans.*, 87 (1991) 1951.
 36. R.L. June, A.T. Bell and D.N. Theodorou, *J. Phys. Chem.*, 96 (1992) 1051.
 37. Hernandez and C.R.A. Catlow, *Proc. R. Soc. Lond. A*, 448 (1995) 143.
 38. G. Schrimpf, B. Tavitian and D. Espinat, *J. Phys. Chem.*, 99 (1995) 10932.
 39. G. Sastre, A. Corma and C.R.A. Catlow, *Topic in Catalysis*, (in press).
 40. J.A. Horsley, J.D. Fellmann, E.G. Derouane and C.F. Freeman, *J. Catal.*, 147 (1994) 231.
 41. R.C. Deka and R. Vetrivel, *Chem. Commun.*, 1996, 2397.
 42. R.C. Deka and R. Vetrivel, *J. Catal.*, 174 (1998) 88.
 43. R.C. Deka, R. Vetrivel, S. Yashonath, K. Mizukami, H. Takaba, M. Kubo and A. Miyamoto, *Third Tokyo Conference on Advanced Catalytic Science and Technology*, Tokyo, Japan, 1998.
 44. L. Verlet, *Phys. Rev.*, 159 (1967) 98.
 45. A. Alberti, P. Davoli and G. Vezzalini, *Z. Kristallogr.* 175 (1986) 249.
 46. P. Dauber-Osguthorpe, V.A. Roberts, D.J. Osguthorpe, J. Wolff, M. Genest, A.T. Hagler, *Proteins: Struc., Function Genetics*, 4 (1988) 21.
 47. M.P. Allen and D.J. Tildesley, *Computer Simulation of Liquids*, Clarendon Press, Oxford, 1987.
 48. DISCOVER, Biosym Technologies Inc., San Diego, 1993.

CHAPTER 6

INFLUENCE OF ZEOLITE COMPOSITION ON ACIDITY AND ETHYLATION ACTIVITY: A QUANTUM CHEMICAL STUDY

ABSTRACT

In this chapter, the modifications of frontier molecular orbital energy of the guest molecules located inside a microporous zeolitic cavity are studied by quantum chemical calculation. MNDO (Modified Neglect of Diatomic Overlap) method has been used to study fully siliceous cluster models of sites in the 12-m channel of mordenite. The interaction of isobutylbenzene (IBB) with the cluster models representing the wall of the 12-m channel of mordenite is studied. It is found that the highest occupied molecular orbital (HOMO) energy of IBB increases when it is inside the zeolite pore compared to its gas phase. The changes in HOMO energy of ethylbenzene (EB), *o*-, *m*- and *p*-isobutylethylbenzene (IBEB) when they are confined inside zeolites relative to gas phase are also presented.

The effect of the chemical composition on the acidity is studied by isomorphous substitution of Si by trivalent atoms such as Al, Ga and B using *ab initio* calculations. The local softness decreases in the order: (Al, Si) > (Ga, Si) > (B, Si) when they are isomorphously substituted for Si in the framework. The softness of the acid site plays an important role in catalytic activity especially for orbital-controlled reactions. The catalytic implications of the changes in the softness of various sites in zeolites have been brought out from results of quantum chemical calculations. The local softness values for various atoms in IBB are useful to understand the selectivity in its ethylation reaction.

1. INTRODUCTION

Over the last three decades, significant advances have been made concerning: (i) the synthesis of aluminosilicates including the isomorphous substitution of silicon or aluminium by other elements,¹⁻³ (ii) tailoring the physicochemical properties of zeolites by post-synthesis solid state treatments to enable them as host structures with characteristics, which suit the specific requirements of each process⁴ and (iii) the structural characterization of these solids by means of recently available instrumental techniques such as solid state NMR, X-ray photoelectron spectroscopy (XPS) and both neutron and synchrotron based diffraction.⁵

However, despite the considerable volume of information obtained recently and the important catalytic role played by such isomorphously substituted zeolites, many facets of their behavior are poorly understood. For example, regarding the acidic properties, it is found that the intrinsic strength of the sites depends not only on the nature of atoms in next neighbour coordination sphere but also on the crystalline structure of the zeolite.

The reactant molecules experience the influence of the strong electric fields existing in the cavities which produce an induced polarization of the guest.⁶⁻⁸ Detailed maps showing electrostatic potentials have been reported for some zeolites using cluster models^{9,10} and periodic Hartree-Fock models.¹¹ It has been realized that not only ionic interaction but covalent interactions also play an important role in some reactions catalyzed by zeolites. The formation of activated complexes inside zeolite cages and the mechanisms of transfer of electrons between zeolite and adsorbate could be understood only by invoking the above two interactions.¹²⁻¹⁴ In the case of ethylation of aromatic molecules with ethylene, the reactivity of aromatics as electron donors is related to the energy of their highest occupied molecular orbital (HOMO).^{15,16} The higher HOMO energy of donor aromatics when they are confined inside zeolite pores relative to gas phase, leads to higher covalent interaction according to the general theory of reactivity.¹⁷⁻¹⁹ According to Pearson's hard-soft acid-base (HSAB) principle, the feasibility of electron transfer can be described within a perturbational semi-empirical approach. The feasibility of electron transfer is inversely proportional to the HOMO-LUMO energy gap between the electron donor and acceptor.¹⁸

In a different approach using density functional theory, the feasibility of electron transfer between donor and acceptor is inversely proportional to the hardness of both the molecules involved in the process.^{20,21} The chemical hardness of a molecule may be influenced even by a small difference between its LUMO and HOMO energy values. It is expected that a decrease in the HOMO-LUMO gap will lead to softness of the molecule, since they will undergo polarization more easily and consequently the reactivity will be altered.

These concepts can be applied in a straightforward manner when one considers reactions in either the gas or even liquid phase. However, when the reaction occurs in a confined space, it has to be considered that the electronic properties of some molecules can change due to confinement inside zeolite pore.²² It has been shown that the change in energy of the molecular orbitals of the confined molecules is inversely proportional to the size of the zeolite pore.²³ This effect becomes particularly important when the size of the molecule matches the size of the pore. This electronic effect arising due to the confinement of the molecule inside zeolite pores may be defined as 'electron confinement effect'. The electron confinement effect essentially affects the orbital energies of the confined molecules and becomes more important when the pore size of the structure decreases and when the molecular orbitals are more diffuse. For ethylene and aromatic molecules, the HOMO energy seems to be more sensitive to the electron confinement effect than the LUMO energy and thus a decrease in the HOMO-LUMO band gap is expected.¹⁵

The acid strength of zeolite sites have been calculated for various cluster models to study the influence of structure and composition on Brønsted and Lewis acidity.²⁴⁻³⁰ However, theoretical studies on the local hardness and softness of acid sites in zeolites are limited. Local hardness and softness parameters have been used as descriptors of reactivity.³¹ Global hardness, which is defined as the second derivative of energy with respect to the number of particles at constant temperature and external potential and its inverse, global softness are related to the stability of the systems.³² The affinity of two systems to react has been proposed by Pearson.³³ The principle of maximum hardness (PMH), proposed by Parr and Pearson,³² which is rigorously proved by Parr and Chattaraj,³⁴ relates the stability of the systems at constant chemical potential to the

hardness. The PMH was tested by several authors using *ab initio* and density functional theoretic level.³⁵⁻³⁷ To describe the reactivity, a local quantity namely Fukui function was first proposed by Parr and Yang.³⁸ Local softness, which is related to the Fukui function, through a factor of global softness, is introduced as another reactivity parameter. The local hard-soft acid-base (HSAB) principle based on the polarizability was originally proposed by Parr and Yang,³⁸ and later proved by Gazquez and Mendez³⁹ HSAB principle predicts the reactivity centers in two reacting systems based on equal softness. Krishnamurty *et al.*⁴⁰ have shown the validity of local HSAB principle in cases of interaction of small gaseous molecules with the zeolite surfaces. Fukui functions and local softness parameters have been successfully used in various studies by Geerlings and coworkers.^{31,41-43} Recently, a new scheme based on the relative electrophilicity and nucleophilicity has been proposed by Roy *et al.*⁴⁴ to explain the reactivity aspects of some carbonyl compounds such as aldehydes and ketones.

Achieving a very high selectivity with zeolite catalysts is an essential requirement to use them for the production fine chemicals. Although the shape selectivity is the major controlling factor, there are several studies in literature to show that electronic factors also play a subtle role in controlling selectivity. In this context, the aim of this work is to calculate the change in the frontier molecular orbital energies of aromatics such as EB, IBB, *o*-, *m*- and *p*-IBEB upon confinement in the pores of mordenite. Local softness of the ring carbons of IBB molecule is studied to predict the direction of the alkylating group. Variation of local softness of the acidic hydrogen and the alkylating group is calculated when the Si atom is isomorphously substituted by Al, Ga or B.

2. METHODOLOGY

2.1. Theory

The concept of HSAB was introduced by Pearson³³ based on the polarization properties of acid and base centres. There are two theoretical approaches to explain HSAB principle.

The first was developed by Klopman⁴⁵ and Salem⁴⁶ simultaneously by using second-order perturbation approximation to the molecular orbital theory. This approach relates the HSAB principle to the frontier molecular orbital theory of Fukui *et al.*⁴⁷⁻⁴⁹ If

one considers product formed from two reactants, A and B, by the formation of a covalent bond, one can decompose the Hamiltonian of the system into two terms. The first describing the system composed by the noninteracting reactants and the second describing the perturbation of each fragment by the other. Developing this in second-order perturbation theory, Klopman obtained the expression for the change of energy during the reaction as given in Equation 1.

$$\Delta E = -\sum_{ab} (q_a + q_b) \beta_{ab} S_{ab} + \sum_{k < l} \frac{Q_k Q_l}{\epsilon_o R_{kl}} + \left(\sum_r^{occ} \sum_s^{virt} - \sum_s^{occ} \sum_r^{virt} \right) \frac{2 \left(\sum_{ab}^c c_{ra} c_{sb} \beta_{ab} \right)^2}{E_r - E_s} \quad (1)$$

where the indexes a and b refer to the atomic orbitals of reactants A and B; k and l to the atoms of each reactant; r and s to the molecular orbital of each reactant without interaction. The first and second terms correspond to the first-order approximation. The first term represents the closed shell repulsion between the occupied orbitals of each reactant. The second term represents the coulombic interaction between the atoms of each reactant considering them as point charges Q_i . The third term is a second order approximation and depends mainly on the energy differences between the occupied molecular orbitals of one fragment and the virtual orbitals of the other. The chemical meaning of this term refers to the energy related to the formation of a covalent bond and can be associated with the hardness of the reactants.

Applying the frontier orbital theory, which says that the terms other than those with the smallest difference ($E_r - E_s$), that is, ($E_{LUMO} - E_{HOMO}$) can be neglected, the energy related to the second order can be approximated by

$$\Delta E^{(2)} \approx \frac{2 \left(\sum_{ab}^c c_{ra} c_{sb} \beta_{ab} \right)^2}{E_r - E_s} \quad (2)$$

where r is HOMO of fragment A (donor) and s is LUMO of fragment B (acceptor). This depends only on the energy difference ($E_r - E_s$), the resonance integral β_{ab} and the coefficients C_{ra} that correspond to the contribution of each atomic orbital to the HOMO and LUMO, i.e., to the frontier orbital density. The hardness and softness of a species

(molecule or atom) can be calculated using Koopmans theorem. According to Koopmans theorem, the frontier orbital energies are given by

$$IP = -E_{\text{HOMO}}$$

$$EA = -E_{\text{LUMO}}$$

where IP and EA are the first ionization potential and electron affinity of the species. Following Pearson,⁵⁰ for a closed-shell species, the hardness parameters can be obtained using Koopmans theorem for the eigenvalues corresponding to the highest occupied and lowest unoccupied molecular orbitals as

$$\eta = \frac{1}{2}(E_{\text{LUMO}} - E_{\text{HOMO}}) \quad (3)$$

The second approach involves the calculation of total energies of the molecule and its monocationic and mononegative ions. From the calculated total energies one can derive the hardness, using finite difference approximation. The global hardness is defined as the second derivative of the energy with respect to the number of particles for a given external potential:

$$\eta = \left(\frac{\partial^2 E}{\partial N^2} \right)_{v(\bar{r})} = \left(\frac{\partial \mu}{\partial N} \right)_{v(\bar{r})} \quad (4)$$

where E is the total energy, N is the number of electrons of a chemical species and μ is the chemical potential. The corresponding global softness is expressed in terms of the inverse of global hardness as:

$$S = \frac{1}{2\eta} = \left(\frac{\partial^2 N}{\partial E^2} \right)_{v(\bar{r})} = \left(\frac{\partial N}{\partial \mu} \right)_{v(\bar{r})} \quad (5)$$

By applying the finite difference approximation, we get what are known as the operational global hardness and softness as:

$$\eta = \frac{IP - EA}{2} \quad (6)$$

$$S = \frac{1}{IP - EA} \quad (7)$$

The local softness $s(\bar{r})$ may be defined as,

$$s(\bar{r}) = \left(\frac{\partial Q(\bar{r})}{\partial \mu} \right)_{v(\bar{r})} \quad (8)$$

so that, $\int s(\bar{r})d\bar{r} = S$

Combining equations 8 and 5 we can write,

$$s(\bar{r}) = \left(\frac{\partial \rho(\bar{r})}{\partial N} \right)_{v(\bar{r})} \cdot \left(\frac{\partial N}{\partial \mu} \right)_{v(\bar{r})} = f(\bar{r}) \cdot S = \left(\frac{\partial \mu}{\partial v(\bar{r})} \right)_N \cdot S \quad (9)$$

where $f(\bar{r})$ is defined as the Fukui function by Parr and Yang.³⁸ $f(\bar{r})$ defines the sensitivity of chemical potential to the local external perturbation at point r . From the definition of the local softness, one can infer that local softness can also be used as reactivity measure. Local HSAB principle states that the local softness is a better reactivity descriptor with respect to the reaction partner. The definitions of $f(\bar{r})$ and $s(\bar{r})$ involve derivatives of $\rho(\bar{r})$ with respect to the number of electrons. A finite difference scheme has been used to define three different types of local softness for nucleophilic, electrophilic and radical attacks as given below:

$$s_k^+ = [\rho_k(N_o + 1) - \rho_k(N_o)] \cdot S \quad (10)$$

$$s_k^- = [\rho_k(N_o) - \rho_k(N_o - 1)] \cdot S \quad (11)$$

$$s_k^o = \frac{1}{2} [\rho_k(N_o + 1) - \rho_k(N_o - 1)] \cdot S \quad (12)$$

where $\rho_k(N_o)$, $\rho_k(N_o + 1)$ and $\rho_k(N_o - 1)$ are the Mülliken populations on atom k in the N_o , $(N_o + 1)$ and $(N_o - 1)$ electron systems, respectively.

2.2. Computational Details

The reactivity parameters used in this study include global hardness, global softness, O–H bond length (r_{OH}) of bridging hydroxyl group, net charges (q_H) of the acidic hydrogen, ionicity $|q_H q_O|$ of O–H bond, local softness (s_H^+) of acidic hydrogen and its relative electrophilicity (s_H^+ / s_H^-). The quantum chemical calculations have been carried out at the MNDO⁵¹ and *ab initio* Hartree-Fock⁵² level with different basis sets. The Hartree - Fock calculations were carried by GAMESS package developed by Dupuis and coworkers⁵³ in a SGI-Indy workstation. The calculation of IP and EA as the difference of separate SCF energy values of neutral and monpositive or mononegative ions of same cluster model is explained elsewhere.⁴⁰

Cluster models of mordenite zeolite containing 118 atoms are taken for MNDO calculations. The stoichiometry of the cluster model is $H_{44}Si_{32}O_{42}$. Acidity of zeolite

clusters is studied in small clusters which are represented as: $H_3SiO(H)TH_3$ where $T = Al, Ga$ and B . The influence of zeolite composition on ethylation activity is studied in these clusters substituting the acidic hydrogen atoms by ethyl group.

3. RESULTS AND DISCUSSION

By screening several zeolites using energy minimization calculations for the selective production of *p*-IBEB, we found that mordenite is the most potential candidate (please see Chapter 4). Hence, here we analyze the electronic confinement effect of the reactant and product molecules inside the pores of mordenite.

3.1. Influence of Mordenite Pore on Frontier Molecular Orbitals of Guest Molecules

When studying the interaction of guest organic molecule with zeolite host, the first aspect to be considered is the location of the guest molecule and the part of the zeolite lattice which provides the interacting part of the whole zeolite lattice. The minimum energy configuration of the molecules in the channel of mordenite are those obtained using the force field energy minimization technique as discussed in Chapter 4. A cluster is

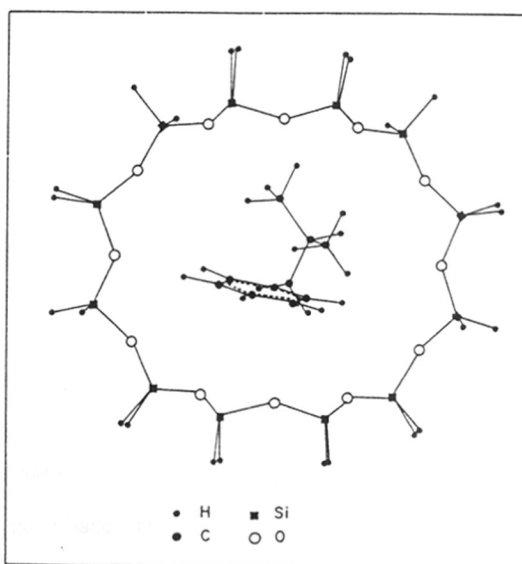


Figure 1. Cluster of mordenite terminated by hydrogens showing the position of isobutylbenzene molecule at the minimum energy configuration as derived from force field energy minimization calculations.

generated to study the electronic confinement effect by MNDO calculations. This cluster model contains in addition to the molecule, a full layer of a 12-m ring which has the maximum interaction with the molecule and the other SiO₄ units which are closer to the molecule. The unsaturated valency of silicon atoms in the 12-m ring are saturated by attaching hydrogen atoms to them. Figure 1 shows a typical cluster model for representing the confinement of IBB inside the 12-m ring of mordenite. The stoichiometry of the cluster model to represent the zeolite framework is H₄₄Si₃₂O₄₂. Similar type of clusters are taken for other molecules based on their minimum energy configurations. We performed single geometry calculations for all the cluster models. The HOMO and LUMO energies of EB, IBB, *o*-, *m*- and *p*-IBEB in the gas phase and when they are in their minimum energy configuration in the pore of mordenite are given in Table 1.

Table 1. Frontier orbital energies (au) and hardness (au) of the EB, IBB, *o*-, *m*- & *p*-IBEB molecules in gas phase and upon confinement inside the channel of mordenite at their minimum energy configurations derived by force field energy minimization technique.

Molecules	Gas phase			Inside zeolite cavity		
	HOMO	LUMO	η	HOMO	LUMO	η
EB	-0.34054	0.00945	0.17500	-0.25638	0.07270	0.16454
IBB	-0.34115	0.00911	0.17513	-0.25593	0.07250	0.16422
<i>o</i> -IBEB	-0.33900	0.00713	0.17306	-0.26244	0.07245	0.16745
<i>m</i> -IBEB	-0.33943	0.00717	0.17348	-0.25898	0.07232	0.16565
<i>p</i> -IBEB	-0.33720	0.00514	0.17117	-0.26100	0.07200	0.16650

The results show the effect of the confinement on the frontier orbitals of the molecules when they are inside the pores of mordenite. It is seen from Table 1 that both HOMO and LUMO energies of confined molecules increase with respect to the values obtained in the gas phase. However, the HOMO energy values are more sensitive than the LUMO energy values. Differences in HOMO energy values observed for the molecules are large enough to expect reasonable differences in the chemical behaviour of the molecules inside zeolite pores with respect to gas phase.

Global hardness values calculated according to Equation 3 are also given in Table 1. The chemical hardness is a qualitative parameter to estimate the extent of the electron confinement effect. A decrease in the hardness after confinement is seen in Table 1. In other words softness of the molecules increases when they are inside the pores of mordenite.

In Chapter 4, it is shown that the interaction energy becomes favourable as the molecule approaches the walls of the zeolite. The minimum energy configuration is found when the molecule is near the walls and the maximum energy is observed when it is at the centre of the zeolite channel. The total energy, HOMO, LUMO energies and hardness of IBB in gas phase as well as at minimum and maximum energy configurations obtained from force field energy minimization calculation are shown in Table 2. It is seen from Table 2 that when the molecule moves more close to the walls of the zeolite, the HOMO energy increases with respect to the gas phase molecule. The LUMO energy also experiences a slight increase when the molecule moves from the center of the channel towards the walls of the zeolite. The energy difference between the minimum and maximum energy configuration calculated using MNDO quantum chemical method is 24.16 kJ/mol. From force field energy minimization calculations this energy was found to be 10.13 kJ/mol. The difference in energy obtained by quantum chemical calculation and energy minimization may be due to the artifact of the cluster model.

Table 2. Total energy, HOMO, LUMO and hardness of IBB in the gas phase and at minimum and maximum energy configurations inside the 12-m channel of mordenite.

	Gas phase	Inside the pore of mordenite	
		Maximum energy	Minimum energy
Total energy (au)	-54.28916	-681.85489	-681.86409
HOMO (au)	-0.34115	-0.26478	-0.25593
LUMO (au)	0.00911	0.07188	0.07250
Hardness, η (au)	0.17513	0.16833	0.16422

3.2. Influence of Chemical Composition on Acidity

The cluster models chosen to study the influence of isomorphous substitution of Al, Ga or B in place of Si is shown in Figure 2. The zeolite cluster models $\text{H}_3\text{Si}-\text{O}(\text{H})-\text{AlH}_3$, $\text{H}_3\text{Si}-\text{O}(\text{H})-\text{GaH}_3$ and $\text{H}_3\text{Si}-\text{O}(\text{H})-\text{BH}_3$ are denoted by (Al, Si), (Ga, Si) and (B, Si) respectively. Si—O—T bridge is bonded to hydrogen atoms to fix the boundary conditions. The Si—H and T—H distances are fixed as 1.5 Å with the H atoms lying along the vectors, Si—O and T—O, respectively. The initial geometry of these cluster models are derived from the crystal structure reported for the faujasite lattice.⁵⁴ However, to make it a general utility for all zeolites, the geometry of all the atoms in these cluster models are optimized (fully optimized cluster). Trial calculations are also carried out for the initial geometry (rigid cluster). Calculations are performed for the geometry where peripheral hydrogen atoms are held fixed and only the geometry of central atoms are optimized (partially optimized cluster). The exact prediction of the acid strength of these isomorphously substituted zeolite observed in the experimental studies⁵⁵⁻⁵⁷ are used as criteria to fix these calculation parameters. Experimentally the acid strength in substituted zeolites are found to be decreasing in the order (Al, Si) > (Ga, Si) > (B, Si). Although a larger cluster model is desired, we observed that the cluster models where the T atoms are terminated by -OH groups, are unsuitable to analyze the HSAB results. The oxygen atoms bridging a T and H (T—O—H) have larger electronegativity than the oxygen atoms bridging two Ts (T—O—T). Due to the unrealistic electrostatic potential created by O in T—O—H in the vicinity of Brønsted acid sites, these cluster models become unsuitable. The electronic structures are calculated for the neutral, anionic and cationic cluster models. The global softness of the cluster models and the local softness on the acidic sites are computed according to the Equations 7 and 10 respectively.

3.2.1. Calculations with 3-21G Basis Set

Table 3 shows the reactivity parameters of the fully optimized zeolite cluster models calculated using 3-21G basis set. These parameters are given only for the bridging H atoms obtained through both the Mulliken and Lowdin population analysis. The values of the charge on the bridging H atom, q_{H} , indicate that the acidity decreases in the order (Al, Si) > (Ga, Si) > (B, Si). The values of the OH bond length, r_{OH} , which is an indication of the strength of the bond and therefore the acidity of the hydroxyl group are

also in perfect agreement with experimental data.⁵⁵⁻⁵⁷ The same conclusions are arrived when considering $|q_{\text{H}}q_{\text{O}}|$, which is a measure of the ionicity of the OH bond.

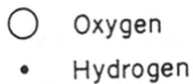
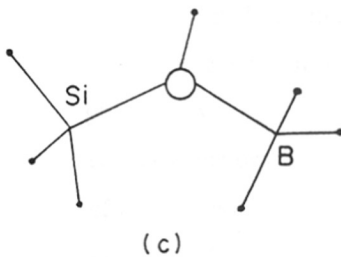
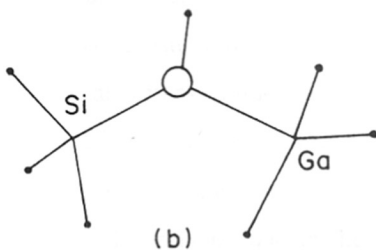
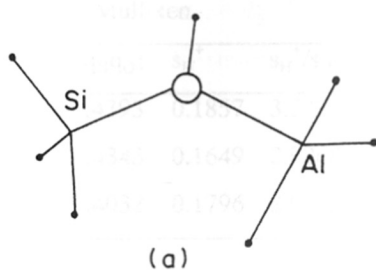


Figure 2. The geometry of the cluster model: $\text{H}_3\text{SiO}(\text{H})\text{TH}_3$ (where $\text{T} = \text{Al}, \text{Ga}$ or B) used to study the influence of chemical composition on the acidic properties. The geometry is fully optimised using 3-21G and DZV basis sets. The properties calculated for these cluster models are given in Tables 3 and 5.

Table 3. Calculated values of the reactivity parameters (au) of the bridging hydroxyl group for the fully optimized cluster models using 3-21G basis set

Cluster	r_{OH} (Å)	Mulliken				Lowdin			
		q_{H}	$ q_{\text{H}}q_{\text{O}} $	s_{H}^+	$s_{\text{H}}^+/s_{\text{H}}^-$	q_{H}	$ q_{\text{H}}q_{\text{O}} $	s_{H}^+	$s_{\text{H}}^+/s_{\text{H}}^-$
(Al, Si)	0.966	0.4706	0.4393	0.1857	3.5427	0.3250	0.1740	0.1394	3.9462
(Ga, Si)	0.965	0.4691	0.4343	0.1649	2.9268	0.3226	0.1726	0.1322	3.4324
(B, Si)	0.963	0.4666	0.4032	0.1796	2.0205	0.3225	0.1396	0.1291	2.1126

However, local softness (s_{H}^+) values calculated using Mulliken population are in the order: (Al, Si) > (B, Si) > (Ga, Si), which is not in agreement with experiments. The explanation for the less accurate description of the acidity by the local softness may be due to its dependence on basis sets. Cluster model may also have effect on local softness. It is interesting to see that the local softness values (s_{H}^+) calculated using Lowdin population follow the experimental trend. Thus s_{H}^+ (or s_{H}^-) values are strongly influenced by basis set and/or cluster models. However, the ratio ($s_{\text{H}}^+/s_{\text{H}}^-$), which involves two differences of electron densities of systems differing by one in their number of electrons at constant nuclear framework, is expected to be less sensitive to the basis set and/or cluster model. The bridging H atom having the highest $s_{\text{H}}^+/s_{\text{H}}^-$ value is the most acidic proton. The $s_{\text{H}}^+/s_{\text{H}}^-$ values for all the three clusters are presented in Table 3. It is seen that the new parameter, the relative electrophilicity ($s_{\text{H}}^+/s_{\text{H}}^-$) is good indicator of acidity. The $s_{\text{H}}^+/s_{\text{H}}^-$ values are larger for the systems with higher acidity.

The fully optimized disiloxane analogs, $\text{H}_3\text{Si}-\text{O}(\text{H})-\text{TH}_3$ (T = Al, Ga, B), do not belong to any particular type of zeolite. We imposed little constraints in the cluster models to mimic experimental geometry. The H—T—H (T = Si, Al, Ga, B) angles are held fixed at their crystallographically determined geometry and only the central part of the cluster is optimized which is reasonable to take care the geometry distortions due to isomorphous substitution of Si by other trivalent cations. The reactivity parameters for these clusters are given in Table 4. All the reactivity parameters calculated using Mulliken population analysis are in agreement with acidity trends in contrast to previous case. The ionicity of the OH bond, $|q_{\text{H}}q_{\text{O}}|$, local softness, s_{H}^+ , and relative electrophilicity, $s_{\text{H}}^+/s_{\text{H}}^-$ values calculated by Lowdin population analysis are also in agreement with experimental acidity

trend. The charges on acidic hydrogen, q_H , calculated from Mulliken or Lowdin population do or do not follow the experimental acidity trend. Even in cases where they follow experimental acidity their numerical values show minor variation. Hence, it may be concluded that s_H^+/s_H^- is a more reliable parameter to predict acidity.

Table 4. Calculated values of the reactivity parameters in au of the bridging hydroxyl group for the partially optimized cluster models using 3-21G basis set

Cluster	r_{OH} (Å)	Mulliken				Lowdin			
		q_H	$ q_H q_O $	s_H^+	s_H^+/s_H^-	q_H	$ q_H q_O $	s_H^+	s_H^+/s_H^-
(Al, Si)	0.968	0.4861	0.4597	0.2594	4.6712	0.3361	0.1779	0.1886	5.0196
(Ga, Si)	0.966	0.4854	0.4549	0.2373	4.1611	0.3340	0.1759	0.1792	4.5636
(B, Si)	0.963	0.4813	0.4169	0.2322	2.2952	0.3351	0.1393	0.1622	2.2771

3.2.2. Calculations with DZV Basis Set

We used a larger basis set namely DZV basis and calculated the reactivity parameters mentioned above. These values, calculated by both Mulliken and Lowdin population analysis for fully optimized cluster are given in Table 5. The calculated r_{OH} , $|q_H q_O|$, s_H^+ , and s_H^+/s_H^- are in good agreement with the experimental values; however, the q_H values for (B, Si) cluster calculated by Lowdin population is larger than (Ga, Si) cluster. The same trend is observed in the rigid cluster models using DZV basis set as shown in Table 6. Hence, it can be concluded that when larger basis sets are used the local softness and relative electrophilicity are reliable parameters to describe the acidity.

Table 5. Calculated values of the reactivity parameters in atomic units (au) of the bridging hydroxyl group for the optimized models using DZV basis set

Cluster	r_{OH} (Å)	Mulliken				Lowdin			
		q_H	$ q_H q_O $	s_H^+	s_H^+/s_H^-	q_H	$ q_H q_O $	s_H^+	s_H^+/s_H^-
(Al, Si)	0.953	0.4969	0.5698	0.2317	3.8471	0.3653	0.2919	0.1481	4.7210
(Ga, Si)	0.952	0.4891	0.5436	0.2064	2.9183	0.3625	0.2856	0.1369	3.6342
(B, Si)	0.949	0.4874	0.4945	0.1981	2.2639	0.3642	0.2528	0.1197	2.4496

Table 6. Calculated values of the reactivity parameters in atomic units (au) of the bridging hydroxyl group for the rigid models using DZV basis set

Cluster	r_{OH} (Å)	Mulliken				Lowdin			
		q_{H}	$ q_{\text{H}}q_{\text{O}} $	s_{H}^+	$s_{\text{H}}^+/s_{\text{H}}^-$	q_{H}	$ q_{\text{H}}q_{\text{O}} $	s_{H}^+	$s_{\text{H}}^+/s_{\text{H}}^-$
(Al, Si)	0.955	0.5129	0.5967	0.3534	5.4834	0.3762	0.2974	0.2209	6.3598
(Ga, Si)	0.953	0.5041	0.5680	0.3265	4.7431	0.3718	0.2882	0.2061	5.4333
(B, Si)	0.950	0.5039	0.5053	0.2788	3.1725	0.3753	0.2466	0.1620	3.1851

3.3. Influence of Chemical Composition on Ethylation Activity

Quantum chemical calculations are also carried out on the isobutylbenzene (IBB) molecule in order to understand the position (*o*-, *m*- or *p*) where ethylation occurs in this molecule and the results are given in Table 7. It is observed that the local softness values at various carbon atoms of IBB are in the order: para > ortho > meta positions. The net charges calculated indicate that nucleophilic attack will take place in the order: ortho > para > meta. Hence a proton or an alkylating agent is expected to produce more ortho isomer. However, based on the local softness values, an alkylating agent with higher softness value is expected to attack the para position.

Table 7. The electronic properties in atomic units (au) of the fully optimized isobutylbenzene (IBB) molecule.

Molecule	Total energy	Global softness	Mulliken charges			Local softness		
			<i>o</i> -C	<i>m</i> -C	<i>p</i> -C	<i>o</i> -C	<i>m</i> -C	<i>p</i> -C
IBB	-386.7332	2.5218	-0.3183	-0.1924	-0.2189	0.1189	0.0433	0.3841

The formation of surface alkoxy groups due to the activation of alcohols are an established fact in the literature.^{58,59} Quantum chemical cluster calculations in the literature also have indicated the formation of surface alkoxy groups on the Bronsted acid sites.⁶⁰ Hence we carried out calculations on the cluster models shown in Figure 3 in order to understand the ethylation capability of zeolites with different chemical composition. The results of the calculations are given in Table 8. Thus the alkylating agent is modeled by replacing the acidic hydrogen by an ethyl group. The zeolitic O—C₁ of C₂H₅ group

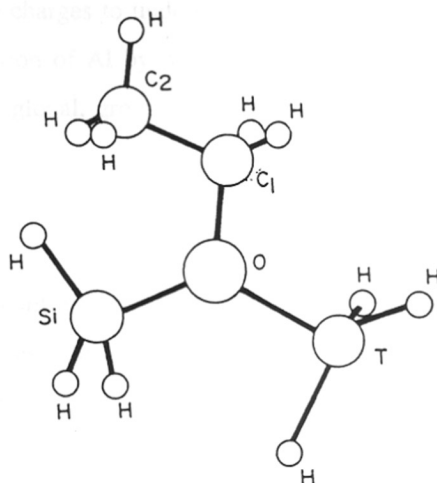


Figure 3. The geometry of the cluster model used to study the alkylating agent, namely the surface ethoxy group; T = Al, Ga or B. The proton at the Brønsted acid site is replaced by the ethyl group. The calculated electronic properties are given in Table 8.

Table 8. The electronic properties of fully optimized (with $r_{O-C} = 1.8 \text{ \AA}$) $H_3Si(OC_2H_5)TH_3$, (where T = Al, Ga or B) cluster models.

Cluster models	Mulliken charges				$ q_O q_{C_2H_5} $	$r_{O-C_2H_5}$ (\AA)	Global softness	Group softness $s_{C_2H_5} +$
	q_O	q_{C2}	q_{C1}	$q_{C_2H_5}$				
SiAl:Et	-1.1970	-0.4897	0.0529	0.6144	0.7355	1.80	2.6270	1.9746
SiGa:Et	-1.1434	-0.4894	0.0535	0.5955	0.6809	1.80	2.6000	1.9137
SiB:Et	-1.0136	-0.4939	0.0694	0.6012	0.6094	1.80	2.4548	1.8474

distance is fixed at 1.8 \AA and the geometry of all the other atoms in the cluster model, shown in Figure 3 are optimized. The global softness values and ionicity of $O-C_2H_5$ bond are found to follow the trend of the acid strength of these zeolites. The group softness of the $-C_2H_5$ group shows clear dependence on the chemical composition. The

global softness are in the order of (SiAl:Et) > (SiGa:Et) > (SiB:Et). But the group charge of -C₂H₅ group does not follow the trend. Thus group softness is found to be a better parameter than group charges to understand reactivity. In this work we have studied the isomorphous substitution of Al by other trivalent elements. It is also possible to study reactivity in terms of global, group and local softness for bigger clusters by varying the Si/Al ratio.

4. CONCLUSIONS

The electron confinement effect for organic molecules have been calculated by confining the molecules into all silica clusters of mordenite. The increase in HOMO energy is found to be higher as the molecule occupies sites nearer to the wall of zeolite. The HOMO energy value and HOMO-LUMO band gap, point to the fact that IBB molecule becomes softer after confinement in the microporous environment of mordenite and this will alter the reactivity of this molecule in zeolite catalyzed reactions.

In this study, we also show that Pearson acidity based on HSAB principle is an important parameter to describe the acidity and selectivity. Local softness, a parameter to quantify Pearson acidity is derivable from quantum chemical calculations. The influence of chemical composition explored in this study indicates that it is possible to optimize the catalytic activity and selectivity by controlling both acid strength and acid softness. It is found that 'relative electrophilicity' (defined as s_H^+ / s_H^-) emerges as a better parameter to study the acidity and reactivity in ethylation reaction.

REFERENCES

1. H. Kessler, in *Comprehensive Supramolecular Chemistry*, G. Alberti and T. Bein (eds.) Pergamon, Oxford, Vol. 7, 1996, p. 425.
2. M.E. Davis, *Acc. Chem. Res.*, 26 (1993) 111.
3. C.-Y. Chen, H.-X. Li and M.E. Davis, *Microporous Mater.*, 2 (1993) 17.
4. *Introduction to Zeolite Science and Practice*, H. van Bekkum, E.M. Flanigen and J.C. Jansen (eds.), Elsevier, Amsterdam, 1991.
5. A. Corma, *Chem. Rev.*, 95 (1995) 559.
6. J.A. Rabo, C.L. Angell, P.H. Kasai and V. Schoemaker, *Discuss. Faraday Soc.*, 41

- (1996) 328.
7. E.J. Dempsey, *J. Phys. Chem.*, 73 (1969) 3660.
 8. E. Kassab, K. Seiti and M. Allavena, *J. Phys. Chem.*, 95 (1991) 9425.
 9. A. Goursot, F. Fajula, C. Daul and J. Weber, *J. Phys. Chem.*, 92 (1988) 4456.
 10. H.V. Brand, L.A. Curtiss and L.E. Iton, *J. Phys. Chem.*, 97 (1993) 12773.
 11. (a) J.C. White and A.C. Hess, *J. Phys. Chem.*, 97 (1993) 6398; (b) J.B. Nicholas and A.C. Hess, *J. Am. Chem. Soc.*, 116 (1993) 5428.
 12. A. Corma, in *Guidelines for Mastering the Properties of Molecular Sieves, Vol. 221, NATO ASI Series*, D. Barthomeuf, E.G. Derouane and W. Holderich (eds.), Plenum Press, New York, 1990, p. 299.
 13. K.P. Wendlandt and H. Bremer, *Proceedings of the 8th International Congress on Catalysis*, Verlag-Chemie, Weinheim, (1988) p. 507.
 14. A. Corma, G. Sastre, P.M. Viruela and C. Zicovich-Wilson, *J. Catal.*, 136 (1992) 521.
 15. G. Sastre, P. Viruela and A. Corma, *Chem. Phys. Lett.*, 264 (1997) 565.
 16. A. Corma, H. Garcia, G. Sastre and P.M. Viruela, *J. Phys. Chem. B*, 101 (1997) 4575.
 17. G. Klopman, *Chemical Reactivity and Reaction Paths*, Wiley, New York, 1974.
 18. K. Fukui, *Theory of Orientation and Stereoselection*, Springer, Berlin, 1970.
 19. M.J.S. Dewar, *J. Mol. Struct. (Theochem)*, 200 (1989) 301.
 20. R.G. Parr, R.A. Donnelly, M. Levy and W.E. Palke, *J. Chem. Phys.*, 168 (1978) 3801.
 21. R.G. Parr, *Ann. Rev. Phys. Chem.*, 34 (1983) 631.
 22. B.G. Baekelandt, W.J. Mortier and R.A. Schoonheydt, in *Modelling of Structure and Reactivity in Zeolites*, C.R.A. Catlow (ed.), Academic Press, London, 1992, p. 157.
 23. C. Zicovich-Wilson, J.H. Planelles and W. Jaskolshi, *Int. J. Quantum Chem.*, 50 (1994) 429.
 24. J. Sauer, in *Modelling of Structure and Reactivity in Zeolites*, C.R.A. Catlow (ed.), Academic Press, London, 1992, p. 183.
 25. P.E. Sinclair and C.R.A. Catlow, *J. Chem. Soc., Faraday Trans.*, 93 (1997) 333.
 26. M.S. Stave and J.B. Nicholas, *J. Phys. Chem.*, 99 (1995) 15046.
 27. R. Vetrivel, R.C. Deka, A. Chatterjee, M. Kubo, E. Broclawik and A. Miyamoto, in *Molecular electrostatic potential: concepts and applications*; J.S. Murray and K. Sen, (eds.), Elsevier, Amsterdam, 1996, p 509.

28. G.J. Kramer and R.A. van Santen, *J. Am. Chem. Soc.*, 115 (1993) 2887.
29. J. Sauer, *Chem. Rev.*, 89 (1989) 199.
30. R.A. van Santen and G.J. Kramer, *Chem. Rev.*, 95 (1995) 637.
31. W. Langenaeker, N. Coussement, F. De Proft and P. Geerlings, *J. Phys. Chem.*, 98 (1994) 3010.
32. R.G. Parr and R.G. Pearson, *J. Am. Chem. Soc.*, 105 (1983) 7512.
33. R.G. Pearson, *J. Am. Chem. Soc.*, 85 (1963) 3533.
34. R.G. Parr and P.K. Chattaraj, *J. Am. Chem. Soc.*, 113 (1991) 1854.
35. R.G. Pearson and W.E. Palke, *J. Phys. Chem.*, 96 (1992) 3283.
36. J.L. Gazquez, A. Martinez and F. Mendez, *J. Phys. Chem.*, 97 (1993) 4059.
37. S. Pal, N. Vaval and R.K. Roy, *J. Phys. Chem.*, 97 (1993) 4404.
38. R.G. Parr and W. Yang, *J. Am. Chem. Soc.*, 106 (1984) 4049.
39. J.L. Gazquez and F. Mendez, *J. Phys. Chem.*, 98 (1994) 4591.
40. S. Krishnamurty, R.K. Roy, R. Vetrivel, S. Iwata and S. Pal, *J. Phys. Chem. A*, 101 (1997) 7253.
41. F. De Proft, W. Langenaeker and P. Geerlings, *J. Phys. Chem.*, 97 (1993) 1826.
42. F. De Proft, S. Amira, K. Choho and P. Geerlings, *J. Phys. Chem.*, 98 (1994) 5227
43. S. Damoun, W. Langenaeker, G. Van de Waude and P. Geerlings, *J. Phys. Chem.*, 99 (1995) 12151.
44. R.K. Roy, S. Krishnamurty, P. Geerlings and S. Pal, *J. Phys. Chem.* (in press)
45. G. Klopman, *J. Am. Chem. Soc.*, 90 (1968) 223.
46. L. Salem, *J. Am. Chem. Soc.*, 90 (1968) 543.
47. K. Fukui, T. Yanezawa and H. Shingu, *J. Chem. Phys.*, 20 (1952) 722.
48. K. Fukui, T. Yanezawa and H. Shingu, *J. Chem. Phys.*, 22 (1954) 1433.
49. K. Fukui and H. Fujimoto, *Bull. Chem. Soc. Jpn.*, 41 (1968) 1989.
50. R.G. Pearson, *Proc. Natl. Acad. Sci.*, 89 (1986) 1827.
51. J.J.P. Stewart, *J. Compt.-Aided Mol. Design*, 4 (1990) 1.
52. E.U. Condon and H. Odabasi, *Atomic Structure*, Cambridge University Press, 1980.
53. GAMESS, General Atomic and Molecular Electronic Structure System, Department of Chemistry, North Dakota State University and Ames Laboratory, Iowa State University; by Schmidt, M. W.; Baldrige, K. K.; Boatz, J. A.; Elbert, S. T.; Gordon,

- M. S.; Jensen, J. H.; Koseki, S.; Matsunga, N.; Nguyen, K. A.; Su, S. J.; Windus, T. L.; Dupuis, M.; Montgomery, J. A. *J. Comput. Chem.* **1993**, *14*, 1347.
54. D.H. Olson, *J. Phys. Chem.*, *74* (1970) 2758.
55. C.T. Chu and C.D. Chang, *J. Phys. Chem.*, *89* (1985) 1569.
56. J. Datka and M. Kawalek, *J. Chem. Soc., Faraday Trans.*, *89* (1993) 1829.
57. S.V. Awate, P.N. Joshi, M.J. Eapen and V.P. Shiralkar, *J. Phys. Chem.*, *97* (1993) 6042.
58. V.B. Kazansky, *Acc. Chem. Res.*, *24* (1991) 379.
59. V.B. Kazansky and I.N. Senchenya, *J. Catal.*, *119* (1989) 108.
60. S.R. Blazkowski and R.A. van Santen, *Topics in Catal.* *4* (1997) 145.

CHAPTER 7

SUMMARY AND CONCLUSIONS

In this thesis, several molecular modeling techniques have been systematically used to design suitable zeolite catalysts for the synthesis of fine chemicals. Alkylation of aromatic compounds is a crucial step in the synthesis of several fine chemicals. Although alkylation of aromatics is commonly carried out over zeolites, the selection of a particular zeolite is rather by chemical intuition. We have used standard but sound theory-based molecular modeling techniques. The specific information that could be generated by each of these techniques has been derived and then they are put together to arrive at the whole picture.

A logical route to design zeolite catalysts has been devised based on the molecular modeling technique. The procedure starts with the crystal structure of zeolites and the chemical formula of the aromatic molecules, proceeds in several steps and finally, the suitable shape selective catalyst is suggested as shown in Figures 1-3. We have studied the selective synthesis of 4,4'-DIBP, which is an intermediate in the synthesis of polymer useful for liquid crystal display application.¹ In this case, several zeolites have been experimentally tested.² The prediction by our molecular modeling technique that ZSM-12 (MTW) will be a suitable catalyst is in good agreement with the experimental findings.³ *p*-IBEB is the key intermediate in the synthesis of the analgesic drug - ibuprofen.⁴ The conventional synthesis route for *p*-IBEB using Friedel-Crafts catalysts lead to low selectivity (17.6%)⁵ whereas Tokumoto *et al.*⁶ have claimed to achieve better selectivity (43%) using a HY zeolite catalyst. However, this reaction has not been studied over other zeolites. Hence, the studies on the selective synthesis of *p*-IBEB over several zeolites described in this study is a 'de Nova' attempt. The computational route to logical design of shape selective zeolite for the production of *p*-IBEB is the main content of this thesis.

The first step in the procedure involves the screening of several zeolites to choose the zeolites which pass the test of structural fitting. The sequence of operations is shown in Figure 1. For *p*-IBEB, it is observed that small and medium pore zeolites are not suitable. Among the

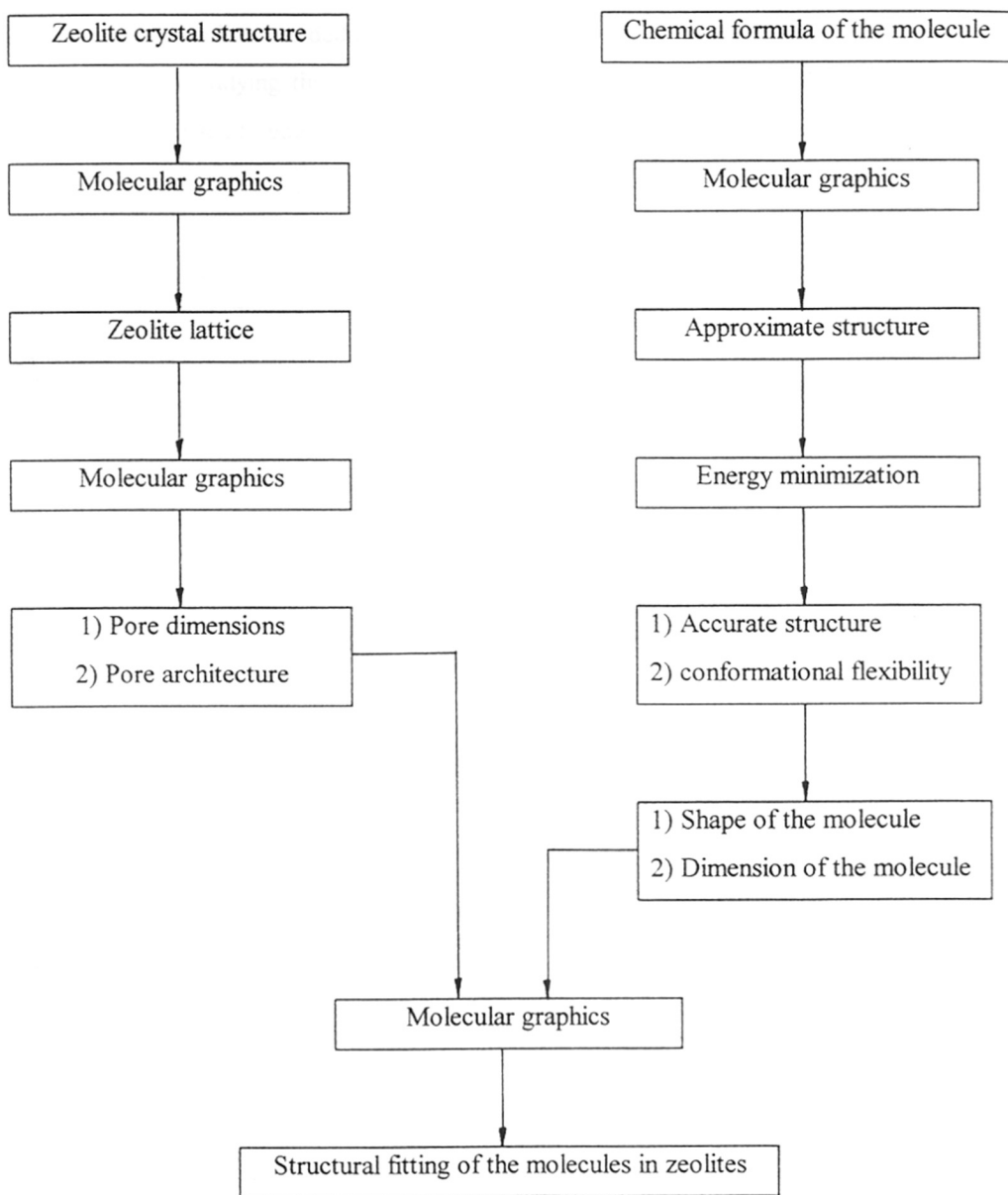


Figure 1. The first step in the screening of zeolite catalysts for shape selective reactions.

twenty large pore zeolites, aluminophosphate frameworks, natural minerals and those with more than one polymorphic structure are not considered in this study. Thus seven large pore zeolites are screened out for further quantitative analysis. Several adsorption sites for the

molecules inside zeolites are deduced by a ‘hybrid method’ as shown in Figure 2. Finally, the steps involved in studying the diffusion characteristics are shown in Figure 3. MD and QC calculations are used to gain better understanding on the adsorption, dynamics and reaction

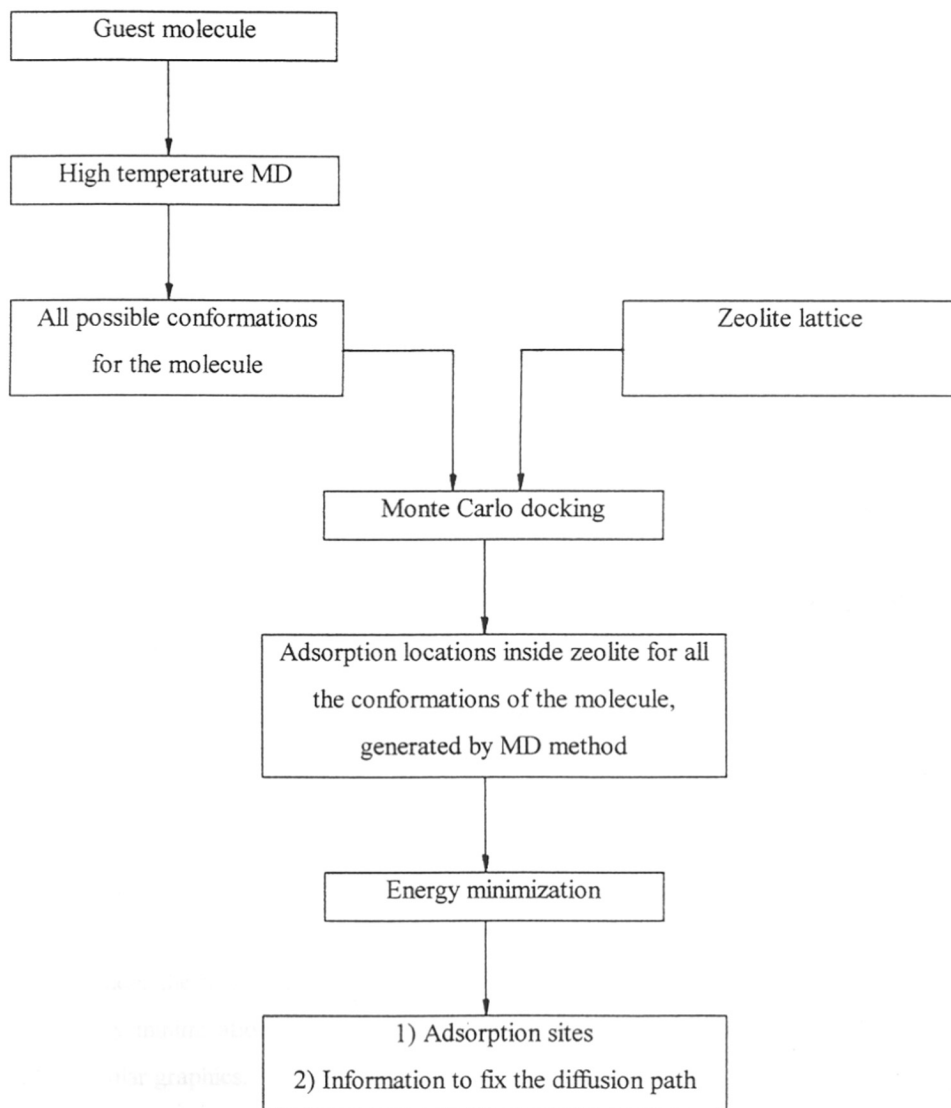


Figure 2. Locating the adsorption sites and predicting the diffusivity by a hybrid method.

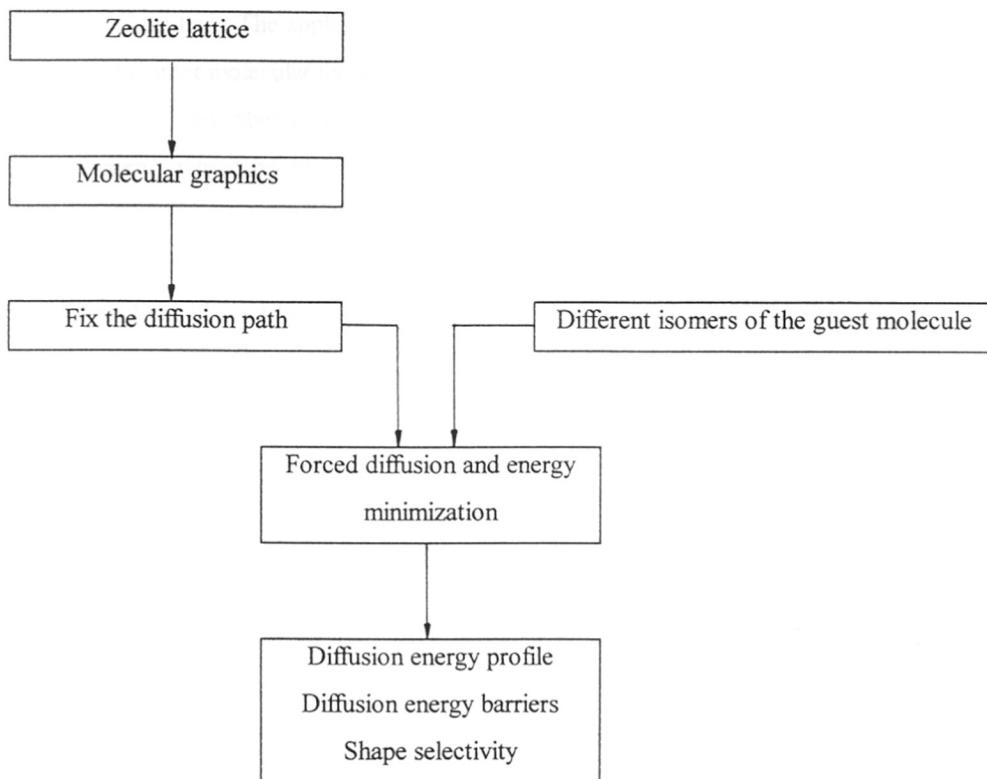


Figure 3. Methodology to predict the shape selective efficiency of zeolites, by calculating the diffusion energy barrier.

mechanism. The details of work and the subsequent outcome from each chapter are given in the following section.

In Chapter 1, we present a general overview of zeolites tracing their development as shape selective catalysts since their discovery in 1756. The scope of the thesis is briefly presented. The theory of several molecular modeling methods adopted in this thesis are detailed under the title - basics of simulation methods. The methods described include force field energy minimization, Monte Carlo, molecular dynamics, quantum chemical calculations and molecular graphics.

Chapter 2 describes the application of molecular graphics and structural fitting of aromatics in large pore zeolites. The usefulness of deriving several informations from this

technique is described. The application of molecular graphics to analyse the results of detailed calculations by other molecular modeling methods is also brought out.

Chapter 3 describes a 'hybrid method' which combines molecular dynamics, Monte Carlo and energy minimization methods to locate the energetically favourable adsorption sites for the guest molecules. Such calculations are performed to locate the isomers of DIBP in three large pore zeolites and the isomers of IBEB in several large pore zeolites. The ratio of mean/minimum energy is used to predict the diffusivity of these molecules qualitatively.

Chapter 4 uses the information derived from Chapter 3 on adsorption sites, to fix the diffusion path for the molecules. The diffusion of isomers of DIBP is studied in LTL, MOR and MTW using energy minimization technique. The diffusion energy barriers are calculated from the energy profile plot obtained by plotting interaction energy versus the distance travelled by the molecule. Similarly, the diffusion of isomers of IBEB is studied in seven large pore zeolites. The diffusion constraint being the main cause of the shape selectivity, the efficiency of these zeolites for the shape selective production of the required isomers are predicted. Additionally, the interaction between the zeolite host and the guest molecules are understood at an atomic level. The influence of pore architecture on the diffusion characteristics of the molecules is also brought out.

Chapter 5 describes the application of MD method to study the diffusion behaviour of *p*-, *m*- and *o*-IBEB inside MOR. The results of these calculations validate the conclusions derived in the earlier chapters. The diffusivity of the molecules are calculated and reported. Further, the dynamics of the molecules and the structural details are brought out from the MD calculations carried out at 298 K.

In Chapter 6, quantum chemical calculations are used to study the electronic interactions using the cluster approach. Fairly large cluster models have been generated to represent the adsorption site in MOR. Then, the interaction of guest molecules with the host zeolite cluster is studied by semi-empirical MNDO method. The variation in the reactivity of the molecules due to their confinement in the micropores of zeolites is brought out from the changes in HOMO value and HOMO-LUMO band gap. Pearson acidity based on Hard-Soft Acid-Base principle is demonstrated as a reliable parameter to describe acidity and it could be calculated by cluster approach. Further, relative electrophilicity derived from the local softness

values is brought out as an indication of reactivity, considering ethylation as the typical reaction.

While the present chapter (Chapter 7) provides the overall summary and conclusions of this thesis, the specific conclusions derived from each chapter is summarised at the end of those chapters. In general, it is seen that the combination of several methods is necessary for obtaining an accurate and reliable information about the adsorption sites and selectivity of zeolites.

REFERENCES

1. D. Fraenkel, M. Cherniavsky, B. Ittah and M. Levy, *J. Catal.*, 110 (1996) 273.
2. Y. Sugi and M. Toba, *Catal. Today*, 19 (1994) 187.
3. A.S. Loktev and P.S. Chekriy, *Stud. Surf. Sci. Catal.*, 84 (1994) 1845.
4. J.-P. Rieu, A. Boucherle, H. Cousse and G. Mouzin, *Tetrahedron*, 42 (1986) 4095.
5. I. Shimizu, Y. Matsumura, Y. Tokumoto and K. Uchida, *Eur. Pat. Appl.*, 373 362, 1990.
6. Y. Tokumoto, I. Shimizu and S. Inoue, *Eur. Pat. Appl.*, 414 207, 1991.

CURRICULUM VITAE

Ramesh Ch. Deka was born in a village, Karaibari, Assam, India, on 1st January, 1970. In 1991, he received his B. Sc. degree in Chemistry from Gauhati University, Assam. In 1994, he received M. Sc. degree in Physical Chemistry from the same University. In the same year he was awarded the CSIR fellowship. He started his research carrier in January 1995 on theoretical modelling of zeolite catalysts with Dr. Rajappan Vetrivel, Catalysis Division, National Chemical Laboratory, Pune. His research interests include use of energy minimisation, Monte Carlo, molecular dynamics and quantum chemical methods to investigate the adsorption sites and catalytic properties of zeolites.

LIST OF PUBLICATIONS

1. **Ramesh Ch. Deka** and Rajappan Vetrivel,
Computer-aided search for shape-selective zeolite catalysts for the synthesis of *p*-isobutylethylbenzene,
Chem. Commun., (1996) 2397.
2. R. Vetrivel, **Ramesh Ch. Deka**, A. Chatterjee, M. Kubo, E. Broclawik and A. Miyamoto,
Studies on the molecular electrostatic potential inside the microporous material and its relevance to their catalytic activity,
in *Molecular Electrostatic Potentials : Concepts and Applications, Theoretical and Computational Chemistry*, J.S. Murray and K. Sen (eds.), Elsevier, Amsterdam, Vol. 3 (1996) 509.
3. T. Selvam, D.N. Iyer, **Ramesh Ch. Deka**, A. Chatterjee and R. Vetrivel,
A computational 'Expert System' approach to design synthesis routes for zeolite catalysts,
Stud. Surf. Sci. Catal., 105 (1996) 133.
4. **Ramesh Ch. Deka** and Rajappan Vetrivel,
Adsorption sites and diffusion mechanism of alkylbenzenes in large pore zeolite catalysts as predicted by molecular modeling techniques,
J. Catal., 174 (1998) 88.
5. **Ramesh Ch. Deka** and Rajappan Vetrivel,
Adsorption and diffusion characteristics of *p*-isobutylethylbenzene in large pore zeolites as derived from molecular modelling methods,
Stud. Surf. Sci. Catal., 113 (1998) 643.
6. S. Sharma, **Ramesh Ch. Deka**, A.P. Singh and R. Vetrivel,
The nature of active site and the mechanism of selective chlorination of aromatics by zeolites K-L as predicted by molecular modelling methods,
Stud. Surf. Sci. Catal., 113 (1998) 675.

7. **Ramesh Ch. Deka**,
Acidity in zeolites and their characterisation by different spectroscopic methods,
Indian J. Chem. Technology, (in press).
8. R. Vetrivel, **Ramesh Ch. Deka**, S.B. Waghmode, S. Sivasanker, K. Mizukami, H. Takaba, M. Kubo and A. Miyamoto,
Molecular modelling of adsorption and diffusion processes in zeolites in relevance to environment protection,
in *Adsorption and its Application in Industry and Environment Protection*,
A. Dabrowski (ed.) Elsevier, Amsterdam (in press).
9. **Ramesh Ch. Deka**, Rajappan Vetrivel and Akira Miyamoto,
Computational studies on the diffusion behaviour of alkylaromatics in large pore zeolites,
Topics in Catal., (in press).
10. **Ramesh Ch. Deka**, Sourav Pal, Annick Goursot and Rajappan Vetrivel,
Influence of zeolite composition on the selectivity of alkylation reaction for the synthesis of p-isobutylethylbenzene: A computational study,
Catal. Today (accepted)
11. **Ramesh Ch. Deka**, Rajappan Vetrivel, Paul Geerlings and Sourav Pal,
Application of Hard-Soft Acid-Base principle to study Bronsted acid sites in zeolite clusters: A quantum chemical study,
J. Phys. Chem., (communicated).
12. P. Bharathi, **Ramesh Ch. Deka**, S. Sivasanker and R. Vetrivel,
Diffusional characteristics of substituted anilines in various zeolites as predicted by molecular modeling methods,
Catal. Lett., (communicated).